UNIVERSITAT POLITÈCNICA DE VALÈNCIA

Departament d'Enginyeria Electrònica

"Mathematical modeling approaches for the diagnosis and treatment of reentrant atrial tachyarrhythmias"

Tesi Doctoral

Autor
Alejandro Liberos Mascarell

Dirigida per:
Dra. María de la Salud Guillem Sánchez
Dr. Batiste Andreu Martínez Climent
Dr. José Millet Roig

València, 25 de Gener de 2016

Agraïments

El temps que transcorre durant la realització d'una tesi doctoral, així com les experiències associades a aquesta, promouen canvis importants en la vida de l'estudiant i la seua percepció del món. Si a més hi afegim la volatilitat social i econòmica en la que es troba la nostra societat, les reflexions i converses s'encadenen donant lloc a un procés profund d'aprenentatge a nivell personal i humà que queda directament lligat al científic.

En el meu cas, les persones que m'han envoltat han estat una peça fonamental en tot aquest procés, és per això que no puc més que agrair als meus companys de laboratori durant tots aquests anys per la seua qualitat intel·lectual i humana: Jorge, Miquel, Ramon, Edu, Ismael, Santi, Xavi, Félix, Alfonso, Cristina, Conrad i molts més heu sigut els millors companys en aquests anys i de segur que la relació personal (i el jolgorio) duraran molt.

Menció especial mereixen Maria i Andreu, als qui vaig conèixer molt joves i que gràcies a la seua empenta i visió, han fet en pocs anys d'un grup de 'xiquillos' –creueu-me que he buscat una paraula més acurada però hagués distorsionat el significat- un grup d'investigació a l'avantguarda en investigació cardíaca. És un orgull formar part d'aquest equip que de segur obtindrà resultats a l'alçada, així com haver estat en moments tan importants de la vostra vida.

També vull agrair a Pepe, Paco, Toni i Álvaro, el haver-me introduït al grup així com l'atenció i el tracte proper durant tots aquests anys. Com no, recordar les hores al laboratori de fisiologia i l'acolliment de Javier Chorro, Lluís Such i tot el seu equip, els desitge els majors èxits professionals i personals.

L'experiència d'una estada prolongada a l'estranger també l'haig d'agrair a aquesta tesi doctoral i una vegada més vaig tenir la sort de comptar amb l'acolliment d'un equip excepcional a nivell científic i personal a la University of Oxford. Gràcies a Blanca, Alfonso, Ana i Elissa per fer-me sentir com a casa durant aquests mesos, de segur que la col·laboració serà continuada en els propers anys.

Res de tot açò hagués estat possible sense el recolzament de la meua família. Gràcies als meus pares pel treball i tenacitat durant més de 35 anys, espere que trobeu en nosaltres, els vostres fills, la recompensa a tots els esforços. Per a nosaltres heu sigut el millor exemple d'esforç i de com afrontar les dificultats amb serenitat. Als meus germans, que a més sempre han sigut els millors amics sempre,

els millors desitjos. Per a tots tres pareix que se'ns albiren moments de canvis i noves experiències, de segur que triem el camí correcte, perquè el 'xarco' no ens distancie.

L'últim lloc per a Pilar per ser com és i ajudar sempre a que el camí siga més clar i fàcil, perquè junts fem el projecte més important que és la nostra vida.

Acronyms

AA	Atrial appendage (LAA and RAA are left and right respectively).
AF	Atrial fibrillation.
AFL	Atrial flutter.
AP	Action potential.
APA	Action potential amplitude.
APD	Action potential duration (APD20, APD50, APD90).
APDratio (f)	APD(N Hz) divided by APD at 1Hz.
ATP	Adenosine triphosphate.
AV	Atrioventricular (node).
AVF	Augmented lead at the left foot.
AVL	Augmented lead at the left arm.
AVR	Augmented lead at the right arm.
BB	Bachmann's bundle.
BCL	Basic cycle length.
BSPM	Body Surface Potential Mapping.
Ca^{2+}	Calcium ion.
cAF	Chronic atrial fibrillation.
CFAE	Complex fractionated atrial electrogram.
C_m	Membrane capacitor.
CPU	Central processing unit.
CRU	Sarcoplasmic reticulum calcium release units, or ryanodine receptor.
CT	Crista terminalis.

CTI	Cavotricuspid isthmus.
CUDA	Compute Unified Device Architecture, parallel programming framework by Nvidia.
CCW	Counterclockwise.
CV	Conduction velocity.
CW	Clockwise.
d	Distance between cells.
dV/dt_{max}	Maximum slope of AP upstroke.
D	Diffusion.
DI	Einthoven Lead I.
DII	Einthoven Lead II.
DIII	Einthoven Lead III.
dV_m/dt	Voltage slope.
ECG	Electrocardiogram.
EGM	Electrogram.
FE	Forward Euler.
FO	Fosa ovalis.
h	Time step.
g_{XX}	Conductance associated to an ionic current
HT	Hilbert transform.
I_{Cab}	Background calcium current.
I_{CaL} / g_{CaL}	Inward L–type Ca2+ corrent / conductance.
I_f	Hyperpolarization–activated inward current.
I_{ion}	Resulting current through cell membrane.
I_{K1} / g_{K1}	Inward–rectifier current/conductance.
I_{Kr} / g_{Kr}	Rapid repolarizing potassium corrents / conductance.
I_{Ks} / g_{Ks}	Slow repolarizing potassium corrents / conductance.
I_{Kur} / g_{Kur}	Ultra–rapid delayed K+ current / conductance.
I_{Na} / g_{Na}	Fast sodium corrent / conductance.

I_{Nab}	Background sodium current.
I_{NaK}	Sodium–potassium pump current.
$I_{NaK,max}$	Sodium–potassium màximum pump current.
I_{NCX} / k_{NCX}	Sodium calcium exchanger current.
I_{PMCA}	Calcium pump current.
I_{to} / g_{to}	Transient outward corrent / conductance.
$J_{rel,RyR}$	Constant modulating CRUs.
K^+	Potassium ion.
k_{NCX}	Constant modulating I_{NCX}.
GP–GPU	General Purpose – Graphic Processing Unit.
LA	Left atrium.
MV	Mitral valve.
Na^+	Sodium ion.
ODE	Ordinary differential equation.
PCr	Partial Correlation index.
PLB	Phospholamban.
PM	Pectinate muscles.
PN	Patient number N.
PV	Pulmonary veins.
R&D	Research and development.
RA	Right atrium.
RL	Rush–Larsen.
RM	Rotor meandering.
RMP	Resting membrane potential.
RP	Refractory period.
S	Septum.
SA	Sinoatrial (node).
SD	Standard deviation.
SERCA	Sarcoplasmic reticulum Ca^{2+} ATPase pump.

SLN	Sarcopilin.
SP	Singularity point.
SR	Sarcoplasmic reticulum.
t	Time.
tAFL	Typical atrial flutter.
TA	Tricuspid Annulus.
V20	Potential at 20% of APD90.
VN	Precordial lead (N = [1,6]).
VC	Vena cava.
V_m	Membrane potential.
WL	Wavelength.
WCT	Wilson central terminal.

Contents

List of figures

Abstract

Atrial tachyarrhythmias present a high prevalence in the developed world, and several studies predict that in the coming decades it will be increased. Micro or macro-reentrant mechanisms of the electrical wavefronts that govern the mechanical behavior of the heart are one of the main responsibles for the maintenance of these arrhythmias. Atrial flutter is maintained by a macro-reentry around an anatomical or functional obstacle located in the atria. In the case of atrial fibrillation, the hypothesis which describes high frequency rotors as dominant sources of the fibrillation and responsible for the maintenance of the arrhythmia, has been gaining relevance in the last years. However, the therapies that target high frequency sources have a limited efficacy with current techniques.

Radiofrequency ablation allows the destruction of parts of the cardiac tissue resulting in the interruption of the reentrant circuit in case of macro-reentries or the isolation of micro-reentrant circuits. The non-invasive location of reentrant circuits would increment the efficacy of these therapies and would shorten surgery interventions.

In parallel, pharmacological therapies modify ionic expressions associated to the excitability and electrical refractoriness of the cardiac tissue with the objective of hindering the maintenance of reentrant behaviors. These therapies require a deep knowledge of the ionic mechanisms underlying the reentrant behavior and its properties in order to be effective. The research in these mechanisms allows the evaluation of new targets for the treatment and thus may improve the efficacy in atrial fibrillation termination.

In this thesis, mathematical modeling is used to go forward in the minimization of the limitations associated to these treatments. Body surface potential mapping has been evaluated, both clinically and by means of mathematical simulations for the diagnosis and location of macro-reentrant circuits. The analysis of phase maps obtained from multiple lead electrocardiographic recordings distributed in the whole torso allowed the discrimination between different reentrant circuits. It is the reason why this technique is presented as a tool for the non-invasive location of macro and micro-reentrant circuits.

A population of mathematical models designed in this thesis based on the action potentials recordings of atrial cardiomyocites from 149 patients, allowed the

evaluation of the ionic mechanisms defining the properties of reentrant behaviors. This study has allowed us defining the blockade of I_{CaL} as a target for the pharmacological treatment. The blockade of this current is associated with the increase of the movement in the core of the rotor which easies the collision of the rotor with other wavefronts or anatomical obstacles promoting the extinction of the reentry. The variability observed between patients modeled in our population has allowed showing and explaining the mechanisms promoting divergent results of a single treatment. This is why the introduction of populations of models will allow the prevention of side effects associated to inter-subject variability and to go forward in the development of individualized therapies.

These works are built through a simulation platform of cardiac electrophysiology based in Graphic Processing Units (GPUs) and developed in this thesis. The platform allows the simulation of cellular models, tissues and organs with a realistic geometry and shows features comparable to that of the platforms used by the most relevant electrophysiology research groups at the moment.

Resum

Les taquiarítmies auriculars tenen una alta prevalença en el món desenvolupat, a més diversos estudis poblacionals indiquen que en les pròximes dècades aquesta es veurà incrementada. Els mecanismes de micro o macro–reentrada dels fronts d'ona elèctrics que regeixen el comportament mecànic del cor, es presenten com una de les principals causes del manteniment d'aquestes arítmies. El flutter auricular és mantingut per una macro–reentrada al voltant d'un obstacle anatòmic o funcional en les aurícules, mentre que en el cas de la fibril·lació auricular la hipòtesi que defineix als rotors d'alta freqüència com a elements dominants i responsables del manteniment de l'arítmia s'ha anat imposant a la resta en els últims anys. No obstant això, les teràpies que tenen com a objectiu finalitzar o aïllar aquestes reentrades tenen encara una eficàcia limitada.

L'ablació per radiofreqüència permet eliminar zones del teixit cardíac resultant en la interrupció del circuit de reentrada en el cas de macro–reentrades o l'aïllament de comportaments micro–reentrants. La localització no invasiva dels circuits reentrants incrementaria l'eficàcia d'aquestes teràpies i reduiria la durada de les intervencions quirúrgiques.

D'altra banda, les teràpies farmacològiques alteren les expressions iòniques associades a la excitabilitat i la refractaritat del teixit amb la finalitat de dificultar el manteniment de comportaments reentrants. Aquest tipus de teràpies exigeixen incrementar el coneixement dels mecanismes subjacents que expliquen el procés de reentrada i les seues propietats, la recerca d'aquests mecanismes permet definir les dianes terapèutiques que milloren l'eficàcia en l'extinció d'aquests comportaments.

En aquesta tesi el modelatge matemàtic s'utilitza per a fer un pas important en la minimització de les limitacions associades a aquests tractaments. La cartografia elèctrica de superfície ha sigut testada, clínicament i amb simulacions matemàtiques com a tècnica de diagnòstic i localització de circuits macro–reentrants. L'anàlisi de mapes de fase obtinguts a partir dels registres multicanal de derivacions electrocardiogràfiques distribuïdes en la superfície del tors permet diferenciar diferents circuits de reentrada. És per açò que aquesta tècnica de registre i anàlisi es presenta com una eina per a la localització no invasiva de circuits macro i micro–reentrants.

Una població de models matemàtics, dissenyada en aquesta tesi a partir dels registres dels potencials d'acció de 149 pacients, ha permès avaluar els mecanismes

iònics que defineixen les propietats associades als processos de reentrada. Açò ha permès apuntar al bloqueig del corrent I_{CaL} com a diana terapèutica. Aquesta s'associa a l'increment del moviment del nucli que facilita l'impacte del rotor amb altres fronts d'ona o obstacles extingint-se així el comportament reentrant. La variabilitat entre pacients reflectida en la població de models ha permès a més mostrar els mecanismes pels quals un mateix tractament pot mostrar efectes divergents, així l'ús de poblacions de models matemàtics permetrà prevenir efectes secundaris associats a la variabilitat entre pacients i aprofundir en el desenvolupament de teràpies individualitzades.

Aquests treballs es fonamenten sobre una plataforma de simulació de electrofisiologia cardíaca basat en Unitats de Processament Gràfic (GPUs) i desenvolupada en aquesta tesi. La plataforma permet la simulació de models cel·lulars cardíacs així com de teixits o òrgans amb geometria realista, mostrant unes prestacions comparables amb les de les utilitzades per els grups de recerca més importants en aquesta área.

Resumen

Las taquiarritmias auriculares tienen una alta prevalencia en el mundo desarrollado, además diversos estudios poblacionales indican que en las próximas décadas ésta se verá incrementada. Los mecanismos de micro o macro–reentrada de los frentes de onda eléctricos que rigen el comportamiento mecánico del corazón, se presentan como una de las principales causas del mantenimiento de estas arritmias. El flutter auricular es mantenido por un macro–reentrada alrededor de un obstáculo anatómico o funcional en las aurículas, mientras que en el caso de la fibrilación auricular la hipótesis que define a los rotores de alta frecuencia como elementos dominantes y responsables del mantenimiento de la arritmia se ha ido imponiendo al resto en los últimos años. Sin embargo, las terapias que tienen como objetivo finalizar o aislar estas reentradas tienen todavía una eficacia limitada.

La ablación por radiofrecuencia permite eliminar zonas del tejido cardiaco resultando en la interrupción del circuito de reentrada en el caso de macro–reentradas o el aislamiento de comportamientos micro–reentrantes. La localización no invasiva de los circuitos reentrantes incrementaría la eficacia de estas terapias y reduciría la duración de las intervenciones quirúrgicas.

Por otro lado, las terapias farmacológicas alteran las expresiones iónicas asociadas a la excitabilidad y la refractoriedad del tejido con el fin de dificultar el mantenimiento de comportamientos reentrantes. Este tipo de terapias exigen incrementar el conocimiento de los mecanismos subyacentes que explican el proceso de reentrada y sus propiedades, la investigación de estos mecanismos permite definir las dianas terapéuticas que mejoran la eficacia en la extinción de estos comportamientos.

En esta tesis el modelado matemático se utiliza para dar un paso importante en la minimización de las limitaciones asociadas a estos tratamientos. La cartografía eléctrica de superficie ha sido testada, clínicamente y con simulaciones matemática,s como técnica de diagnóstico y localización de circuitos macro–reentrantes. El análisis de mapas de fase obtenidos a partir de los registros multicanal de derivaciones electrocardiográficas distribuidas en la superficie del torso permite diferenciar distintos circuitos de reentrada. Es por ello que esta técnica de registro y análisis se presenta como una herramienta para la localización no invasiva de circuitos macro y micro–reentrantes.

Una población de modelos matemáticos, diseñada en esta tesis a partir de los registros de los potenciales de acción de 149 pacientes, ha permitido evaluar los mecanismos iónicos que definen las propiedades asociadas a los procesos de reentrada. Esto ha permitido apuntar al bloqueo de la corriente I_{CaL} como diana terapéutica. Ésta se asocia al incremento del movimiento del núcleo que facilita el impacto del rotor con otros frentes de onda u obstáculos extinguiéndose así el comportamiento reentrante. La variabilidad entre pacientes reflejada en la población de modelos ha permitido además mostrar los mecanismos por los cuales un mismo tratamiento puede mostrar efectos divergentes, así el uso de poblaciones de modelos matemáticos permitirá prevenir efectos secundarios asociados a la variabilidad entre pacientes y profundizar en el desarrollo de terapias individualizadas.

Estos trabajos se cimientan sobre una plataforma de simulación de electrofisiología cardiaca de basado en Unidades de Procesado Gráfico (GPUs) y desarrollada en esta tesis. La plataforma permite la simulación de modelos celulares cardiacos así como de tejidos u órganos con geometría realista, mostrando unas prestaciones comparables con las de las utilizadas por los grupos de investigación más potentes en el campo de la electrofisiología.

Chapter 1

Introduction

The growth of biomedical engineering as a discipline in the last decades has had an important impact on improving the quality of life of citizens. And it is because, this bridge between technologists and clinicians has enabled the introduction of high technology and instruments in the diagnosis and therapy protocols that are faced by physicians and patients every day.

Despite the progress already achieved, the room for improvement is still very large so that, together with the great impact of this discipline in society, it sparks the interest of industry and institutions. Note the introduction in recent years of degrees and Masters in biomedical engineering in several Spanish universities, as well as the support from Spanish and European public and governmental entities that is reflected in the program for R&D financing "Horizon 2020" and in the Spanish Strategy for Science and Technology and Innovation 2013–2020:

- To develop, as part of a continuous process of exploration and research chasing clinical efficiency, emerging and cutting–edge therapeutic tools.
- To facilitate the link between the actors involved in the Spanish health and technological innovation process through collaboration with clinical groups, basic and technical research, as well as companies of international relevance

Cardiac electrophysiology is one of the areas to that biomedical engineering preeminently faces. Since the first manifestations of the electrical activity of the myocardium and its link with pumping efficiency of the heart due to the excitation–contraction binomial, through the introduction into clinical practice of the electrocardiogram (ECG) ***(Einthoven 1906)***, much progress has been made in the knowledge of the electrical mechanisms driving healthy or pathological episodes of the heart.

However, in the field of atrial tachyarrhythmias – among which include atrial fibrillation (AF) and atrial flutter (AFL) – the mechanisms of initiation and maintenance are not fully understood, at the same time new approaches for

diagnosis and treatment of these arrhythmias are being presented frequently. That is why the research linked to atrial or, in general, cardiac tachyarrhythmias attracts a high scientific interest that brings the celebration of congresses dedicated to this issue or the publication of books and high impact factor articles.

Much of this research has historically required the use of animals or patients in order to test different hypotheses associated with diagnostic or therapeutic advances. In recent years, thanks to the continuous improvement of computing and simulation platforms, the introduction of in–silico experimentation is mitigating technical and essentially ethical problems associated with experimental studies in animals. Simulations of cardiac electrical activity allow the evaluation of hypotheses with a high control of the variables involved, and serve for its viability analysis avoiding huge economic and ethical costs.

1.1. Motivations

Today, many authors argue that many atrial arrhythmias are caused by macro or micro–reentrant electrical activity. Atrial flutter is maintained by a macro–reentry around an anatomical – typically the tricuspid valve ***(Olgin 1995)*** **–** or functional obstacle in the atria. The case of atrial fibrillation (AF) is much more discussed, many authors ***(Berenfeld 2000, Jalife 2002, Atienza 2006)*** argue that high frequency rotors are the mechanism responsible of this pathological activity. This, coupled with that AF is the most common cardiac arrhythmia, has led many research projects in order to better understand the behavior of the rotors easing the development of new pharmacological treatments or address its isolation or extinction by radiofrequency ablation or drug treatment.

Mathematical modeling has been in the last decades one of the strategies to meet the challenges associated with cardiac electrophysiology research. However, the simulating platforms used in the last decades needed from huge investments that were not possible for most research groups. Our group needed mathematical models to validate our hypothesis, so the introduction in this thesis of simulation platforms based in General Purpose – Graphic Processing Unit (GP–GPU) which represent lower costs compared with the clusters used in other platforms, supposed a step forward for our research. Simulations will ease the location and understanding of the mechanisms responsible of reentrant arrhythmias, and they will allow the identification of the most favorable therapeutic strategy.

We hypothesized that Body Surface Potential Mapping (BSPM) can help in the identification and location of macro and micro–reentries, and thus be used as a tool in the diagnosis and ablation procedures of atrial arrhythmias.

In parallel, the pharmacological treatment of atrial fibrillation requires deep research to understand the ionic mechanisms responsible for maintenance of AF. It is because the drugs used today are moderately effective at the time of ending the arrhythmia and maintain sinus rhythm ***(Climent 2015b)***, especially in the case of

persistent or permanent AF which implies highly remodeled substrates. A strategy for the extinction of rotors is to increase the area needed for the maintenance of the reentry and promote its collision with other wavefronts or anatomical obstacles ***(Climent 2015b)***. That is why in this thesis the impact of different ionic currents in action potentials and dynamics of rotors are evaluated.

Cell, organ and human torso level mathematical models supported with experimental data has been used in this thesis to validate our hypotheses. For this the following objectives were proposed:

1.1. Objectives

The goal of the present thesis is to propose and develop methods for the non–invasive location –which will ease ablation procedures– and pharmacological treatment of reentrant drivers of atrial tachyarrhythmias. Signal analysis and mathematical models will be used, resulting in the following secondary objectives:

- To develop a GP–GPU based platform for the simulation of human atrial cell, tissue and geometrical models.
- To obtain spatial parameters from Body Surface Potential Mapping (BSPM) recordings in patients able to improve the diagnosis of atrial flutter.
- To simulate different patterns of macro–reentrant tachycardias in the atria and to evaluate the mechanisms reflected in the torso surface, and the diagnosis methods proposed.
- To develop a population of cell models which reproduce the variability in action potential biomarkers observed in chronic atrial fibrillation patients.
- To evaluate in the population of models of chronic atrial fibrilation the effect of different currents in the action potential and reentrant biomarkers.
- To propose and to evaluate pharmacological treatments with the objective of destabilizing rotors by incrementing the area needed for the maintenance.

1.2. Structure of the thesis

This thesis is structured in the following chapters:

Chapter 2: State of the art. In this chapter, the main concepts implied in this thesis are introduced and reviewed. Cardiac electrophysiology and electrocardiography are introduced including the body surface potential mapping (BSPM) technique. The different mechanisms discussed as responsible of the maintenance of atrial tachyarrhythmias, as the features of the arrhythmias analyzed in this thesis are described. Moreover, the background of cardiac modeling in the level of cell, tissue and geometrical

models are described, finally the use of GP–GPUs in the resolution of cardiac models is also described.

Chapter 3: General materials and methods. The aim of this chapter is to describe the simulation platform developed in this thesis and to describe the main characteristics of the electrophysiological and geometrical models used. Phase analysis and singularity point detection are also introduced as it will be used in the main parts of this thesis.

Chapter 4: Non–invasive Characterization of Atrial Macroreentries during Typical and Atypical Atrial Flutter. Phase analysis of body surface potential mapping is used both in AFL patients and simulations. The simulations used in this thesis complete the chain ionic channels–atrial myocyte–atria–human torso. Different propagation patterns can be identified depending on the structure that sustains the macro–reentrant circuit.

Chapter 5: Role of Main Ion Channel Currents on Atrial Fibrillation Electrophysiological Characteristics: An in Silico Inter–subject Variability Study. A population of models representing inter–subject variability of atrial fibrillation patients is used to evaluate the importance of the different ionic currents in action potential and reentrant biomarkers. Populations of models explain why a single pharmacological treatment can have divergent effects due to inter–subject variability.

Chapter 6: Discussion and conclusion. The results and main findings introduced in this thesis are discussed and compared with previous works and summarizing the main findings. The conclusions are listed and a guideline for future works is proposed.

Chapter 7: Contributions. The scientific contributions associated to this thesis and derived from the present dissertation are listed in this chapter. The scientific framework in which this thesis has been involved is also described including the research stays and collaborations.

Chapter 2

State of the art

This is a chapter that reviews the fundamentals on the different research fields that are discussed in this thesis. This is a multidisciplinary work that comprises different fields, as cardiology, computing simulation or electrocardiographic interpretation. This is why an introduction to these issues that will facilitate the understanding of the rest of the work is needed.

2.1. Introduction to electrocardiography

2.1.1. The heart

The heart is a muscular viscera located in the center of the thoracic cavity. It forms the circulatory system together with the blood and blood vessels, whose main function is to supply the nutrients and oxygen necessary for the survival of all cells in the body. The heart pumps blood throughout the body by means of rhythmic contractions allowing a continuous flow of blood.

The heart consists of four chambers, two atria and two ventricles, on the top and the bottom of the heart respectively. The septum divides the heart into the left and right halves with one atrium and ventricle each, which are connected together. The atria are responsible for the reception while the ventricles are known as blood ejection chambers; both atria and ventricles contract in coordination, first the atria contract together then the ventricles contract. The right side is responsible for receiving blood from the whole body and pumps it to the lungs for oxygenation. In parallel, left atrium and ventricle receive oxygenated blood to be distributed again through the body.

Valves force the blood to flow in the right direction and improve the mechanical efficiency of the pump. Between the right atrium and ventricle it is the tricuspid valve, and between the left atrium and ventricle the mitral valve is placed. The pulmonary valve obstructs the reverse flow of blood from the pulmonary

arteries to the right ventricle, while the aortic valve does the same between the aorta and left ventricle. Anatomy of the heart, valves and vessels is depicted in Figure 2.1.

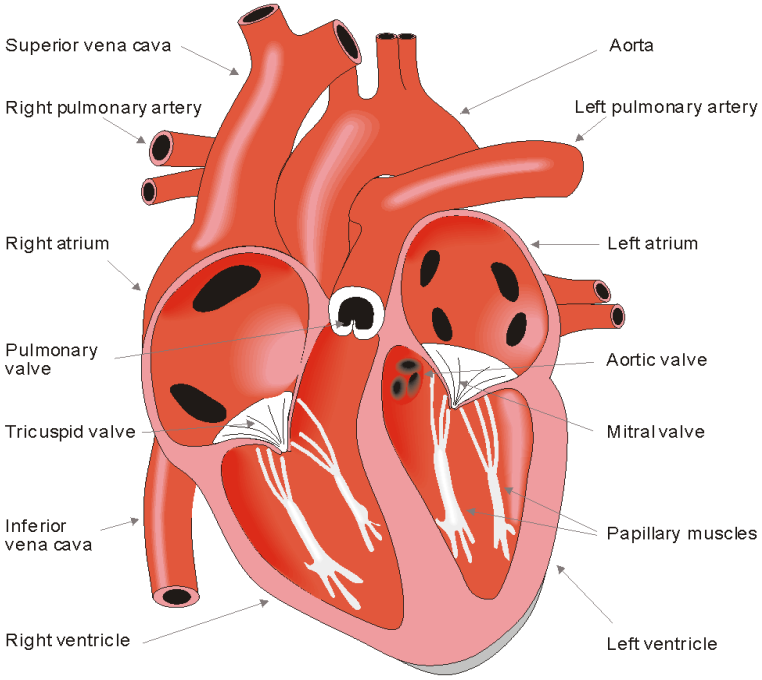

Figure 2.1 – Anatomy of the heart (Malmivuo and Plonsey 1995).
Frontal section of the heart, the most important elements of heart anatomy are depicted.

The efficiency of the mechanical activity of the heart is closely related to the synchrony of the muscle fibers when they contract. This synchronization is provided by the cardiac electrical activity. The electrical stimulation triggering cardiac contraction is spontaneously generated in a structure that works as the natural pacemaker of the heart and it is placed in the upper wall of the right atrium, the sinoatrial (SA) node. The stimulus spreads throughout the atria to reach the atrioventricular (AV) node, in this tissue at the bottom of the right atrium the signal undergoes a delay due to the slow conduction velocity, and the reflection on the mechanical behavior is a delay which sufficies to fill the ventricles with blood. After the delay, the electrical activation spreads into the bundle of His, which is divided into two branches located within the interventricular septum and which lead to Purkinje fibers. These are very thick fibers which allow a very rapid spread causing an almost simultaneous contraction of the entire ventricle. In the following sections, the principles of these electrical signals, known as action potentials (AP), will be detailed.

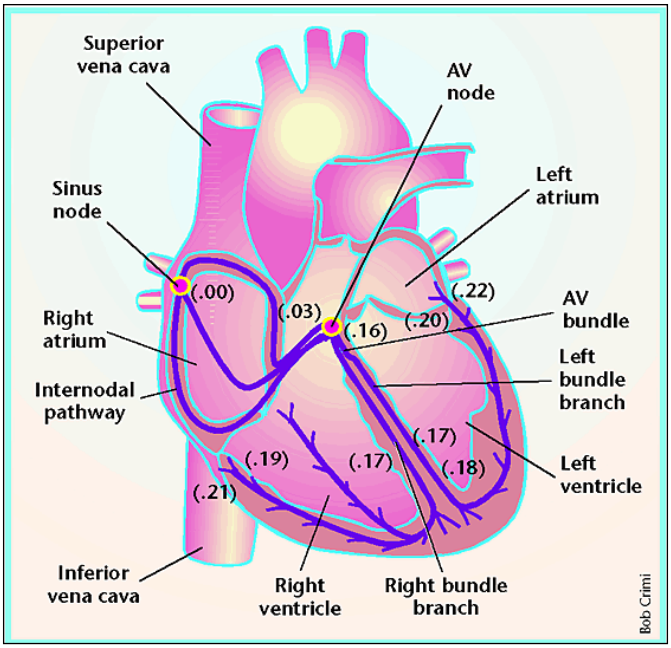

Figure 2.2 – Intrinsic electrical spread in the heart (Robbins and Dorn 2000). *The figure shows that the origin is in the sinus node (00), the rest of time references in seconds correspond to the description given.*

2.1.2. Atrial anatomy

The atria are two cavities with an irregular rounded shape (Figure 2.3), approximately spherical the right atrium (RA), more oval the left atrium (LA). The primary function of the walls of the atria is to receive the blood from the veins, thus, atrial walls are much thinner than those of the ventricles.

The atrial septum is constituted by a fibrotic tissue, except for a thin middle portion called fossa ovalis (FO), which it is formed by two serous membranes lining the atria and circumscribing the FO ring. The perimeter of the atrioventricular orifices is also formed by fibrotic tissues that support the valves. Both atria have a volume of tissue with closed bottom that extends over the front of the heart, surrounding the origin of the aorta and the pulmonary artery, the left and right atrial appendages (LAA and RAA).

The right atrium in its upper part near the septum has two large holes not provided with valves corresponding to the mouth of superior and inferior vena cava (VC) respectively. The bottom of the right atrium is almost entirely occupied by a large hole on which the tricuspid valve is located; between its posterior margin and the mouth of the inferior vena cava, there is the mouth of the coronary sinus, which discharges blood from the coronary system circulation.

The left atrium presents, in its rear–posterior portion, the mouths of the pulmonary veins (PV), two of them on the right near the septum, two of them on the left in the lateral portion of the atrium. The bottom is almost entirely occupied by the atrioventricular orifice, on which the mitral or bicuspid valve is located.

Electrical conduction paths are defined by the orientation of the muscle fibers and bundles and connections between both atria. Anatomical studies both on humans and animals suggest that atrial muscle bundles as Bachmann's bundle ***(Wang 1995, Bachmann 1916)*** and an interatrial bundle placed around the fossa ovalis ***(Spach 1985)*** are the preferred paths for electrical propagation between right and left atria. Some studies suggest the existence of other routes between the two atria as is the connection between the coronary sinus and the left atrial isthmus ***(Chauvin 2000, Antz 1998)***. Bachmann's bundle consists of muscle fibers which start from the roof of the right atria and reach the upper part of the wall of the left atrium ***(Lemery 2003)***. As the main conduction path between the atria, it plays a role in atrial conduction and atrial arrhythmias ***(Lemery 2007)***.

The longest and strongest bundle in the atria is located in the right atrium and it is known as crista terminalis. It starts at the anterior part of the septum and, after ascending to skirt the superior vena cava mouth, it goes down through the right atria free wall to end in the atrioventricular hole ***(Sanchez-Quintana 2002).***

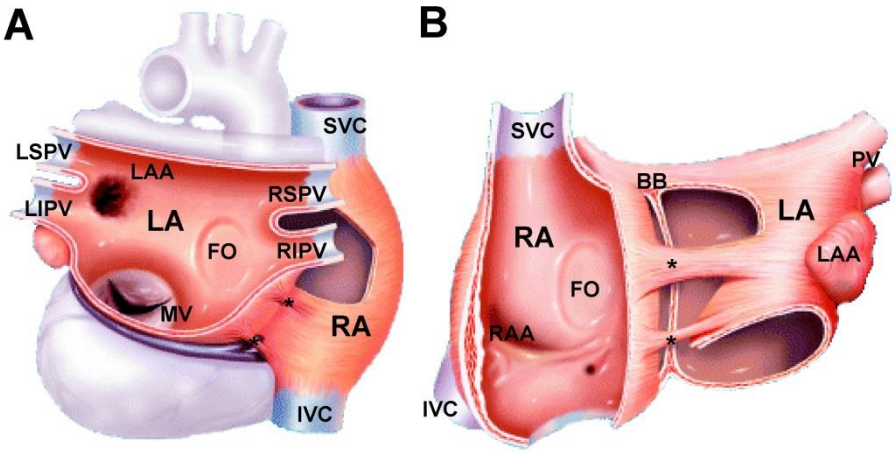

Figure 2.3 – Section views of the atria. Modified from (Olsson 2001).
Section views focusing on the left atrium (LA) in Panel A and in the right atrium (RA) in Panel B are depicted. Superior and inferor vena cava (VC), pulmonary veins (PV), left and right atrial appendages (AA), fosa ovalis (FO), mitral valve (MV), Bachmann's bundle (BB) and interatrial routes (*) can be found.

The inner walls of both atria show, especially in the more distal parts of the septum, the shape of muscle bundles arranged in parallel and called pectinate muscles. Thus, the left atrial walls are usually smooth and pectinate muscles are

exclusively in the appendage while in the right atrium both in the appendage and the right atrial free wall pectinate muscles are found. Pectinate muscles in the right atrial wall start from the crista terminalis forming a right angle, these fibers are divided into numerous branches in the lateral and posterior walls of the right atrium.

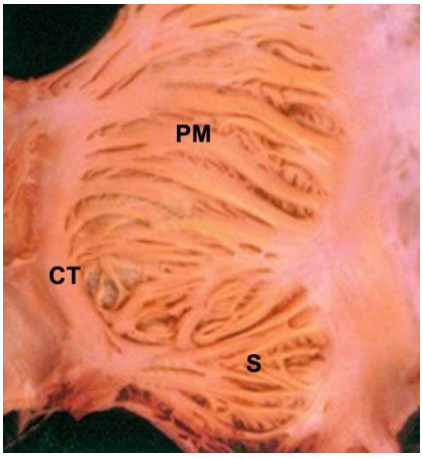

Figure 2.4 – Crista terminalis and pectinate muscles. Modified from (Sanchez-Quintana 2002).
Crista terminalis (CT) and pectinate muscles (PM) form a right angle. The septum (S) is placed in the bottom of the picture.

2.1.3. Action potential

As previously introduced in section 2.1.1, the mechanical efficiency of the heart is closely associated with its electrical behavior. Neurons and muscle cells are electrically excitable and therefore have the ability to spread electrical activity through the tissue. The electrical activity constitutes an oscillation of membrane potential known as action potential (AP). In the case of heart tissue, myocyte contraction is associated with AP, and more specifically to dephosphorylation of ATP in actin and myosin fibers due to an increase in intracellular calcium concentration ***(Malmivuo and Plonsey 1995, Bers 1993)***.

Membrane potential is defined as the electric potential difference between the intracellular and extracellular medium, which at the same time is defined by the concentration gradients between calcium (Ca^{2+}), potassium (K^{+}) and sodium (Na^{+}) ions, among others. As the cell membrane is impermeable to the passage of ions, ion channels, pumps and exchangers are responsible for the modulation of electrochemical fluxes ***(Malmivuo and Plonsey 1995, Jalife 2009)***. These are

proteins that are inserted into the membrane and allow specific and selective passage of ions between the two media, which modulates AP tracings.

Ion channels open and close in accordance with external stimuli. These stimuli are mainly associated to voltage or intracellular or extracellular chemical messengers known as ligands. The force affecting the ions promotes the flux across the cell membrane which is proportional to the difference between the membrane voltage and the equilibrium voltage, described by the Nernst equation ***(Malmivuo and Plonsey 1995)***.

The second ion transportation mechanism is known as active transportation and moves molecules across the cell membrane against their electrochemical gradient. That is why this process requires an energy input. Depending on the energy source these processes are divided into two groups: electrogenic pumps which use chemical energy, such as adenosine triphosphate (ATP) hydrolysis, to move ions against the ion concentrations and ion exchangers, which provide active transport by using another molecule that crosses the membrane by using the same protein structure but favoured by the electrochemical gradient. Cytoplasm subspaces also have an effect in the AP: the sarcoplasmic reticulum stores Ca^{2+} ions that stores and releases the ions during the AP reinforcing the excitation–contraction coupling ***(Courtemanche 1998)***.

In the absence of stimulation, the cells maintain a value of electronegative membrane potential (–60 to –90V) known as resting membrane potential (RMP). AP of atrial and ventricular cells is defined by five phases or parts that start from the RMP (see Figure 2.5). The different phases observed in the AP and main governing currents are described below:

The zero or fast depolarization phase is characterized by a steep rise to a positive voltage around 20mV (dV_m/dt= 393 V/s ***(Kleber and Rudy 2004)***). Na^+ leads this process in the same direction of the electrochemical gradient. After opening of Na^+ channels, many Na^+ ions enter the cell and then the channels close when reaching the equilibrium potential of Na^+ (about +30mV). This phase is essential when driving spread conditions ***(Jalife 2009)***.

Once Na^+ ions enter the cell, the partial repolarization phase promotes a rapid decrease in transmembrane potential due to the decrease in sodium influx and this activates transient potassium currents that eject potassium out of the cell.

The following phase is the longest. During phase 2 or plateau, the potential remains more or less constant around 0 mV. This phase is balanced by the voltage–dependent activation of I_{CaL} channels promoting Ca^{2+} influx and depolarization of the cell added to the repolarizing potassium currents (I_{Kr} e I_{Ks}).

In the third or repolarization phase, output potassium currents prevail and repolarize the cell to reach the RMP. This is due to deactivation of the calcium channel and an increased activity of currents (I_{Kr} and I_{Ks}) which together with the inward–rectifier current (I_{K1}) activation accelerates K^+ output and makes the potential more negative.

Finally, RMP is reached again. This phase involves I_{K1}, that is responsible for maintaining the resting potential near the equilibrium potential of K^+, and the sodium–potassium pump (I_{NaK}), that generates an ion current by expelling Na^+ and bringing in K^+ ions with a ratio of 3 to 2 respectively.

Once the AP has started, the membrane does not respond to a second stimulus until after a time interval called refractory period (RP) has passed. This period depends on the intensity of the second stimulus and the frequency at which the heart is beating. This feature allows at least partial relaxation from the previous contraction and provides a one–way propagation front electrical propagation ***(Jalife 2009)***.

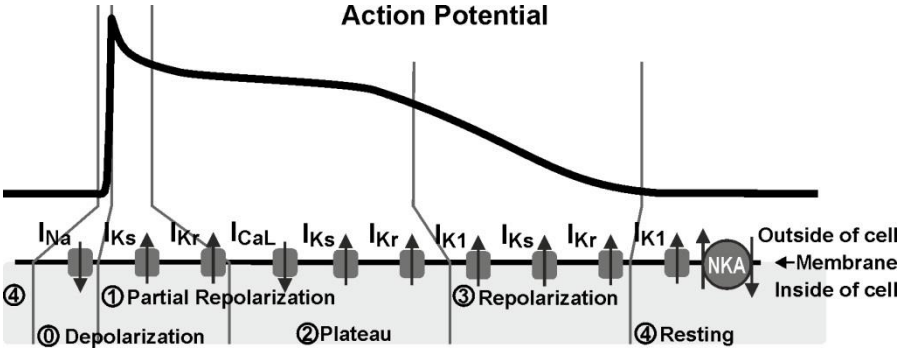

Figure 2.5 – Action Potential.
AP tracing on top and the most important ionic channels and pumps in each AP phase are depicted. Arrows show the direction of transportation of the ions.

Experimental data from animal studies show that both the morphology of APs and the levels of expression of ion channels differ depending on where the cell is located within the heart. It happens both in the atrium ***(Sarmast 2003)*** and in the ventricles ***(Qi 2015)***.

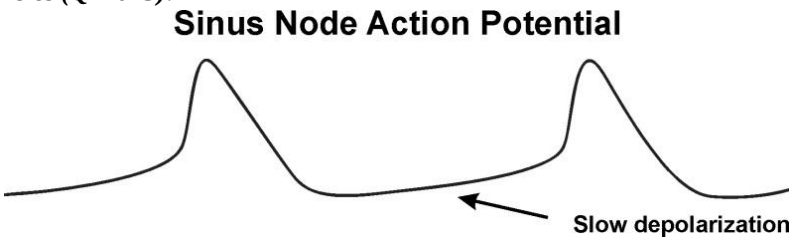

Figure 2.6 – Sinus node AP. Modified from (Jalife 2009).
Slow depolarization in phase 4 that promotes spontaneous depolarization can be observed.

Denote the cells located at the sinus and atrioventricular nodes and in the Purkinje fibers. These cells are capable of spontaneous (also called pacemaker) activity –meaning without any external stimulus–, this is because the potential in

these cells does not remain constant in stage four of the AP. Rather the opposite, there is a slow depolarization in this phase which when a threshold potential is reached triggers a new AP. Under normal conditions, the fastest spontaneous activity occurs in the sinus node acting as the heart pacemaker. On the contrary, Purkinje cells are the ones with the slowest spontaneous activity ***(Jalife 2009)***.

2.1.4. Action potential propagation

In the myocardium, neighboring cells are connected to each other through proteins that conform low resistance paths called gap junctions, these junctions allow the propagation of electrical impulses. The voltage gradient between the intracellular medium of an active cell with its neighboring cells at rest generates a current through the gap junctions. If the neighbor cell is not refractory, this current works as a stimulus and triggers depolarization by sodium entrance.

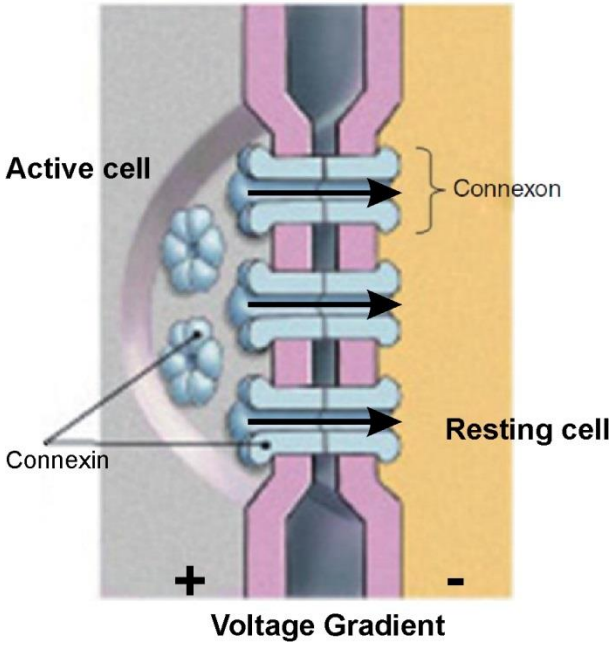

Figure 2.7 – Gap Junction. Modified from (Jalife 2009).
The voltage gradient promotes the flow of positive charges (depicted with arrows) that promote cell depolarization. Connexins and connexon are also shown.

Cardiac cells have an elongated shape and show high variability in length and diameter. They are distributed, depending on the muscle area, forming "brick stone" like patterns or in a more diffuse way. The concentration of gap junctions tends to be higher at the ends of the cells and much less on the sides, producing a strong anisotropy in conduction velocity in brick–stone–like structures. These are

the most powerful muscle fibers ***(Kleber and Rudy 2004)***, such as the crista terminalis or pectinate muscles in the atrium.

Gap junction channels are made up of two connexons, one from each of the adjacent cells. A connexon is composed of six subunits known as connexins. Connexin 43 is the most abundant in heart tissue and in many other organs, Connexin 40 and Connexin 45 are also important in the cardiac tissue. As the rest of ion channels, gap junctions are also regulated by voltage or ligands and can be blocked pharmacologically ***(Jalife 2009)***.

2.1.5. The surface electrocardiogram

Cardiac electrical activity can be monitored from the body surface by acquiring the electrocardiogram (ECG). This was first recorded in 1903 by Willem Einthoven using a galvanometer ***(Einthoven 1906)***. Since this discovery analysis of the ECG signals has been used to diagnose heart diseases noninvasively.

Willem Einthoven determined the standard ECG leads by placing 3 electrodes on the right arm, left arm and left foot respectively, electrode positions define a triangle with the heart in the center called Einthoven's triangle:

$$\begin{aligned} &\text{Lead I:} && DI = \phi_L - \phi_R \\ &\text{Lead II:} && DII = \phi_F - \phi_R \\ &\text{Lead III:} && DIII = \phi_F - \phi_L \end{aligned} \tag{2.1}$$

where

DI = the voltage of Lead I
DII = the voltage of Lead II
$DIII$ = the voltage of Lead III
ϕ_L = potential at the left arm
ϕ_R = potential at the right arm
ϕ_F = potential at the left foot

Goldberger introduced three additional leads by measuring the potential between a single electrode and the midpotential of the two remaining electrodes that is used as a reference. Due to the augmentation of the signal, these leads are known as augmented leads.

$$\begin{aligned} AVR &= \phi_R - \frac{\phi_L + \phi_F}{2} \\ AVL &= \phi_L - \frac{\phi_R + \phi_F}{2} \\ AVF &= \phi_F - \frac{\phi_R + \phi_L}{2} \end{aligned} \tag{2.2}$$

Notice that the augmented leads are fully redundant with respect to the Einthoven leads, and obtain the information from the projection of cardiac activity on a single plain defined by the three electrodes. Six more electrodes were placed

on the anterior and left side of the chest, defining the precordial leads labelled as V1, ... V6. As depicted in Figure 2.8, electrodes corresponding to V1 and V2 are located at the fourth intercostal space on the right and left side of the sternum respectively, V4 is in the fifth intercostal space at the midclavicular line; V3 between V2 and V4; V5 at the same horizontal level of V4 but on the anterior axillary line and V6 in line with V4 and V5 but in the midaxillary line. Precordial leads are measured referenced to the Wilson Central Terminal (WCT) which is defined as the center of Einthoven's triangle and is calculated as an average of the potential in the three electrodes:

$$V_{WCT} = \frac{\phi_R + \phi_L + \phi_F}{3} \tag{2.3}$$

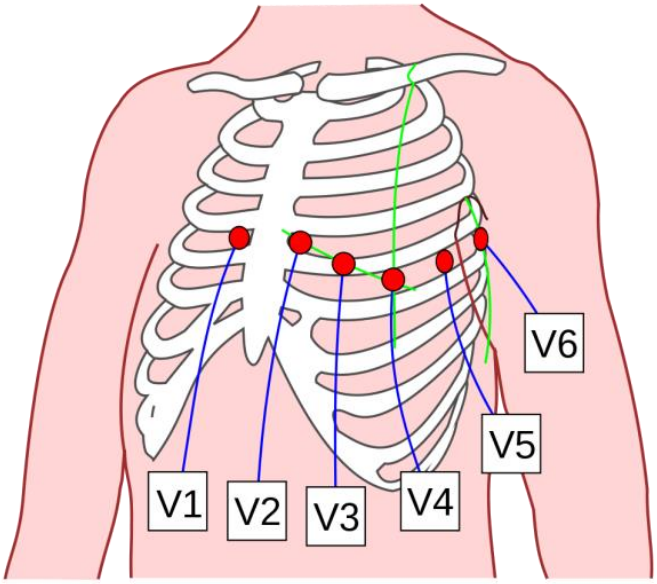

Figure 2.8 – Precordial leads in the torso. By Jmarchn [CC BY–SA].
Electrodes and its location on the rib cage, midaxillary and midclavicular lines are also depicted.

An ECG tracing shows several deflections or waves that reflect the electrical activity of heart chambers. At each time instant, the ECG represents a spatial summation of the APs active in the heart, a normal electrocardiogram is depicted in Figure 2.9. The so–called P wave corresponds to the depolarization in the atria, after the P wave the delay introduced by the AV node can be observed as an inactive period. Then, ventricular depolarization occurs and it is reflected in the QRS complex. Note that the amplitude of this complex is higher due to the bigger mass of the ventricles and the synchronization in which the ventricles contract,

thanks to that the bundle of His and Purkinje fibers allow a very rapid spread. The T wave corresponds to the ventricular repolarization or return to the resting state while the depolarization of the atria is masked by the QRS complex ***(Malmivuo and Plonsey 1995)***.

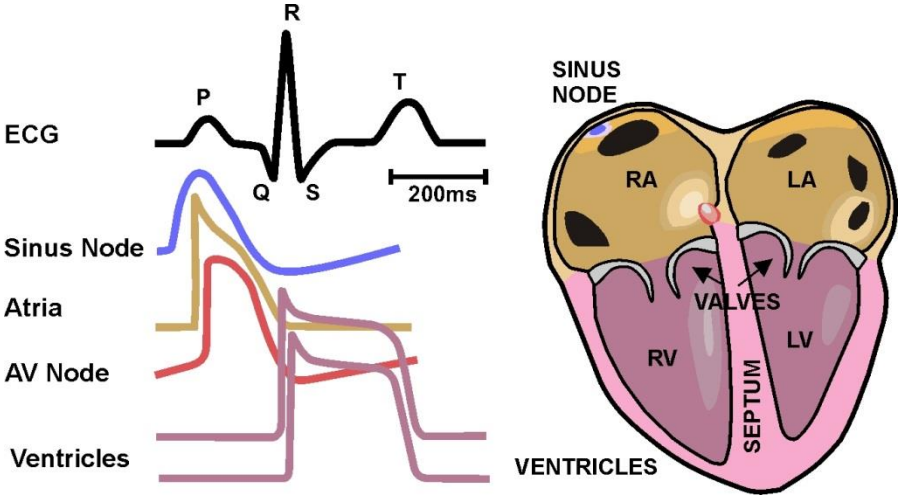

Figure 2.9 – Normal ECG tracing synthesis. From (Rodrigo 2014a)
ECG tracing in black and the APs responsible of each wave are depicted. Colors in APs correspond to those presented in the scheme of the heart. It can be observed how depolarization of atrial cells corresponds with the P wave, QRS complex and T wave correspond with depolarization and repolarization in the ventricles respectively.

2.1.6. Body Surface Potential Mapping

For a long time it was thought that 12–lead ECG was able to extract all the clinically relevant electrocardiographic information available on the torso. Frank ***(Frank 1954)*** affirmed that approximately 95 % of the QRS complex could be modeled as an equivalent single dipole with a fixed localization. This theory was refuted years later by Taccardi ***(Taccardi 1963)*** which showed that some pathologies show distributions in the torso with multiple maximum and minimum potential areas and therefore required several dipoles to obtain a correct model. This principle has been applied to diseases such as Brugada syndrome ***(Guillem 2010)*** and it is of special interest in diseases involving simultaneous wavefronts such as atrial fibrillation ***(Rodrigo 2014b, Guillem 2013, Guillem 2009b)***. In order to improve the noninvasive diagnosis of these complex diseases, the record of the electrocardiographic activity present in the whole surface of the torso was proposed.

Body Surface Potential Mapping (BSPM) is a technique that consists of the mapping of the potential in the whole torso surface in order to get more

information of the cardiac electrical activity than that provided by the conventional electrocardiogram. It allows the detection of phenomena that in the 12–lead ECG could not be detected ***(Taccardi 1998, Carley 2003, Finlay 2005)***. Therefore, the heart electric field is recorded on the entire surface of the torso with a number of electrodes that ranges between 32 and 256 ***(Hoekema 1999)***. Although there is no standard number of electrodes or location, most research groups tend to place more electrodes on the front of the torso as the potential variation at the front is significantly higher.

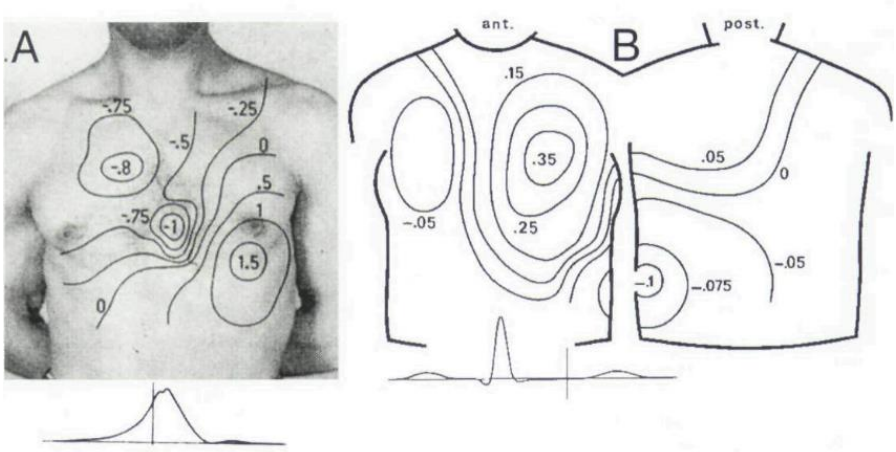

Figure 2.10 – Body surface potential maps. From Taccardi el al. (Taccardi 1998) *Panel A shows a normal BSPM after 30ms of QRS onset. Panel B shows a map of a patient with angina, during de ST interval, an abnormal minimum can be observed in the left–posterior part of the torso, this area is not registered in the 12–lead ECG.*

Several studies showed an improved diagnosis by using BSPM. Bruns et al. ***(Bruns 2002)***, by analyzing the QRS integral and the gradient of the ST segment in BSPM recordings elucidated that upper right precordial leads allowed an improved detection of ECG markers of Brugada syndrome. Eckardt et al. ***(Eckardt 2002)*** proved that the presence of late potentials and ST segment elevation on BSPM recordings allowed the prediction of the inducibility of ventricular tachyarrhitmias in Brugada syndrome patients. Dubuc et al. ***(Dubuc 1993)*** used isopotential maps from BSPM recordings for the localization of accessory pathways in Wolf–Parkinson–White patients to guide catheter ablation. In the field of diagnosis of atrial arrhythmias, SippensGroenewegen et al. showed that the origin of focal tachycardias ***(SippensGroenewegen 1998)*** or the reentrant circuit during atrial flutter ***(SippensGroenewegen 2000)*** could be determined by analysis of BSPM maps. Guillem et al. introduced the wavefront propagation maps as a technique to summarize the electrical propagation pattern into a single map during atrial flutter ***(Guillem 2009a)*** and to characterize the organization degree during atrial

fibrillation ***(Guillem 2009b)***. Guillem et al. also showed that spatial gradients of activation frequency in human AF can be detected on BSPM recordings by computing the power spectral density of multiple surface leads ***(Guillem 2013)***, which cannot be accomplished by using the standard 12–lead ECG . Rodrigo et. al. ***(Rodrigo 2014b)*** introduced band–pass filtering and phase map analysis to distinguish atrial fibrillation episodes driven by the right atria from those driven from the left atria. These works show how many techniques for computing and displaying clinically relevant information obtained from BSP recordings have been developed, however the need for validation of these results in larger population hampers the introduction of BSPM into the clinical practice.

Nowadays, BSPM together with three–dimensional models of the torso and heart, obtained from segmentation of the computed tomography or magnetic resonance images, are being used to solve the inverse problem of the electrocardiography. This area of research is attracting great interest, as it would allow the display of information on myocardial models in a similar way to that of invasive catheterization techniques already introduced in clinical practice ***(Hocini 2015, Pedrón-Torrecilla 2013, Pedron-Torrecilla 2012, Haissaguerre 2013)***.

Therefore, it is expected that the inverse problem of electrocardiography will introduce BSPM recording procedures in the clinical practice resulting in a major development and validation of BSPM techniques.

2.2. Atrial tachyarrhythmias

As it has been presented, the mechanical activity of the heart is synchronized by its electrical activity. When the electrical activation of the heart does not follow the spread initiated from the sinus node that has previously been described at a rate of 60 to 100 beats per minute (the so–called sinus rhythm), the heart is suffering an episode of cardiac arrhythmia. Cardiac arrhythmias can be classified as ventricular arrhythmias or supraventricular arrhythmias, when they involve heart structures over the atrio–ventricular node. While some ventricular arrhythmias can be lethal, supraventricular arrhythmias decrease the quality of life of patients and are a major issue in terms of epidemiology in the developed countries.

2.2.1. Mechanisms

The mechanisms involved in the triggering and maintenance of atrial tachyarrhythmias are not completely understood. However, important improvements have been developed in describing basic mechanisms related to cardiac arrhythmias, being ectopic focci, reentrant activity and multiple wavelets the most discussed mechanisms from the early twentieth century.

Atrial tachyarrhythmias can be driven by groups of cells with enhanced pacemaker activity. As described, the sinoatrial node, the atrioventricular node and

His–Purkinje cells presents in phase four of the AP a slow depolarization that brings automaticity to these cells. The rest of cardiac cells do not present automatic activity, however abnormal automaticity can be adopted under pathological conditions, usually associated to inward Ca^{2+} currents in phase four. An enhanced activity in this phase, due to alterations in the ionic currents involved, can promote a variety of ectopic tachycardias ***(Jalife 2009)*** and for many authors it can be the source of atrial fibrillation activity especially in the pulmonary veins area ***(Haissaguerre 1998)***.

The second mechanism is the reentrant circuit. Under certain conditions it is possible that the spread initiated in a heartbeat is not extinguished and rotates around an area in repetitive cycles, either around an anatomical obstacle (anatomical reentry) or not (functional reentry) ***(Kleber and Rudy 2004)***.

Mayer ***(Mayer 1916)*** made the first experimental demonstration of reentry on jellyfish tissue. Making a premature stimulation on a muscle ring with an appropriate period promotes a unidirectional block and a single wave propagating in the opposite direction. The reentrant activity could be maintained for many days.

Mines ***(Mines 1913)*** reproduced Mayer's experiments in ring–like cardiac tissues and hypothesized about the responsibility of reentrant activity in cardiac tachyarrhythmias. He also defined as a basis of the initiation of reentrant activity the need of a unidirectional conduction block and described the relation between conduction velocity (*CV*), refractory period (*RP)* and the minimum length of the reentrant circuit or wavelength (*WL*).

$$WL = CV \cdot RP \tag{2.4}$$

In the case that the reentrant circuit was longer than *WL*, the excitable gap becomes longer and the reentry remains stable in terms of frequency. If the size of the circuit is approximately *WL*, the complexity increases and the reentry becomes irregular.

Thanks to the development of multielectrode mapping techniques it was possible to prove that the reentrant activity could be maintained without the need of an obstacle that defines a reentrant circuit ***(Allessie 1973, Allessie 1976, Allessie 1977)***. It is defined as a functional reentry and was hypothesized fifty years before by Garrey ***(Garrey 1924)***.

Allesie and co–workers defined the "leading circle" concept, the functional reentries are defined by the relation between the wavefront and the refractory tail, so the leading circuit was defined as "the smallest possible pathway in which the impulse can continue to circulate", and "in which the stimulating efficacy of the wavefront is just enough to excite the tissue ahead which is still in its relative refractory phase" ***(Allessie 1977)***.

The leading circle theory implied that inside the circle the tissue remains in a state of refractoriness, defining a functional obstacle. This theory prevailed for

approximately 20 years but became insufficient to explain the dynamics of atrial and ventricular fibrillation. The main limitation of the theory was that if the circle is not excitable there is no possibility of drifting or meandering of the center of the rotation, and high resolution recordings demonstrated the movement of reentrant activity especially in the case of heterogeneous substrates. The leading circle was replaced by the term rotor that was proposed as the most important organizing centre (or driver) of fibrillation. A 'spiral wave' is the wave of excitation promoted by a rotor in a two–dimensional tissue and consists in a spiral with increasing convex curvature toward the center of the reentry. A 'scroll wave' is the equivalent in a three–dimensional tissue, this mechanism is present in many systems of chemical, physical or biological origin ***(Jalife 2009, Jalife 2011, Kleber and Rudy 2004)***.

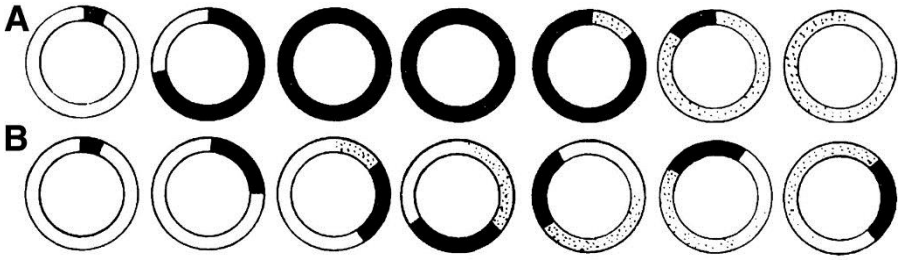

Figure 2.11 – Model of anatomical reentry. By (Mines 1913).
Excited and refractory tissue is depicted in black, white areas are completely excitable, and areas depicted with dots are relatively refractory. Both panels show a clockwise propagation as a block in the counterclockwise direction is supposed. In panel A λ is longer than the reentrant circuit and the wavefront collides with its own refractory tail so the reentry becomes extinct. Panel B shows an example where the reentry is maintained, the reentrant circuit is much longer than λ so the wavefront finds an excitable tissue.

Conduction velocity depends in part on the shape of the wavefront. Thus, while planar waves propagate faster than convex waves, in a spiral wave the wavefront becomes more convex towards the centre of the reentry, so, in the core, the curvature reaches a critical value that reduces the strength of the wavefront at the time of depolarizing by the activation of reaction ionic channels and electrotonic diffusion becomes more important in cell depolarization. It promotes an AP duration shortened in the core of the reentry. As both conduction velocity and refractory period varies from the center of the rotor towards the periphery of the spiral or scroll wave it makes the definition of wavelength inaccurate for characterizing functional reentries ***(Jalife 2011)***.

In a functional reentry the velocity and length also depends on the excitability of the partially refractory tissue and on the efficacy of the wavefront at the time of

depolarizing the tissue ahead. It is at the same time defined by the upstroke and amplitude of the AP and the passive properties of the tissue as it can be the gap–junctional connections ***(Kleber and Rudy 2004)***. It was also observed that functional reentries can appear in pairs rotating in opposite directions and defining "figure–8" or "double–loop" reentries. As described, the heart presents structures that determine the propagation of wavefronts, so anisotropic functional reentries are also observed due to the orientation of the myocardial fibers implied ***(Jalife 2009)***.

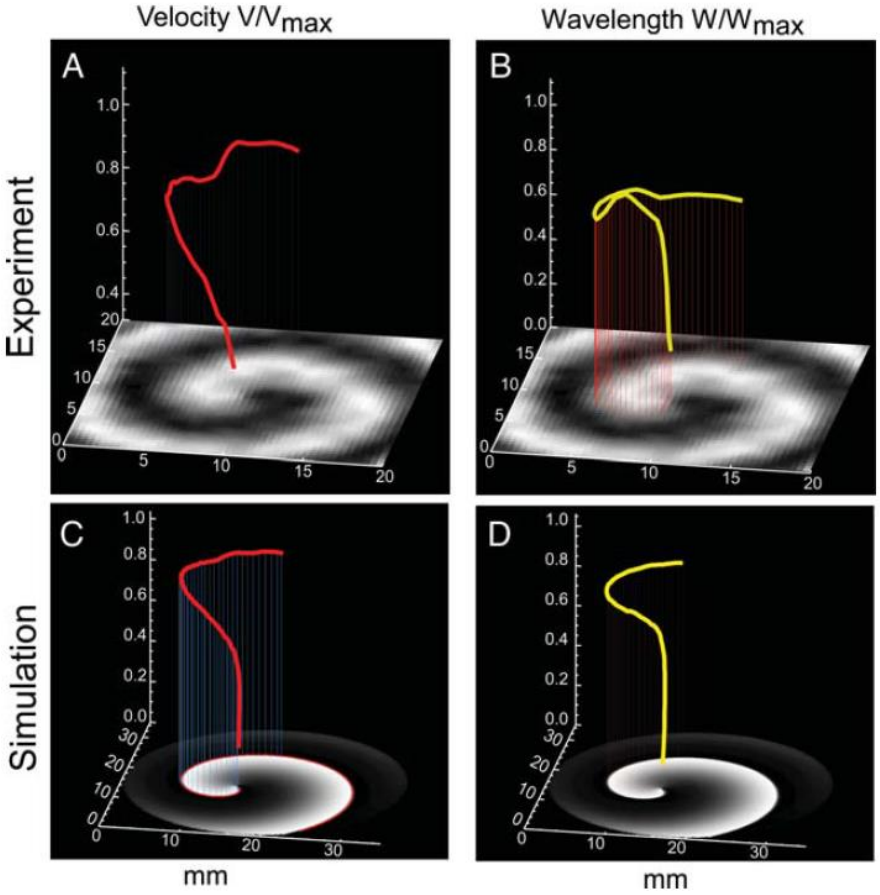

Figure 2.12 – Spiral wave and variation in conduction velocity and wavelength. By (Jalife 2011).

Spiral waves in both experimental and in–silico recordings are presented, conduction velocity and wavelength increases from the core of the reentry towards the periphery of the spiral wave.

Another important theory regarding fibrillation was formulated by Gordon Moe. He argued that during these episodes cardiac activity was totally disorganized

and defined the arrhythmia as the result of 'randomly wandering wave fronts, ever changing in number and direction'***(Moe 1956)***. Later Moe and Abildskov presented that atrial fibrillation propagation was independent of its initiation and that inhomogeneous depolarization was essential for the maintenance of the arrhythmia ***(Moe and Abildskov 1959)***. 'Multiple wavelet' was proposed by Moe and hypothesized that randomness in time and space of tissue properties played important roles in atrial fibrillation ***(Moe 1962)***. Then, mapping studies in animals and humans gave additional support to this theory due to the complexity of the recordings obtained and especially due to the good results of the surgical MAZE procedure that consists in the compartmentation of the atria hindering the sustainability of multiple wavelets ***(Cox 1991a, Jalife 2011)***. However, this theory implies randomness and it is not what it happens in fibrillation were hierarchical distribution in terms of dominant frequencies can be observed both in animals and humans. Furthermore, it has been demonstrated the ability to cease fibrillation by removing or isolating high frequency sources, it made multiple wavelet theory less relevant in recent years ***(Guillem 2013, Atienza 2006, Mansour 2001, Sanders 2005)***.

2.2.2. Atrial flutter

Atrial flutter (AFL) is a high frequency tachycardia (240–350 bpm), that shows a continuous oscillation in the ECG. The maintenance mechanism of the arrhythmia is macroreentry around obstacles constituted by anatomical structures (valvular or venous orifices), scars or areas of functional block ***(Garcia-Cosio 2012)***.

Typical AFL is known for its dependence on the anatomical structure of the right atrium, being the tricuspid valve the obstacle around which the reentry is maintained. In 90% of cases the reentry is counterclockwise, descending through the right atrium free wall and ascending through the septal wall. On the contrary, atypical AFL refers to the set of macroreentrant tachycardias which cannot be classified as typical AFL ***(Garcia-Cosio 2012, Saoudi 2001, Cosio 2003)***.

Typical AFL ECG is characterized by complex undulation in the lower leads and, in the case of counterclockwise typical AFL positive deflections in V1, while in the case of counterclockwise typical AFL W like waveforms can be recorded in V1 . In the case of atypical AFL ECG leads differ from those observed in typical flutter and the localization of the reentries circuit needs from invasive electrophysiological studies ***(Garcia-Cosio 2012)***.

Radiofrequency ablation of some segment of the reentrant circuit is the most effective therapy of AFL. In the case of typical AFL cavotricuspid isthmus ablation is performed since this is the narrowest segment of the reentrant circuit. In the case of atypical flutter an electrophysiology study is needed to locate the best area to ablate ***(Morady 1999)***.

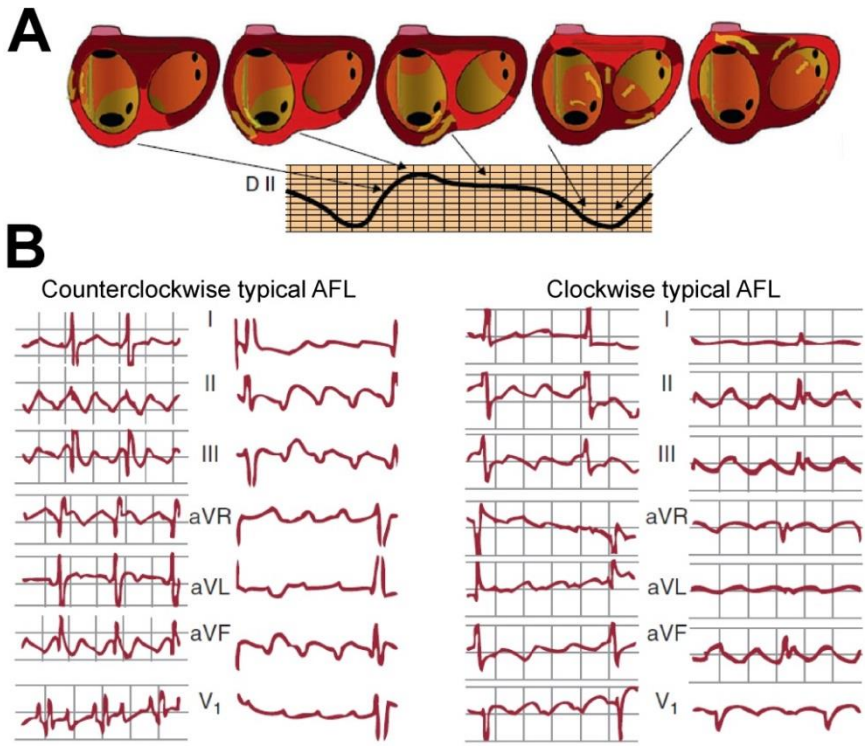

Figure 2.13 – Typical atrial flutter. Modified from (Garcia-Cosio 2012).
Panel A shows an schematic representation of the reentrant circuit during counterclockwise typical atrial flutter with an ascending propagation in the septum followed by a descending propagation in the right atrium free wall, the complex wave that can be observed in inferior lead II is also presented. Panel B shows examples of counterclockwise and clockwise typical AFL registers. Complex waves in inferior leads II, III and aVF can be observed in all patients, V1 presents positive deflections in counterclockwise typical AFL patients while W like waveforms can be observed in clockwise examples.

2.2.3. Atrial fibrillation

Atrial fibrillation (AF) is the most prevalent cardiac arrhythmia ***(Haissaguerre 2000, Pedersen 2006)*** and is characterized by a chaotic activation of the atrial cells that results in an inefficient blood emptying of these cavities that increases the risk of embolism due to blood coagulation.

During atrial fibrillation cells depolarize at very high frequencies that can reach 400 to 600 beats per minute. Atrioventricular node filters the number of electrical wavefronts and reduces the number of propagations to the ventricles allowing patients to survive. Nevertheless, the ventricular rate does not match with the sinus rhythm and, therefore, does not adapt to the needs of the patient in each

moment resulting in irregular ventricular depolarization ***(Nattel 2002, Climent 2011)***.

The mechanisms responsible for the initiation and maintenance of AF are not completely understood and are still a topic of discussion since the early twentieth century. As described before, ectopic focci, reentrant activity represented by rotors and multiple wavelets, have focused efforts by many researchers throughout this period at the time of explaining AF. While multiple wavelets theory tries to explain the atrial irregular activity itself as a chaotic behavior ***(Moe 1962, Jalife 2011)***, rotors and ectopic focci are supposed to be high frequency drivers that promote turbulent propagations due to the variability in refractoriness present in the fibrillary substrate ***(Nattel 2002)***.

As described the evidence of a hierarchical distribution in terms of dominant frequency during AF episodes, has led the scientific community to defend that the initiation and maintenance of AF need a driver (rotor or ectopic focus) or a variable number of drivers and a substrate that promotes a turbulent propagation through the atrium ***(Jalife 2011, Climent 2015b)***.

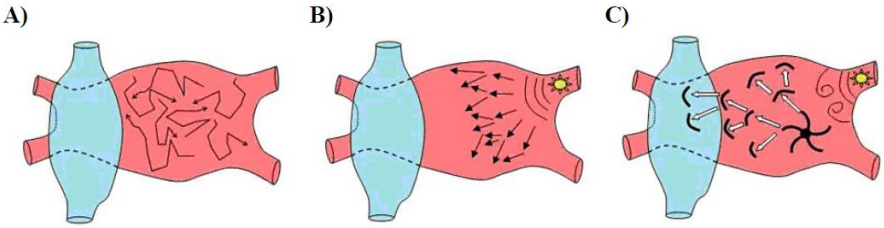

Figure 2.14– Maintenance mechanisms of AF. Modified from (Atienza 2006). *Multiple wavelet (A), ectopic focci (B) and rotor (C) theories are depicted.*

While by treating paroxysmal AF the isolation of these drivers can be sufficient to terminate the arrhythmia ***(Atienza 2009, Narayan 2012)***, in the case of patients suffering of persistent AF, removing these sources is less effective ***(Atienza 2009)***. This is in part due to the strong electrical and structural alterations in the atrial tissue known as remodeling. Electrical remodeling consists in changes in AP biomarkers being the most important the shortening of AP duration and the effective refractory period, while structural remodeling includes increased fibrosis, cell and chamber dilatation ***(Doessel 2012, Climent 2015b)*** and even an increment in the endo–epicardial decoupling and perpendicularity ***(Maesen 2013)***. Tissue remodeling is caused by long periods of sustained AF or other cardiovascular diseases, and results in a tissue with a heterogeneously reduced conduction velocity and AP duration, which results in a reduced wavelength that favors the maintenance of AF.

Experimental and numerical methods have suggested that electrical remodeling is mainly based on an increased activity of the inward–rectified current (I_{K1}) and a decreased expression of the inward L–type Ca^{2+} current (I_{CaL}) ***(Tobon 2008, Zhang 2009, Koivumaki 2014, Climent 2015b)***. Structural remodeling implies a disconnection between cells and a reduction of gap junctions which results in a decreased tissue conductivity ***(Zhang 2009)***. Recordings in animals and humans suggest that the more remodeled the tissue is, the more complex the fibrillatory activity, patients suffering of persistent AF present faster activation rates and a more turbulent propagation or increased number of wave fronts ***(Allessie 2010, Climent 2015b)***.

2.2.4. Clinical treatment of atrial fibrillation

Electrical cardioversion is one of the therapies used to terminate AF by applying controlled electrical impulses, which synchronize the electrical activity of the atria. However, this technique does not supress the cause of AF, making AF episodes to be repetitive in time. When intending to eliminate or inhibit the causes of the arrhythmia pharmacological or radiofrequency ablation treatments are used. AF treatments tend to combine both types of treatments to reinforce the results:

Antiarrhythmic drugs

Pharmacological therapy is the most common methodology in reducing AF episodes or its symptoms. The main objectives of these drugs are preventing arrhythmia episodes, controlling cardiac frequency –sinus and atrioventricular nodes–, anticoagulating blood or performing chemical cardioversion.

Antiarrhythmic drugs are classified depending on the receptor or ionic mechanisms affected, note that antiarrhythmic drugs can have an effect in many ionic currents at the same time despite having a prevalent effect in some ion channels. According to Vaughan–Williams classification, the following families of antiarrhythmic drugs are distinguished ***(Vaughan Williams 1984, Nattel and Singh 1999)***:

- Class I: Have an important effect in Na^+ channels and are classified in three subclasses depending on the effect in AP duration. These drugs reduce excitability of cells, and are for this reason called Membrane Stabilizing agents.
  - Class Ia: These drugs slow phase zero and results in a retardation of the repolarization and an increment of effective refractory period.
  - Class Ib: These antiarrhythmic agent have an important effect in Na^+ channels at high but not in low frequencies at the time of slowing phase zero. However, in this case this effect is attached with a reduction of AP duration and effective refractory period.

  - Class Ic: It also have an effect on Na^+ channelsbut in this case do not alter the repolarization phase.
- Class II: or β–blockers, block the sympathetic activity of the heart and are used to reduce the number of propagations through the atrioventricular node in the case of supraventricular tachyarrhythmias.
- Class III: These drugs block potassium channels resulting in an elongation of action potential duration and effective refractory period. As Na^+ channels are not affected they hinder the maintenance of reentrant tachyarrhithmias.
- Class IV: These drugs block of I_{CaL} channels and are usually used to reduce the number of propagations trough the atrioventricular node. These drugs have the inconvenient of reducing heart contractility but allow the control of heart rate which is reduced by β–blockers.

However, since antiarrhythmic drugs do not affect only the atria, they have important side effects which increase mortality rates ***(Nattel 1998, Nattel 2002, Calkins 2009)***.

Radiofrequency ablation

Radiofrequency ablation is an invasive therapy which damages the area of the atria causing the arrhythmia and, therefore, eliminates the source of the AF ***(Fuster 2006, Calkins 2009)***. The identification and location of this source is an essential goal to achieve before the ablation of this source. Haissaguerre identified the pulmonary veins as the most frequent location of drivers of AF ***(Jais 1997, Haissaguerre 1998)***, it resulted in a revolution for the clinical treatment of AF, as pulmonary vein isolation became a gold standard in the clinical practice ***(Jalife 2011)***, with success rates of 70% in patients with paroxysmal AF and 22% in patients with persistent AF ***(Oral 2002)***. However, AF sources have been detected in other regions of the atria such as the superior vena cava, left posterior free wall, crista terminalis or the coronary sinus ***(Jais 1997, Haissaguerre 1998)***. Consequently, different strategies based on an electrogram–guided identification of the specific primary AF drivers can be performed in order to increase the success ratios or to reduce the damaged area ***(Calkins 2009)***, in this context the ablation of complex fractionated atrial electrogram (CFAE) areas or highest dominant frequency areas have been evaluated.

CFAE ablation is justified on the assumption that primary AF sources promote fractionated and complex electrograms. However, while some authors support that AF termination by targeting CFAE areas had success for the 95% of patients ***(Nademanee 2004)***, other authors achieved a success rate of only 57% for the same conditions ***(Oral 2007)***. Other authors tried to isolate the regions with faster electrical activity ***(Berenfeld 2000, Mansour 2001, Sanders 2005, Atienza 2006, Atienza 2009)***. Atienza et al. also showed that the ablation success in patients without frequency gradients was very low, corresponding in most cases

with patients with persistent AF ***(Atienza 2009)***, suggesting that in some cases ablation therapies should be avoided.

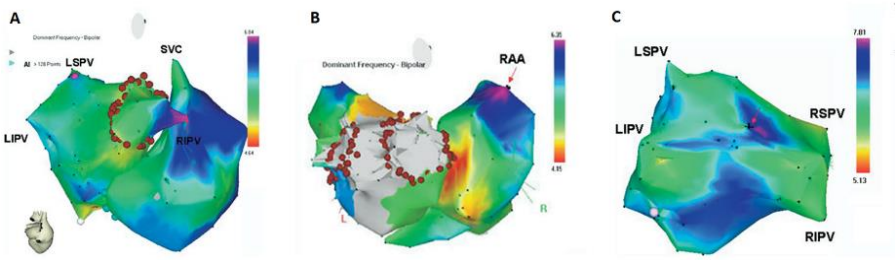

Figure 2.15 – Dominant frequency maps in three AF patients. By (Atienza 2009) *Panel A shows a dominant frequency map for a patient of paroxysmal AF that presented a high dominant region in the right superior pulmonary vein. The fibrillation ended after the isolation of this area with the ablation points depicted in red. Panel B shows a patient with paroxysmal AF. Here the highest dominant frequency was present in the right atria appenddage. Panel C shows a patient with persistent AF with no frequency gradient. The ablation procedure could not stop the arrhythmia.*

Prior to these research works, the initial theories about multiple wavelet or leading circle, led to the introduction of MAZE with the aim of hinder the maintenance of reentrant activity or the propagation of the different wavefronts. At the same time these procedures ensure the propagation between the sinus and the atrioventricular nodes. Different MAZE patterns had been established with the aim of reducing the injured areas of the atria and maintaining sinus rhythm ***(Cox 1991b, Cox 1991a, Cox 1993, Cox 1995, Cox 2000)***.

2.3. Human atria modeling

In the last decades, cardiac modeling has become a tool that contributed to improve the understanding of atrial physiology and pathophysiology. Mathematical modeling allows the access and control of variables that are not available in experimental or clinical research and at the same time reduces costs and avoids technical and ethical problems.

In–silico atrial modeling covers the chain ion–channel, cell, tissue, atrial anatomy and computation of electrocardiograms. Deep research is being conducted with the aim of assessing physiological alterations related mainly with AF.

2.3.1. Action potential modeling

The first AP mathematical model was designed by Hodgkin and Huxley in the 50s ***(Hodgkin and Huxley 1952)***. It was based in experimental data from voltage clamp applied to squid giant axons, and constituted the basis of the most of electrophysiological models that have been developed since that time. In general, the models based on Hodgkin–Huxley formulation are based on the equivalent circuit of a system defined by the membrane and the intra and extracellular mediums as presented in Figure 2.16.

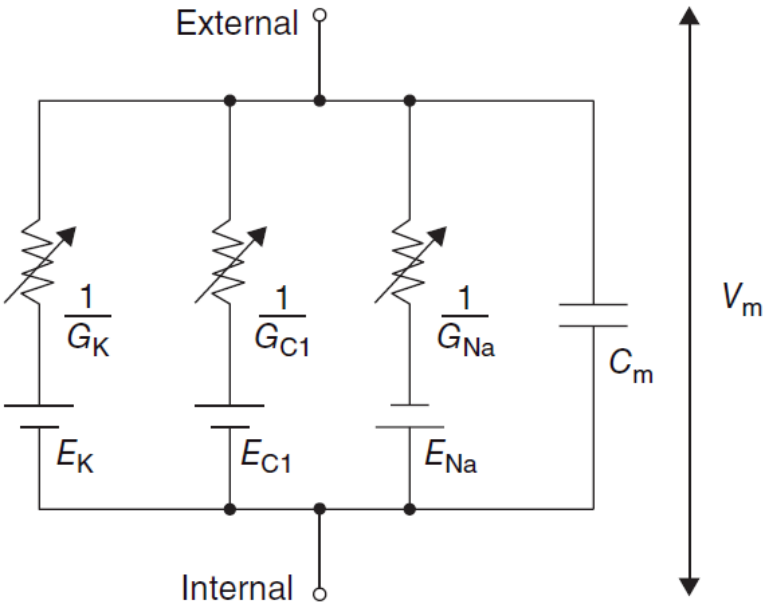

Figure 2.16 – Electric model of a cardiac cell. From (Jalife 2009).
Membrane voltage Vm depends on the charge of the membrane capacitor Cm which is modulated by the ionic channels (modelled as variable resistors or conductances) controlling the different ionic currents.

In the diagram, internal and external mediums are represented and the lipid membrane is presented as a capacitor C_m, the membrane potential (V_m) is the variable which plots APs. The variables that modulate AP shape are ion channels, and it can be opened, closed or inactive depending on different conditions associated with voltage, time or chemical messengers. Electrically, all this activity can be summarized as variable resistors and Ohm's law can be used to define the magnitude of the current circulating in each group of channels, which depends at the same time of the equilibrium potential for each ion:

$$I_x = (V_m - E_x) \cdot G_x \tag{2.5}$$

The currents associated to each group of channels, pumps or ion exchangers are summarized in the resulting current I_{ion} which charges or discharges the capacitor modulating V_m.

$$\frac{\partial V_m}{\partial t} = -\frac{I_{ion}}{C_m} \quad being \quad I_{ion} = \sum_{x=1}^{n} I_x \tag{2.6}$$

Voltage clamp experiments in cardiac cells have demonstrated that cardiac AP presented a higher complexity as compared to squid neurons and required the introduction of additional ionic currents. Denis Noble designed the first models of cardiac myocytes by modifying the Hodgkin–Huxley equations ***(Noble 1962)***. McAllister introduced some repolarizing potassium currents to the Purkinje fibers cells ***(McAllister 1975)***. After that, different models for ventricular cells were also developed ***(Beeler and Reuter 1977)*** and the effect of ionic pumps and exchangers together with some changes in ionic concentrations were introduced ***(Difrancesco and Noble 1985)***. These improvements together with others resulted in the detailed model of mammalian ventricular myocytes by Luo and Rudy ***(Luo and Rudy 1991, Luo and Rudy 1994)***. Regarding to models of human ventricular myocytes, Iyer and ten Tusscher introduced important specific models ***(Iyer 2004, ten Tusscher 2004)***.

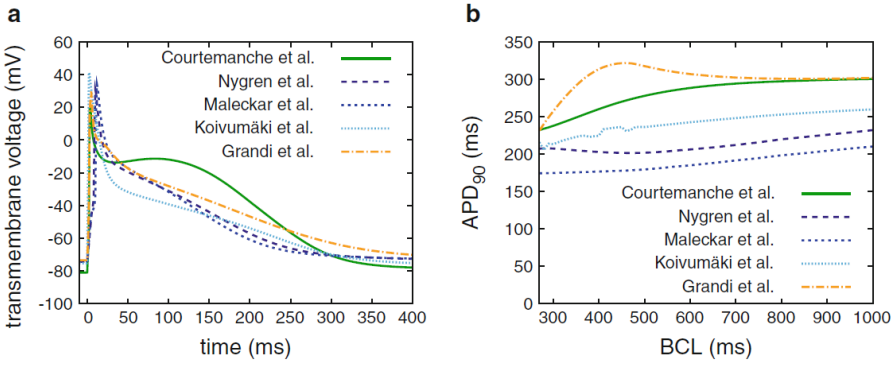

Figure 2.17 – Action potentials and APD90 restitution curves of the different models of human atrial electrophysiology. From (Doessel 2012).

Despite the greater effort in developing ventricular mathematical cell models, big efforts have been invested in the developing of atrial electrophysiological models. Two models of human atrial electrophysiology published in 1998 accelerated the development of atrial modeling: Courtemanche ***(Courtemanche 1998)*** and Nygren ***(Nygren 1998)*** models are based in the same experimental data obtained from humans. However, they present some differences which are evident in AP shape, as it can be observed in Figure 2.17. The Courtemanche model shows an spike–and–dome morphology while the Nygren model shows a more triangular shape. Another important difference is present in the restitution curves for both models, at long basic cycle lengths (BCLs) the Nygren model presents shorter AP

durations at 90% of repolarization (APD90), and APD90 also decreases towards BCL of 470 ms and then increases again at shorter BCL.

These limitations were reduced by Maleckar et al. who improved the Nygren model focusing on rate dependence properties and the reformulation of repolarizing currents ***(Maleckar 2008)***. Also based in the work of Nygren and Maleckar, Koivumaki added a more detailed formulation of the sarcoplasmic reticulum and Ca^{2+} dynamics ***(Koivumaki 2011)***. In this case restitution curves are more similar to those presented by Courtemanche but with shorter APD90s. Finally Grandi presented a model of human atrial cells but in this case modified from a ventricular model of the same group ***(Grandi 2011)***. This model also aims to improve the simulation of intracellular Ca^{2+} dynamics, the AP shape of Grandi model also resembles to that of Nygren, but the APDs are more similar to that presented by Courtemanche, however this model presented long APD90s when BCL was reduced.

Electrical remodeling has been implemented in cell models of atrial electrophysiology. As presented before, electrical remodeling results in a reduction of AP duration and effective refractory period which contributes to the reduction of the wavelength easing the initiation and maintenance of AF. In order to implement the remodeling in atrial cells, in the bibliography the electrical conductances associated to the L–type Ca^{2+} current (I_{CaL}), the transient outward current (I_{to}) and the ultra–rapid delayed K^+ current (I_{Kur}) have been decreased and the inward rectified K^+ current (I_{K1}) has been increased ***(Doessel 2012, Skasa 2001, Workman 2001, VanWagoner 1997, Bosch 1999, Van Wagoner 1999, Brandt 2000, Grammer 2000, Dobrev 2001, Brundel 2001, Christ 2004, Gaborit 2005, Voigt 2009, Caballero 2010)***. The alterations affecting I_{CaL} and I_{K1} were the most important at the time of altering AP shape ***(Koivumaki 2014)***. Besides, it has been shown that a reduced Ca^{2+} handling, which corresponds with lower intracellular Ca^{2+} transients, resulted in a reduction of cell contractility, another characteristic property of remodeled cells ***(Schotten 2001)***.

Rapid and slow delayed rectifiers I_{Kr} and I_{Ks} have also been evaluated as agents involved in AF electrical remodeling. However, contradictory results have been presented, Caballero presented data from human atrium that indicates that I_{Kr} and I_{Ks} are overexpressed in cAF substrates ***(Caballero 2010)***, while decreased or no–change activity is defended by other authors ***(Brundel 2001)***. Other authors evaluated the effect of a K^+ activated Ca^{2+} current, but also presented contradictory results ***(Li 2011, Yu 2012)***.

Changes associated to AF remodeling in the mechanisms of regulating Ca^{2+} handling in the sarcoplasmic reticulum were also evaluated, it was observed that althought having a minor impact on Ca^{2+} signals, restoration of sarcoplasmic reticulum handling, which is decreased in AF may result in a therapeutic option ***(El-Armouche 2006, Shanmugam 2011, Koivumaki 2014)***. Finally, the dilation of atrial cells during AF which results in an increment in the membrane capacitance

has been also documented and simulated ***(Schotten 2002, Corradi 2012, Koivumaki 2014)***.

2.3.2. Tissue level modeling

The AP propagates through the tissue due to depolarizing local current that flow from the depolarized cells to their neighboring myocytes in phase four through gap junctional channels. This current raises the membrane potential and it results in the opening of Na^+ channels which initiates a new action potential.

This behavior is modeled as a continuous excitable medium, with diffusion and local excitation of the membrane voltage, known as reaction–diffusion model. It describes the simplest description of action potential propagation, the monodomain model:

$$\frac{\partial V_m}{\partial t} = -\frac{I_{ion}}{C_m} + \nabla \cdot D\nabla V_m \tag{2.7}$$

As it can be observed the first part of the equation corresponds with 2.6 and summarizes the reaction part of the equation while the first part of the equation implements the diffusion part. ∇ is the gradient operator and D the diffusion coefficient with units m^2/s that describes de efficiency in diffusion of voltage through gap junctional channels. When anisotropy is implemented D is a tensor which depends on the fiber orientation.

As presented above, the transmembrane voltage is the difference between intracellular and extracellular potentials. In contrast with the monodomain model, the bidomain model considers the variation in ionic concentrations and potential in the extracellular space, however the resulting system of equations is much more difficult and increases computational costs. As the monodomain model reproduces the most of the phenomena related with wave propagation, it is the most commonly used ***(Clayton and Panfilov 2008, Doessel 2012)***, however these models cannot address the variations of the extracellular domain such as current injections in defibrillation by electrical cardioversion ***(Trayanova 2006)***.

Many studies have used tissue simulations to evaluate the mechanisms associated with wavefront propagation or rotor dynamics in order to elucidate the mechanisms underlying functional reentries, and the ionic currents involved ***(Pandit 2005, Clayton and Panfilov 2008, Seemann 2010, Sanchez 2012)***.

2.3.3. Geometrical models

The reaction–diffusion formulation allowed development of atrial geometric models. On the one hand, accurate models of some atrial structures –right atrial appendage, crista terminalis...– have been developed ***(Ellis 2000, Zhao 2009)*** and on the other hand, three–dimensional models of the whole human atria have been implemented.

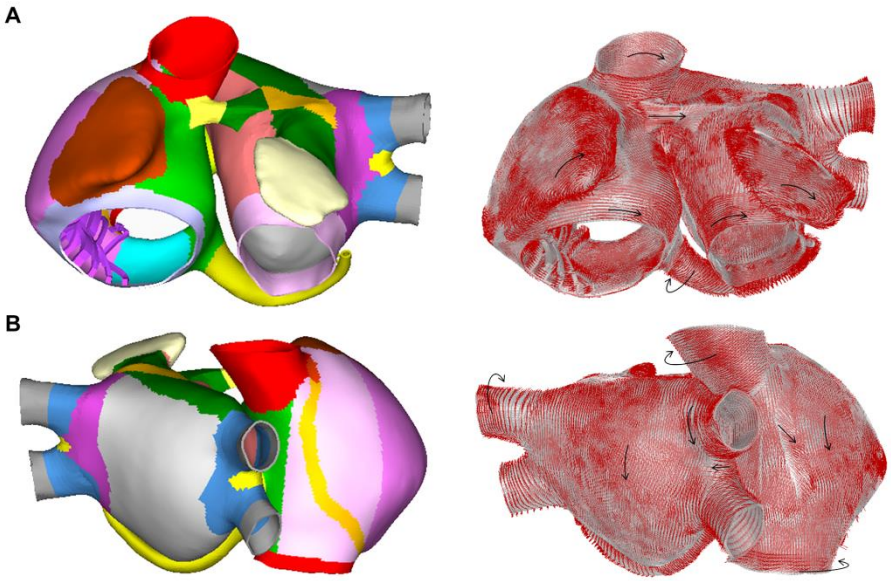

Figure 2.18 – Three dimensional atria model. By (Tobon 2013).
The model is divided in 42 areas depending on the atrial structure and the atrial bundles (left)and fiber orientation is defined by the red lines (right).

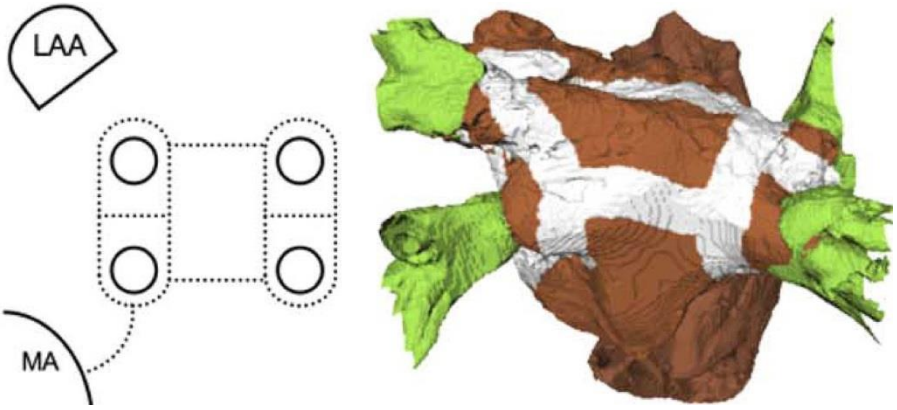

Figure 2.19 – Three dimensional atrial model and ablation strategies. By (Reumann 2008).
See the ablation strategy on the left which describes the isolation of the pulmonary veins and an ablation line from the pulmonary veins to the MA (LAA = Left atrial appendage and MA = Mitral valve Annulus). On the right, the implementation can be observed in the volumes: the volumes in green represent the pulmonary veins, the volumes in white represent the ablated areas and the brown volume is the rest of the atria.

Atria models can be both volumetric ***(Krueger 2011, Aslanidi 2011, Tobon 2013, Krueger 2013)*** or surface models ***(van Dam and van Oosterom 2003, Jacquemet 2006)***, both represent the three dimensional shape of atrial structures but surface models do not reproduce the thickness of atria walls. Another important difference between models is that they can be based on computer axial tomography ***(Burdumy 2012)*** or magnetic resonance ***(Virag 2002)*** images or constructed by using basic volumes as spheres or cylinders ***(Gray and Jalife 1998, Blanc 2001, Dokos 2007)***. Models usually present the most common atrial structure with four pulmonary veins and wall thicknesses in accordance with the literature because of the difficulty of measuring it in non–invasive images. Finally, models can implement anisotropic conduction properties in the most important bundles or atrial structures or not ***(Doessel 2012)***.

The role of anatomical structures in stabilizing macro reentrant tachyarrhythmias ***(Wu 1998)*** and the effect of these structures in atrial flutter reentrant patterns has been evaluated, it was presented the role of crista terminalis anisotropy when stabilizing typical, the role of tissue heterogeneity in the regularity of the reentry, which atrial flutter in atria showing the strong dependence on structural changes in AFL ***(Ellis 2000, Vigmond 2001, Tobon 2013)***.The distribution of reentrant drivers is altered due to the presence of obstacles, it was evaluated in different simulation works ***(Blanc 2001, Virag 2002)***. Depolarization alternants combined with anatomic structures were presented as the most common mechanism in the initiation of AF in another work ***(Virag 2002)***. Another important application of three–dimensional models is to design effective therapies focused on catheter ablation approaches by including ablation lines ***(Blanc 2001, Reumann 2008, Tobon 2010)*** or to evaluate the effect of gaps in ablation lines ***(Dang 2005)***.

2.3.4. GP–GPUs and CUDA in cardiac modeling

A realistic tissue or geometrical model requires thousands or even millions of cells. In addition, depending on the electrophysiological model chosen, each cell is modeled with 15–50 ordinary time–dependent differential equations (ODEs), which implies that the final number of coupled ODEs to be solved may be in the tens or hundreds of millions. With this computational charge the time required to obtain a simulation of a few seconds is in the range of hours or even days.

The development of cardiac modeling is highly dependent on the advances of software tools and computing platforms. In 1952, computing by hand only 8ms of electrical activity in a single cell took 8h to Andrew Huxley ***(Hodgkin and Huxley 1952, Noble 2012)***. Ever since that time, the development of computers, supercomputers and clusters has allowed a big progress in this area of research.

In the past few years, the introduction of General Purpose Graphics Processing Units (GP–GPUs) has been a breakthrough in the field of High

Performance Computing. GPUs can be defined as co–processors which accelerate the processes computed in Central Processing Units (CPUs), these devices were initially designed to perform the calculations needed to display graphic content in a computer screen by using a massively parallel structure. Nowadays, application developers tend to implement massively parallel parts of their codes on the GPU while the CPU leads the serial parts.

Cardiac simulations have to solve large and complex ODE systems replicated in thousands or even millions of locations corresponding to the cells present in a volumetric or surface model, this is a problem with an eminently parallelizable structure, which has led to the use of GP–GPUs ***(Vigmond 2009, Sato 2009, Lionetti 2010, Nimmagadda 2012, Garcia-Molla 2014)***.

GP–GPUs became popular in the field of High Performance Computing thanks to the release of the CUDA software development toolkit in the late 2000's. The CUDA Toolkit started as a set of tools (compiler, libraries…) which allowed the access to GP–GPUs by using the C/C++ language, but nowadays the known as CUDA Ecosystem includes a high number of tools, libraries and applications based on this architecture. The CUDA architecture is supported by the most important nVidia GPU families (i.e. GeForce, ION Quadro and Tesla) and has been used in thousands of published research articles in the last decade.

The most important strength of GP–GPU CUDA platforms is that they are high–performance and available at accessible costs to research groups compared with clusters based in CPUs or supercomputers. At the same time CUDA is compatible with a lot of nVidia devices and the developed application or codes can migrate from one unit to another.

Chapter 3

General Materials and Methods

The general materials and methods employed in this thesis are presented in this chapter. In particular the implementations needed for the simulation in a GP–GPU platform and the basis for phase singularity analysis are described, whereas the electrophysiological and geometrical models used in this thesis are described.

The aim of this chapter is to introduce general concepts that will ease the understanding of the rest of the thesis. Specific materials and method as simulation protocols will be described in each chapter.

3.1. Cardiac simulation GP–GPU platform

All the electrophysiological simulations of this thesis were performed with the GP–GPU available in the lab nVidia TESLA C2075 (Figure 3.1), the main specifications are listed below:

Number of CUDA cores	448
Double precision floating point performance (Peak)	515 Gflops
Single precision floating point performance (Peak)	1.03 Tflops
Total dedicated memory	6GB GDDR5
Memory bandwidth	144 GB/sec

Figure 3.1 – nVidia TESLA C2075.

In the next sections we will describe the implementation of the problem and some details about GPU implementation.

3.1.1. Problem statement

The mathematical model of Koivumaki, and in general all the Hodgkin–Huxley like models, can describe the variation of the transmembrane voltage *V* in time in terms of *V*, of the vector of voltage dependent gating variables $W = w_i, i = 1, \dots, N_w$ and of the vector containing ionic concentrations and other gating variables $\mathrm{X} = x_j, j = 1, \dots, N_x$:

$$\frac{dV}{dt} = I(t, V, X, W) = -\frac{I_{ion}}{C_m}, \tag{3.1}$$

$$\begin{aligned} \frac{dx_j}{dt} &= g_j(V, X, W), \mathrm{j} = 1, \dots, N_x \\ \frac{dw_i}{dt} &= a_i(V)w_i + b_i(V), \mathrm{i} = 1, \dots, N_w \end{aligned} \tag{3.2}$$

With initial conditions V_0, X_0 and W_0, all these variables have associated an ODE, so the whole model has $N_x + N_w + 1$ variables (transmembrane voltage, ionic concentrations and gating variables) and $N_x + N_w + 1$ differential equations.

As presented in section 2.3.2, when using a tissue or geometrical model with a multiple number of cells (Ncells, numbered from 0 to Ncells–1) then the equation 3.1 is modified to include the effect of the neighboring cells, attending to the monodomain model formulation:

$$\frac{\partial V}{\partial t} = -\frac{I_{ion}}{C_m} + \nabla \cdot D\nabla V \tag{3.3}$$

After discretization of the spatial derivatives equation 3.3 for the k–th cell is described by the following ODE:

$$\frac{dV_k}{dt} = -\frac{I_{ion,k}}{C_{m,k}} - D\sum_j \frac{V_k - V_l}{d_{k,l}^2} \tag{3.4}$$

where $d_{k,l}$ is the distance between the neighboring cells *k* and *j* and the sum is performed over the cells neighboring the *k*–th cell. We denote the data vector for

the *k*–th cell as $y_k = [V_k; X_k; W_k]$, and the vector of the transmembrane voltages for all cells as V. Then we wrote the system function f_k for the *k*–th cell as:

$$f_k(t,Y) = f_k(t,V,X_k,W_k) = \begin{cases} \dfrac{dV_k}{dt} = -\dfrac{I_{ion,k}}{C_{m,k}} - D\sum_j \dfrac{V_k - V_l}{d_{k,l}^2} \\ a_i(V_k)w_{i,k} + b_i(V_k), \qquad i = 1,\dots,N_w \\ g_j(V_k,X_k,W_k), \qquad j = 1,\dots,N_x \end{cases} \tag{3.5}$$

Stacking together the data of all cells $Y = [y_0; y_1; \dots; y_{Ncells-1}]$ and the system functions of all cells $F = [f_0; f_1; \dots; f_{Ncells-1}]$, the whole system can be written as an initial value problem,

$$\frac{dY}{dt} = F(t,Y) \tag{3.6}$$

3.1.2. Numerical methods

The forward Euler method

The forward Euler (FE) method is the simplest method for solving initial value ODE systems such as that given by equation 3.6. After selection of a time step h, and given the initial solution Y^0 at time $t = t_0$, an approximate solution is obtained at time $t = t_0 + h \cdot Nsteps$ through the simple loop:

for $j = 1 \rightarrow Nsteps$ **do**
  $Y^{j+1} = Y^j + h \cdot F(t_j, Y^j)$
end for

Algorithm 3.1 – Forward Euler method.

This method has limitations in terms of stability and accuracy, but when solving a cardiac modeling problem in GPU it achieves a reasonable accuracy and speed when combined with the Rush–Larsen method described below and an appropriate time step. Note that the accuracy requested for cardiac modeling is quite gross (1 to 5% ***(Maclachlan 2007)***).

Rush–Larsen method

The Rush–Larsen (RL) method ***(Rush and Larsen 1978)***, was implemented specifically for cell models, and has been well studied ***(Perego and Veneziani 2009, Sundnes 2009, Maclachlan 2007, Marsh 2012)***. This method takes advantage of the special form of the equations governing the gating variables (see

equation 3.2). If V is considered constant over a time interval h (and so the expressions $a_i(V)$ and $b_i(V)$) then the value of the dependent variable after the step $j+1$ can be determined exactly by using the following expression:

$$w_i^{j+1} = \mathrm{e}^{a_i(V)h}\left(w_i^j + \frac{b_i(V)}{a_i(V)}\right) - \frac{b_i(V)}{a_i(V)} \tag{3.7}$$

Rush and Larsen proposed to split the ODE system, solving the equations of the gating variables through equation 3.7 and using the FE method for the rest of the equations. If ng denotes the non–gating functions and variables, the function system can be solved as:

for $j = 1 \rightarrow Nsteps$ **do**
  $Y_{\boldsymbol{ng}}^{j+1} = Y_{\boldsymbol{ng}}^{j} + h \cdot F_{ng}(t_j, Y^j)$
  Apply equation 3.7 to W^j to obtain W^{j+1}
end for

Algorithm 3.2 – Rush–Larsen FE method.

This method makes the problem more stable as the gating equations make the system stiff, and when using the Rush–Larsen method and calculating the exact values the system becomes non–stiff, allowing larger time steps.

3.1.3. GPU Implementation

Here we describe the GPU implementation of the Rush–Larsen FE method. A CUDA program is constructed by pieces of code, called kernels ***(Farber 2011)***. Each kernel is invoked from the main program, to assign a task to the GPU. When a kernel is sent to the GPU, many instances of the kernel are executed in parallel in the GPU. Each of these instances is executed by a thread, and each thread runs in one of the many microprocessors or cores of the GPU. These threads are organized into blocks of threads, that are executed together. In the call to the kernel, the programmer must specify as parameter of the kernel how many blocks (*NBlocks*) and how many threads per block (*NThreadsperBlock*) will be used to execute this kernel.

In our CUDA solver, the parallelism is obtained by simultaneously performing the computations for many cells. The computations for a given cell are carried out by a single CUDA thread. If the number of threads is larger than the number of cells, then each thread will take care of a single cell. If the number of cells is larger than the number of threads, which is usually the case, then several cells are assigned to each thread as follows: suppose that there are *NCells* cells and *NThreads* threads (*NThreads=NBlocks· NThreadsperBlock*), with *NCells>NThreads*. Each thread is identified by an integer number *Tid*,

0≤Tid≤NumThreads. Then, in a given step, thread *Tid* will start processing cell *Tid*. When finished with cell *Tid*, thread *Tid* will process cell *NThreads+Tid*, then cell 2 *NThreads+Tid* and so on,until all the cells have been processed.

The structure of the main loop (executed on the CPU) is described in the Algorithm 3.3, and the kernel (executed on the GPU) is described in Algorithm 3.4:

for $j = 1 \rightarrow Nsteps$ **do**
  $kernel\ RLFE \ll NThreadsperBlock, NBlocks \gg (t, Y^{in}, Y^{out})$
  swap (Y^{in}, Y^{out})
end for

Algorithm 3.3 – CPU main loop, RLFE refers to Rush–Larse forward Euler.

$kernel\ RLFE(t, Y^{in}, Y^{out})$
  $k = Tid$
  while $k < NCells$ **do**
    $y_{k,ng}^{out} = y_{k,ng}^{in} + h \cdot f_{k,ng}(t, y_k^{in})$
    $w_k^{out} = advance\_RushLarsen(w_k^{in}, h)$
    $k = k + NThreads$
  end while

Algorithm 3.4 – kernel RLFE, advance_RushLarsen implements equation 3.7.

All the data needed for the computations and the results are kept in the global memory of the GPU so that all the threads can access the necessary data. An important feature of this problem is that the subroutine that evaluates the system function f_k for each cell is quite complex and uses many variables; for efficiency, these variables are stored in "registers". Generally speaking, CUDA kernels should optimally utilize "shared memory", which is a fast memory that is available to all the threads in a block ***(Farber 2011)***. However, the amount of available shared memory depends on the number of used registers. As many registers have been employed there is a strong limitation in the available so we decided to employ both registers and global memory but no shared memory in our kernels. Instead we decided to reduce the number of accesses to the global memory by doing an efficient use of registers. The structure of the data is also very important at the time of improve the performance. When working on the CPU we used data structures for each cell including all the variables, and then created vectors of this data type, with *NCells* elements. However to obtain a "coalesced access" in the GPU it is more efficient to use a "Structure of Arrays" data layout ***(Farber 2011)***. The access to memory is further improved if the size of the arrays in the structure is a multiple of 32. Therefore, the first multiple of 32 greater than *NCells* (*NCelAux*) is used and the extra cells are not used. The data structure is in a C–like syntax:

$$struct\ celldata \begin{Bmatrix} float\ V[NCelAux] \\ float\ w_1[NCelAux] \\ float\ w_2[NCelAux] \\ \dots \\ float\ x_{Nx}[NCelAux] \end{Bmatrix}$$

The cells not used only have impact in a slight waste of memory but results in a reduction of unaligned memory accesses that is in this way limited to the access to the neighboring cell voltages.

As the data transfer between GPU and CPU is quite slow and it would be very inefficient to store all the calculated steps, we send the data for a predefined *Nsave* steps number. The choice of the step length depends on the problem to be solved based in our works with adaptive step ***(Garcia-Molla 2014)*** and other references depending on the problem.

The simulation platform allows the introduction of stimulation currents in a set of cells configurable in terms of amplitude, duration etc. Electrophysiological variations can be also introduced with different intensities depending on the cell. This information together with the initial values for the variables, the neighboring cells and the conductance connecting each cell with its neighboring cells (which summarizes the diffusion *D* and the distance between cells) is introduced with .txt files generated with Matlab.

3.2. Electrophysiological model of Koivumaki

The electrophysiological model used in this thesis in the model of Koivumaki ***(Koivumaki 2011, Koivumaki 2014)*** which is based in the model of Nygren ***(Nygren 1998)***. As a Hodkin–Huxley like model the resulting current between the intracellular and extracellular mediums modulate the membrane voltage (*V*) in each moment. The Na+, K+ and Ca2+ currents in this model are summarized in Equation 3.8 and depicted in Figure 3.2:

$$I_{ion} = I_{Na} + I_{Nab} + I_{to} + I_f + I_{Kr} + I_{Ks} + I_{Kur} + I_{K1} + I_{CaL} + I_{Cab} + I_{NaK} + I_{PMCA} + I_{NCX} \tag{3.8}$$

Sarcolemma currents are formulated in this model following the model of Nygren, Koivumaki introduced minor changes in some of these currents, introduced I_f and reformulated I_{CaL} but the modeling of sarcoplasmic reticulum (SR) together with the compartmentalization of intracellular and SR media were its main inputs to electrophysiological models.The next sections describe the different currents implemented. The formulation is described in detail in the original reports by Koivumaki: ***(Koivumaki 2011, Koivumaki 2014)***.

3.2.1. Hyperpolarization–activated inward current I_f

The hyperpolarization–activated inward current I_f was introduced by Koivumaki in the atrial electrophysiological model according with the significant role of this current in atrial ectopy and pacemaker activity in the atria as it was suggested by ***(Porciatti 1997, Hoppe and Beuckelmann 1998, Zorn-Pauly 2004, El Chemaly 2007)***. The current mainly introduces potassium in the cell together with sodium and contributes to the pace–maker activity of the cell.

It is formulated attending to the equations of ***(Zorn-Pauly 2004)*** and uses only one gating variable.

3.2.2. Sodium currents

The sodium (Na^+) currents in this model are the fast Na^+ current I_{Na} and the background Na^+ current I_{Nab}.

I_{Na} is an ultra–fast current which introduces in the myocyte an ionic current of several nanoamperes in a very short period of time 1–2 ms. It is the main responsible current of cell depolarization. This current uses 3 gating variables and ODEs (one activation and two inactivation).

I_{Nab} is a current which introduces Na^+ ions depending mainly in the membrane voltage. The main objective of this current is to maintain stable intracellular Na^+ concentrations in phase 4. This current does not use gating variables.

3.2.3. Potassium currents

Potassium currents are outward currents responsible at the time of bringing the membrane potential back to its resting value.

The transient outward potassium current I_{to} is a fast current which activates when the transmembrane voltage gets positive values reducing the membrane potential to plateau values. This current is implemented with one activation and one inactivation gating variables.

The ultrarapid delayed rectifier or sustained outward potassium current I_{Kur} is an atrial specific current with a formulation similar to that of I_{to} (two gating variables) but with a longer duration being present in the first half of the plateau.

The rapid and slow delayed rectifier potassium currents I_{Kr} and I_{Ks} respectively are depolarizing currents with an important role in the repolarization phase which are modeled with a gating variable each.

Finally, the inward rectifier potassium current I_{K1} is a current which remains active during the whole action potential and is very important at the time of maintaining the resting membrane potential, it does not use activation/inactivation gating variables.

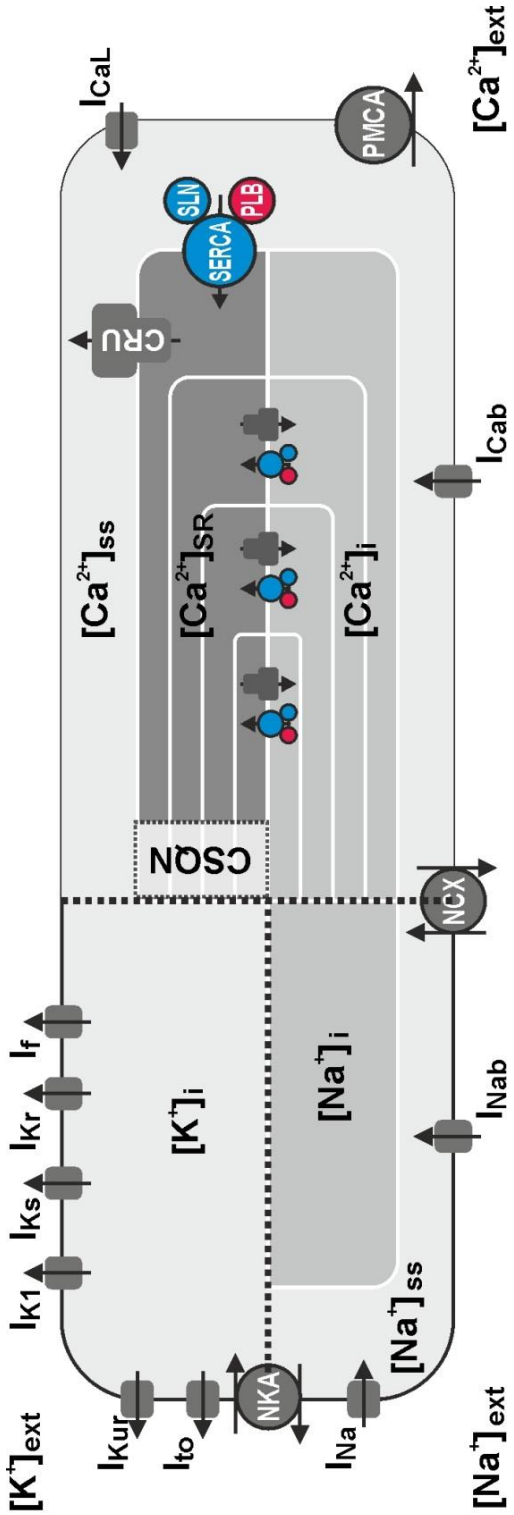

Figure 3.2 – Atrial model implemented scheme. Based in (Koivumaki 2014).
The different sarcolemmal currents and those between the cytosol and sarcoplasmic reticulum are depicted. Also the different subspaces used in the model are depicted.

3.2.4. Calcium currents

The main transmembrane calcium (Ca^{2+}) current is the depolarizing L–type Ca^{2+} current I_{CaL}. It is an inward current much longer than I_{Na}, it is active during the plateau phase and is essential in the shape of the AP. It introduces Ca^{2+} in the myocyte so it plays an important role in the excitation–contraction coupling. Similarly to the I_{Na} it includes one activation and two inactivation gating variables. The changes introduced in this current by Koivumaki were also implemented. See supporting information in ***(Koivumaki 2014)***.

I_{Cab} is a current equivalent to I_{Nab}, but controls the intracellular concentration of Ca^{2+}.

3.2.5. Sarcoplasmic reticulum

In the human atria the Ca^{2+} that flows through the membrane is equivalent to the transit of Ca^{2+} between the cytosol and the sarcoplasmic reticulum (SR). Koivumaki ***(Koivumaki 2011)*** implemented a detailed model to account for the pumping and release of Ca^{2+} from the sarcoplasmic reticulum.

The Ca^{2+} is released from the SR through the calcium activated release channels (which are labelled as CRU in Figure 3.2) and is removed from the cytosol and introduced in the SR through the ATPase pumps SERCA (which is also represented in Figure 3.2). In the model of Koivumaki the SERCA activity is modulated by sarcopilin (SLN) and the phosphorylation of phospholamban (PLB). In terms of Ca^{2+}, bulk cytosol $[Ca^{2+}]_i$ and SR is compartmented in 4 different subspaces which implement the interchange of Ca^{2+}, four different SERCA and CRU connects the four SR subspaces with the junctional cytosol compartment $[Ca^{2+}]_{ss}$ and with three of the bulk cytosolic compartments.

Then Ca^{2+} moves between the bulk cytosol and SR subspaces by diffusion which was modeled by Koivumaki based on Fick's second law of diffusion.

The calcium activated release channels are formulated as Hodgkin–Huxley like channels using three gating variables each and SERCA pumps thus required of one ODE each which is solved with the forward Euler scheme.

3.2.6. Pumps and exchangers

The Na^+–K^+ pump I_{NaK} reestablishes ionic concentrations by introducing 2 potassium ions into the cell and pumping 3 sodium ions. It results in an outward current.

The calcium pump pulls Ca^{2+} ions out of the cell resulting in an outward current. Its main function is to maintain the intracellular concentration of calcium in physiological levels.

The Na^+–Ca^{2+} exchanger I_{NCX} takes advantage of the electrochemical gradient ($[Na^+]_o >> ([Na^+]_i$) and with the introduction of three Na^+ ions pumps one Ca^{2+} ion resulting in an inward current.

None of the pumps or exchangers uses gating variables.

3.2.7. Summary of ODEs

Each ionic concentration ($[Na^+]_i$, $[Na^+]_{ss}$, $[K^+]_i$, $[Ca^{2+}]_i$ –a total of four subspaces–, $[Ca^{2+}]_{ss}$ and $[Ca^{2+}]_{SR}$ –a total of four subspaces–) needs from an ODE which summarizes the ionic exchanges between media depending on the ionic currents obtained or the diffusion in the case of Ca^{2+} and Na^+. Note that the extracellular concentrations remain constant, and that the ionic exchange in the Na^+–K^+ pump and the Na^+–Ca^{2+} exchanger is a multiple of the resulting I_{NaK} or I_{NCX} equivalent currents depending on the ionic concentration calculated.

This total of twelve variables together with the membrane voltage and the four variables associated to SERCA pumps result in a total of 17 variables which are solved with forward Euler scheme.

Furthermore, as it has been described there is a total of 25 gating variables and associated ODEs which are solved with the Rush–Larsen equation. In total the Koivumaki model implemented uses 42 ODEs to solve the AP.

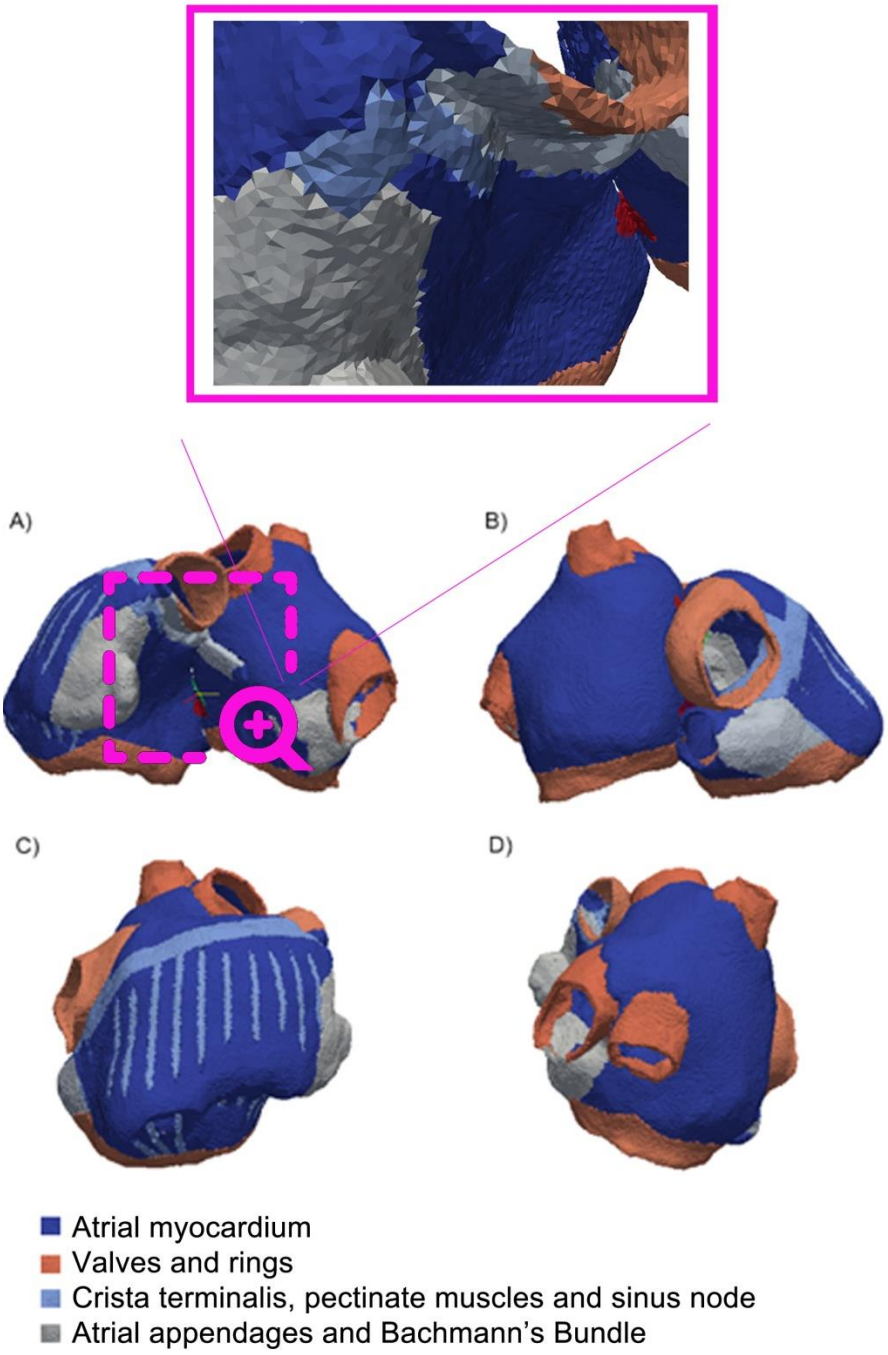

Figure 3.3 – Geometrical model used from different points of view.
Colors depict the different atria area, on top an extended part is shown highlighting the tetrahedron mesh.

3.3. Geometrical model

The geometrical model used in this thesis is based on the free distribution of the model developed by Krueger et al. It is a volumetric three dimensional model of the human atria constructed from medical images (computed tomography and magnetic resonance). The geometric structure consists of tetrahedra and a vector associated to each tetrahedron indicating the direction of the fibers. It includes and distinguishes the most important geometric structures allowing the customization in terms of electrophysiology and propagation (Bachmann's bundle, sinus node, crista terminalis, pectinate muscles, cavotricuspid isthmus, appendages, rings and valves – see Figure 3.3). Fiber modeling was performed using a rule based on a semi–automatic method developed by Krueger et al. ***(Krueger 2011)***.

The anatomical model consists on a three dimensional mesh with 284,578 vertices and 1,353,783 tetrahedra. Each vertex or node is connected to other neighboring vertices, with a number ranging between 4 and 15, and thus the tetrahedra conform the structure. The distance between nodes is 673.38 µm with a standard deviation of 130.31 µm.

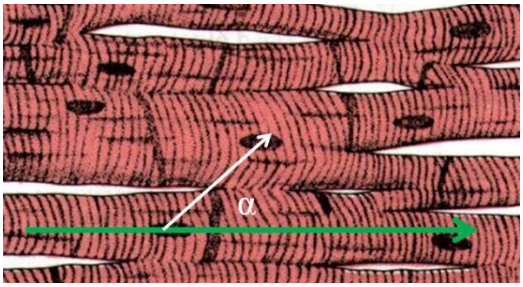

Figure 3.4 – Diffusion between neighboring cells with fiber orientation vectors. *An schematic representation of the cardiac tissue is depicted, the green vector depicts the fiber orientation, the white vector the direction between two neighboring cells.*

As presented in equation 3.4 the conductance between two neighboring cells depends on the diffusion *D* and the distance between cells. When simulating an isotropic tissue *D* is a constant, but when introducing fiber orientation vectors the equivalent $D_{k,l}$ between the neighboring cells *k* and *l*, depends on the angle α between the fiber orientation vector and the direction connecting both neighboring cells attending to the following equation:

$$D_{k,l} = D_{long} \cdot cos^2\alpha + D_{trans} \cdot sin^2\alpha \tag{3.9}$$

Being D_{long} the diffusion value in the direction of the diffusion vector and D_{trans} the diffusion value in the direction perpendicular to the diffusion vector.

Based on the work of Krueger et al. ***(Krueger 2011)***, the diffusion vectors were adjusted to obtain a sinus propagation according to the literature as described in Table 3.1:

Table 3.1– Diffusion values for the different areas of the atria.

Atria region	D_{trans} **µm²/ms**	D_{long}/D_{trans}
Atrial myocardium	0.12	3.75
Appendages	0.12	3.75
Rings and valves	0.12	3.63
Cavotricuspid isthmus	0.12	1
Crista terminalis	0.12	6.56
Bachmann's Bundle	0.12	3.88
Pectinate muscles	0.05	23.25
Sinus node	0.44	1

A sinus propagation takes 118 ms, it can be observed in the Figure 3.5 and it is described below.

The first 5000 ms corresponding to 5 cycles were discarded, taking as a reference the start of the sixth stimulus (t=0ms), the propagation starts in the sinus node in ms 3 and propagates through the right atria following two main fronts, one leading the depolarization in the right atrium and the second to the left atrium. The first front starts in the crista terminalis at after 18 ms and goes through it, due to the anisotropy in this bundle the front takes a convex form through the area connecting both superior and inferior vena cava (see ms 40 and 60). The propagation gets the inferior vena cava in ms 72. The right appendage is totally depolarized after 67 ms. In the right atria the last area to be depolarized is the inferior vena cava in its septal part and completes its activation at ms 112.

The second front gets the Bachmann's bundle at ms 23 and finishes the propagation through this bundle at ms 35 getting the left atria. A wavefront propagates quite isotropically to the right and left pulmonary veins. The wavefront starts the depolarization of the right superior pulmonary vein in ms 55 and the left inferior pulmonary vein in totally depolarized at ms 113. The left atrium is totally depolarized at ms 118 being the the area between the left inferior pulmonary vein and the mitral valve the last to be depolarized.

Note that the interatrial routes in the area of the fossa ovalis and next to the inferior vena cava do not have special relevance during sinus rhythm, being the Bachmann's bundle the main route between the two atria. These results are comparable to that observed in previous simulation works ***(Harrild and Henriquez 2000, Krueger 2011)***.

The computing time needed to obtain 1 second of simulated cardiac activity using the Rush–Larsen forward Euler method with a time step of 20 µs and a sampling frequency of 500 Hz (*Nsave=100*) was 15 minutes and 30seconds.

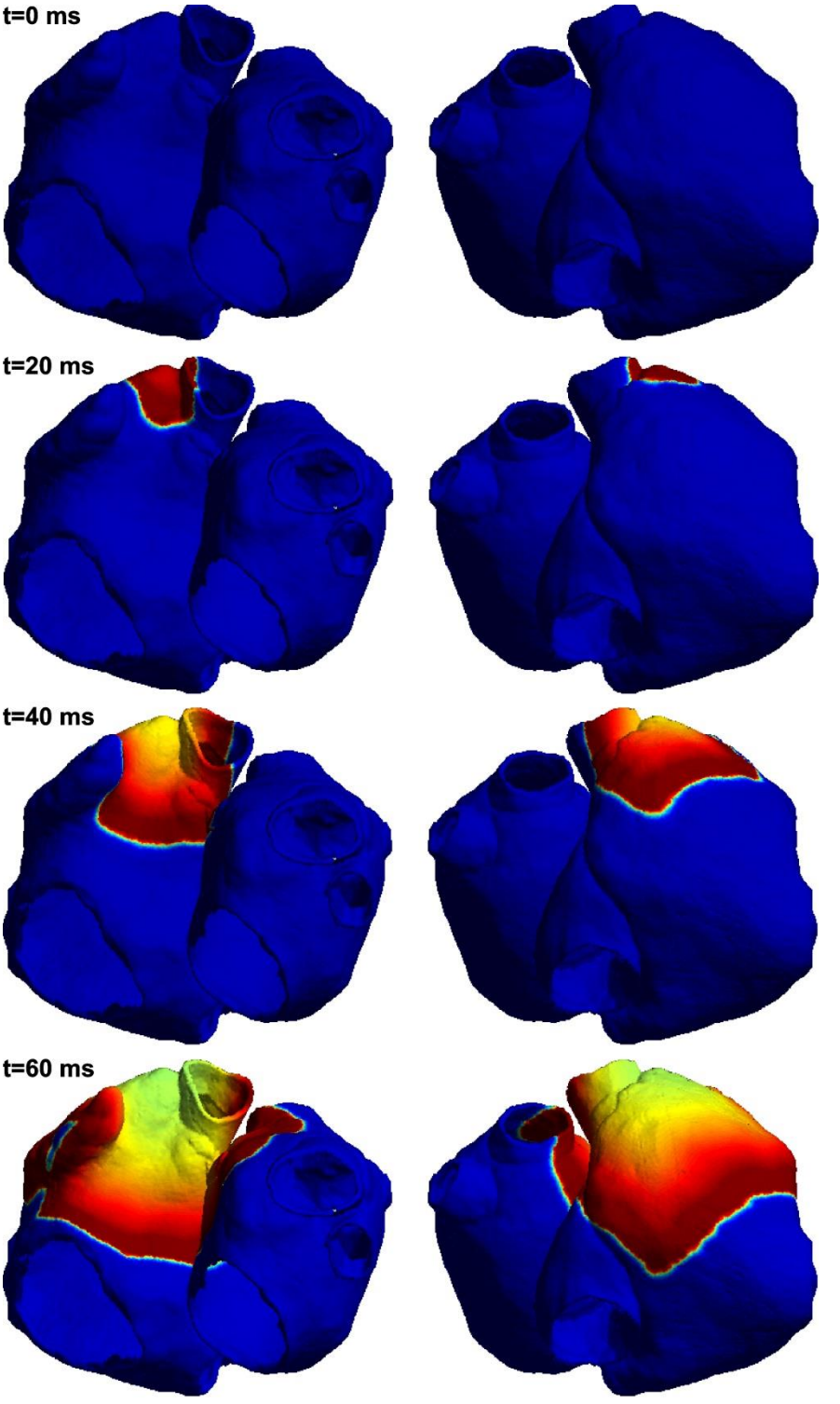
t=0 ms
t=20 ms
t=40 ms
t=60 ms

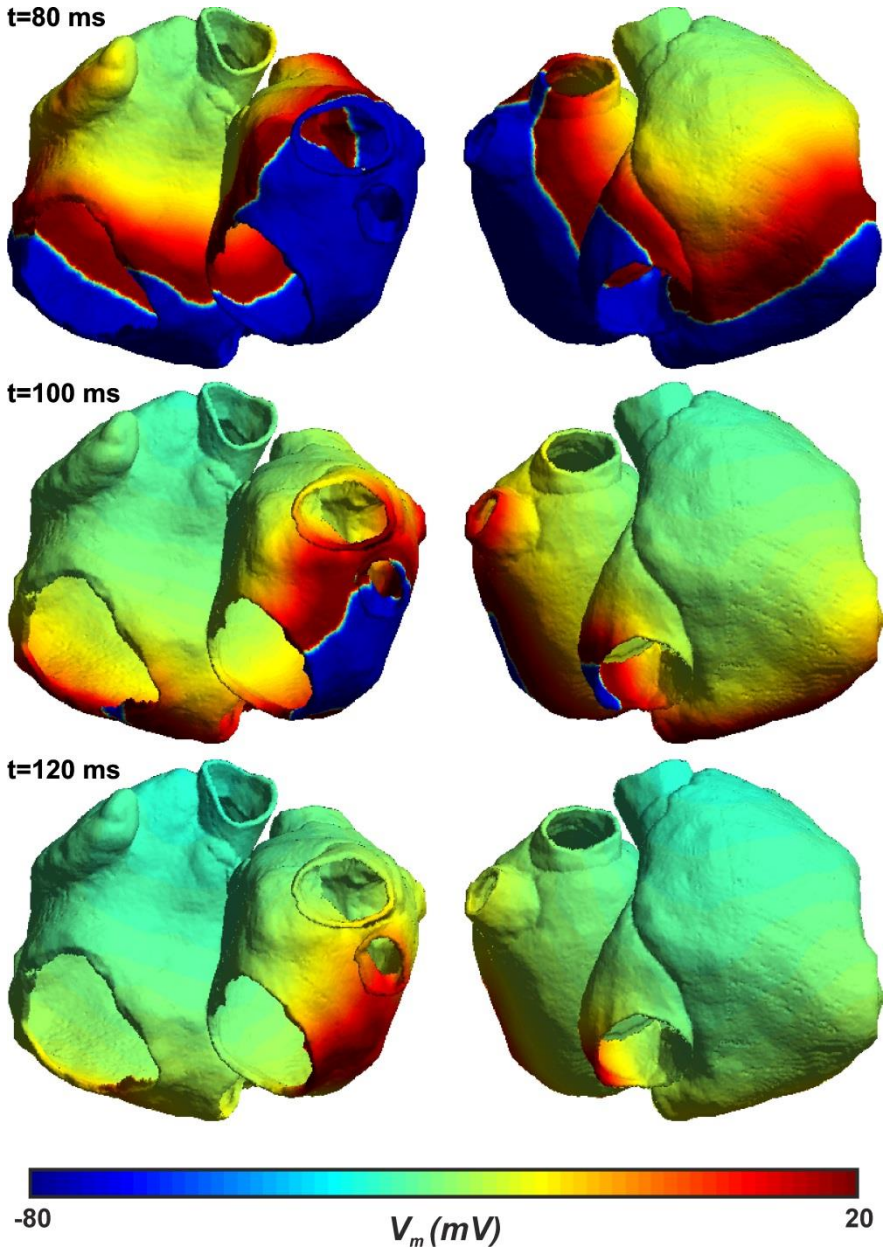

Figure 3.5 – Sinus propagation in the three dimensional atrial model implemented.

Wavefront propagation from two different views and time instants are depicted. The voltage in each cell or area corresponds with the color bar in the bottom.

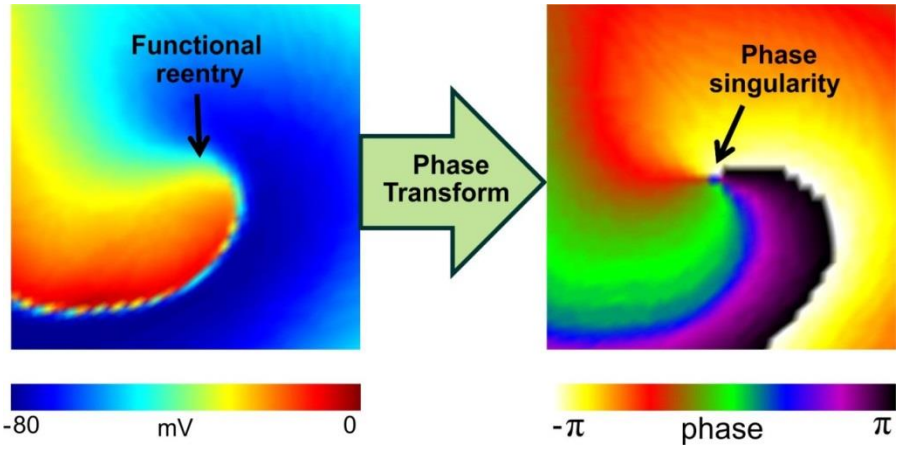

Figure 3.6 – Phase transform.

Action potential map with a reentrant activity (left) and the phase map in the same time instant (right) are depicted. The phase singularity marks the position of the core of the re–entrant activity.

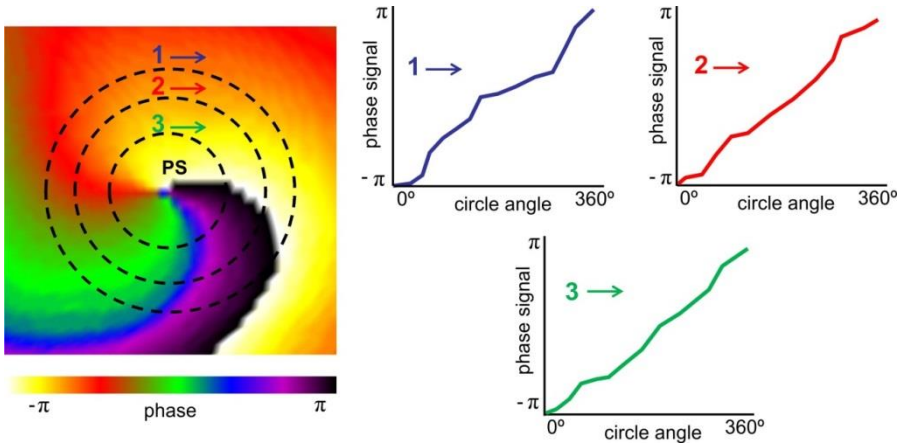

Figure 3.7 – Phase singularity detection methodology.

Phase signals are evaluated in three concentric circles around each candidate to be SP (left). Only those points in which the phase was gradually and monotonically increasing or decreasing in at least two of the three circles are chosen as SP (right).

3.4 Phase analysis

For the detection of the core of reentrant activity, phase maps are used during this thesis both in transmembrane potentials obtained from simulations of atrial tissue or in the torso surface after solving the forward problem of the electrocardiography. Phase maps are obtained from potential maps by calculating the instantaneous phase for each point by using the Hilbert transform ***(Zlochiver 2008, Rodrigo 2014b)***, as described in equation 3.10 where $\angle(\,)$ is the phase operator and $HT(\,)$ the Hilbert transform. The phase signal ranges from 0 to 2π and represents the relative delay of each signal in one period. A singularity point (SP) is defined as the point in a phase map which is surrounded by phases from –pi to pi. The case of a spiral wave or functional re–entry in a simulated tissue is depicted in figure (see Figure 3.6).

$$Phase\ signal\ =\ \angle(\,HT(\,Potential\ Signal\,)) \tag{3.10}$$

To increase reliability, the phase values were obtained along 3 different circles surrounding each evaluated point with radii adjusted depending on the application; an evaluated point was defined as a SP only when the phases of at least two of these three circles were gradually and monotonically increasing or decreasing for a total of 2π (see Figure 3.7).

Chapter 4

Non–invasive Characterization of Atrial Macroreentries during Typical and Atypical Atrial Flutter

4.1. Introduction

Atrial flutter (AFL) is defined as an atrial macroreentrant tachycardia maintained by an electrical wavefront rotating continuously around an anatomical structure, a scar or a functional block area. AFL is manifested in the electrocardiogram (ECG) by repeating atrial complexes with a constant morphology at a rate of 250–300 beats per minute ***(Garcia-Cosio 2012)***. Depending on the structure that defines the re–entrant circuit, AFL is subdivided into two categories: typical AFL, caused by a rotation around the tricuspid annulus (TA) and atypical AFL caused by a rotation around any other structure either in the left or right atria ***(Saoudi 2001)***. AFL can be terminated by ablation of some segment of the reentrant circuit, preferentially the narrowest portion of the circuit ***(Morady 1999)***. While in typical AFL ablation of the cavotricuspid isthmus (CTI) consistently results in an effective arrhythmia termination ***(Garcia-Cosio 2012, Da Costa 2006)***, identification of the ablation target in atypical AFL requires extensive mapping studies in order to determine the circuit responsible of the arrhythmia, which may be especially complex in case of AFL secondary to prior surgical procedures ***(Yokokawa 2013)***.

In this proof–of–concept study we propose that surface representation of the reentrancy circuit of AFL patients may be dependent on the circuit involved in the reentry and thus may allow its identification prior to an ablation procedure. With this objective we analyzed body surface phase maps of AFL patients with either

typical or atypical AFL circuits and propose the spatial inscription of phase singularities as a potential tool for identifying the reentrant circuit. The technique was verified with by using realistic computational models.

4.2. Methods

4.2.1 Patients and body surface potential recording

The study included nine patients admitted at Hospital General Universitario de Valencia with either typical or atypical AFL for an ablation procedure. All patients gave informed consent. The protocol was approved by the Institutional Ethics Committee of the institution.

Recordings were acquired prior to the ablation procedure for 10 minutes with patients in a supine position. In patients with a heart rate faster than 90 beats per minute, a carotid sinus massage was performed during the recording by a trained physicist in order to reduce the heart rate and allow a clear recording of the AFL waves. A total of 67 electrocardiogram (ECG) signals were obtained covering the entire torso surface (see Figure 4.1). A total of 64 electrodes were arranged in a vest with 36 electrodes in the anterior torso and 28 in the posterior torso plus the limb electrodes ***(Guillem 2013, Guillem 2009a)***. Signals were recorded at a sampling rate of 2048 Hz, with a bandwith of 500 Hz and a resolution of 1 microvolt. Quality of all leads was visually evaluated before acquisition and stored for off–line processing.

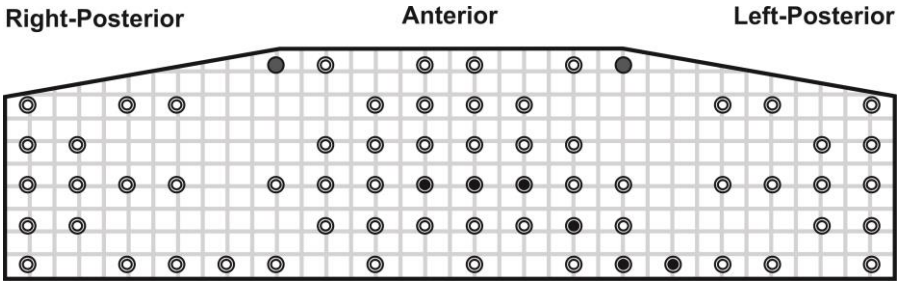

Figure 4.1 – Electrode arrangement in our vest.
Light–gray dots show positioning of right and left arm electrodes. Black dots indicate the location of precordial leads (V1–V6). The center of the sketch corresponds with the anterior chest while the left and right parts of the back are represented on the right and left of the figure respectively.

The diagnostic of typical AFL was confirmed in 3 patients in the electrophysiology laboratory by termination of the arrhythmia after cavotricuspid isthmus (CTI) ablation. The remaining 6 patients had reentrancy circuits not involving the CTI and AFL was terminated by electrical cardioversion.

4.2.2 Computational models

Atrial transmembrane potential calculation

Atrial activity was simulated using the three–dimensional structure described in section 3.3, the action potential for each node was mathematically calculated based on the cellular model of human atria Koivumaki ***(Koivumaki 2011, Koivumaki 2014)*** also described.

As described in sections 2.2.3 and 2.3.1, electrical remodeling is usually associated with a shortening of the action potentials and reduced diffusion in the cardiac tissue, these properties facilitate the maintenance of reentrant behaviors.

We implemented a remodeling by increasing g_{K1} in 31% and decreasing g_{to}, g_{kur} and g_{CaL} in 31%, 19% and 29% respectively, and by decreasing D in 25%, which represents a remodelling degree in between sinus rhythm conditions and atrial fibrillation remodeling implemented by Koivumaki et al. ***(Koivumaki 2014)***. For simulating counterclockwise and clockwise typical AFL, reentrant spread around tricuspid valve was forced, an additional reduction of 40% in D was implemented in cavotricuspid isthmus in order to account for the reduced conduction velocity that is consistently found in patients during AFL ***(SippensGroenewegen 2000, Sasaki 2013)***.

For simulating the reentry around the inferior vena cava the same remodeling was implemented in the atria, instead of the cavotricuspid isthmus, in this case VCI presented a reduction of 50% in D .

For simulating a reentry around the pulmonary veins we emulated a functional block region containing the four pulmonary veins. It consisted in modifications from the model presented in section 3.3 that consisted in a reduction of 90% in D in the area described, and an electrical remodeling (i.e. +62% g_{K1}, –62% g_{to}, –38% g_{Kur} and –59% g_{CaL}) according with the presented for atrial fibrillation by Koivumaki et al. ***(Koivumaki 2014)***. The rest of the tissue presented moderate remodeling variations: in terms of electrical remodeling, conductance variations equal to 10% of the present in the block region were implemented, and in terms of structural remodeling, a reduction of 10% in D from the original values. A transition area with radio 4 cm connected both regions. It resulted in a stable reentry around the whole structure.

A similar model but with the only difference of a more moderate reduction in D in the block area was implemented, in this case the reduction was in a 70% instead of a 90%.

To help interpretation of surface potentials on the torso surface, we also used a simple model consisting of two concentric spheres as atria and torso. The active tissue of the atria consisted of a 2.5 cm radius sphere incorporating 163,842 nodes (average inter–nodal distance of 236,07 ± 15.35 μm) with two inactive caps. A linear stimulus was applied to induce a rotation around the caps.

Numerically the calculations were performed in the simulation platform described in chapter 3.

Torso potential calculation

Simulated electrograms (EGMs) in 2048 points distributed around the epicardium were calculated by using the transmembrane potentials calculated in simulations by the formulation given in Equation 4.1:

$$EGM = \sum_{\vec{r}} \left(\frac{\vec{r}}{r^3} \right) \vec{\nabla} V_m \tag{4.1}$$

where $\vec{r}$ is the distance vector between the measuring point and a point in the tissue domain (r is the euclidean distance –1mm–), $\vec{\nabla}$ denotes the gradient operator and V_m is the transmembrane potential.

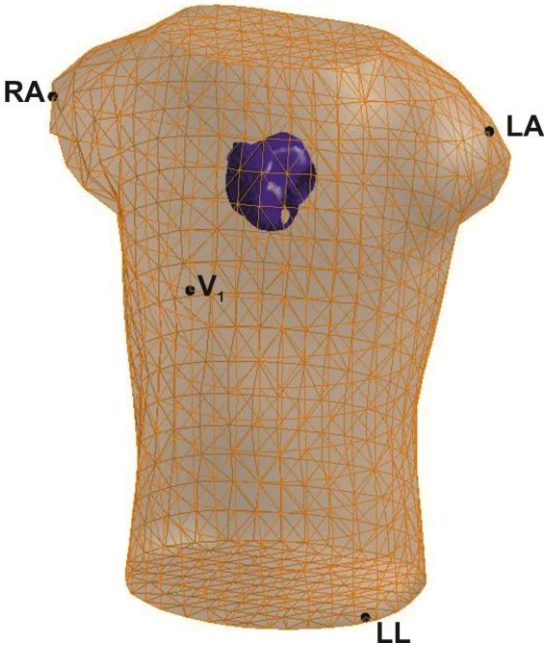

Figure 4.2 – Atria and torso models.
Atrial model with 284.578 nodes is depicted in blue and the torso model with 771 nodes in orange. Nodes corresponding with electrodes: right arm (RA), left arm (LA), left leg (LL) and V1 are depicted as black dots in the figure.

According to Boundary Element Method ***(Horacek and Clements 1997, Rodrigo 2014b)***, potentials on the surface of the torso can be computed from potentials on the heart surface. Specifically, ECGs were computed on a torso

model with 771 nodes and 1538 faces ***(Macleod 1991)*** in the case of the realistic model (see Figure 4.2), and an sphere of 2562 nodes and 5120 faces in the case of the spherical model. The homogeneous and isotropic conductivities assigned to each conductor volume were 0.3 S/m in the case of blood –inside the atria– and 0.2 S/m for the rest of torso tissues.

4.2.3 Signal processing

Signals were processed by using Matlab 7.11 (The Mathworks Inc., The Netherlands). Patient signals were preprocessed as previously described ***(Guillem 2009a, Guillem 2009b)***. Briefly, baseline oscillations were reduced by subtracting the estimated baseline. To estimate the baseline, ECG signals were decimated to 51.2 Hz and filtered with a Butterworth 10th-order low-pass filter with a cut-off frequency of 2 Hz. Baseline was then interpolated to 2048 Hz and subtracted to the original signal. Segments free from ventricular content longer than 400ms were selected after automatic detection of fiducial points of QRSonset and T–waveoffset. The five longest segments free from ventricular content for each patient were included in the study.

In the case of computational models we used the ECG signals obtained with the forward problem of electrocardiography.

Raw ECGs were filtered, by using a 4Hz bandwidth band–pass filter, around the reentrant frequency in the case of models and around the most predominant dominant frequency found on the torso surface in the case of patients, for that the dominant frequency in each lead with a resolution of 0.5 Hz was computed by using the Fast Fourier transform. Body surface potential maps were obtained from the filtered ECG signals by cubic spline interpolation.

4.2.4 Phase maps

Phase maps were obtained from potential maps and singularity points (SP), detected as described in section 3.4. SPs were tracked in time and space and only SPs lasting for at least half rotation were considered. Spatial occurrence of SPs was quantified into histograms, both in two dimensional recurrence maps in the case of patients or in the torso surface in the computational models.

Regions with a higher incidence of SP occurrences of typical AFL patients were defined as typical AFL SP areas and we then quantified the inscription of SPs into these areas.

4.2.5 Multilayer and filaments analysis

In the case of realistic computational models we used multilayer models to evaluate the SP from atria to the torso (see Figure 4.3). In this case, the conductivities inside the atria and for the rest of the tissues of the torso, were again

0.3 S/m 0.2 S/m. A filament was defined as the connection between SPs in the different layers, detected as described above.

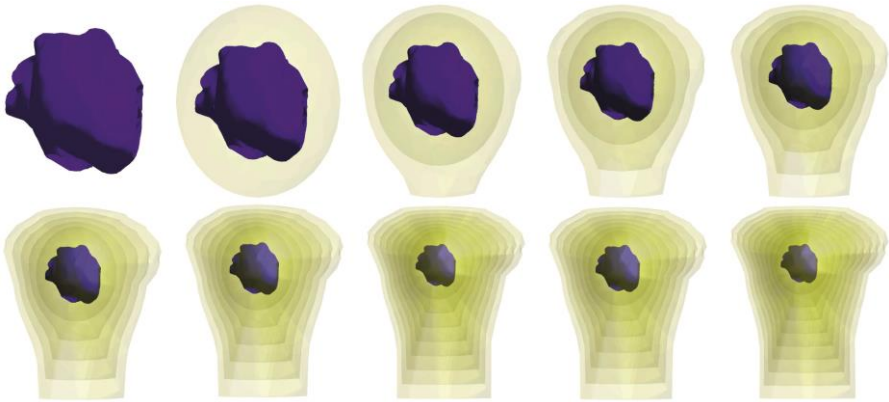

Figure 4.3 – Multilayer torso model.
Atrial model and layers used to evaluate the propagation of SPs from the atria to the torso.

4.2.6 Statistical analysis

Student's T–test was used to evaluate the statistical significance between continuous paired or unpaired variables, and statistical significance was considered for $p<0.01$. All data are reported as mean ± SD (standard deviation).

4.3. Results

4.3.1 Surface representation of typical and atypical atrial flutter in patients

Stable rotational patterns can be observed in consecutive phase maps of typical AFL patients (see Figure 4.4). Phase maps of typical counterclockwise AFL patients (Panel B) display a craniocaudal propagation pattern on the anterior torso and the opposed direction on the posterior torso. Two SPs appear on both midaxillary lines at the center of each rotational pattern and remain stable for consecutive propagations. This propagation was consistent with a counterclockwise rotation around the tricuspid valve with a descending propagation in the right atria free wall followed by an ascending propagation in the interatrial septum.

Panel A shows standard leads with a morphology coherent with previous studies ***(Kalman 1997, Garcia-Cosio 2012)*** with biphasic and positive deflections on lead V1 and a complex ondulation in inferior leads described as a slow descending phase followed by a pronounced negative slope and finally an

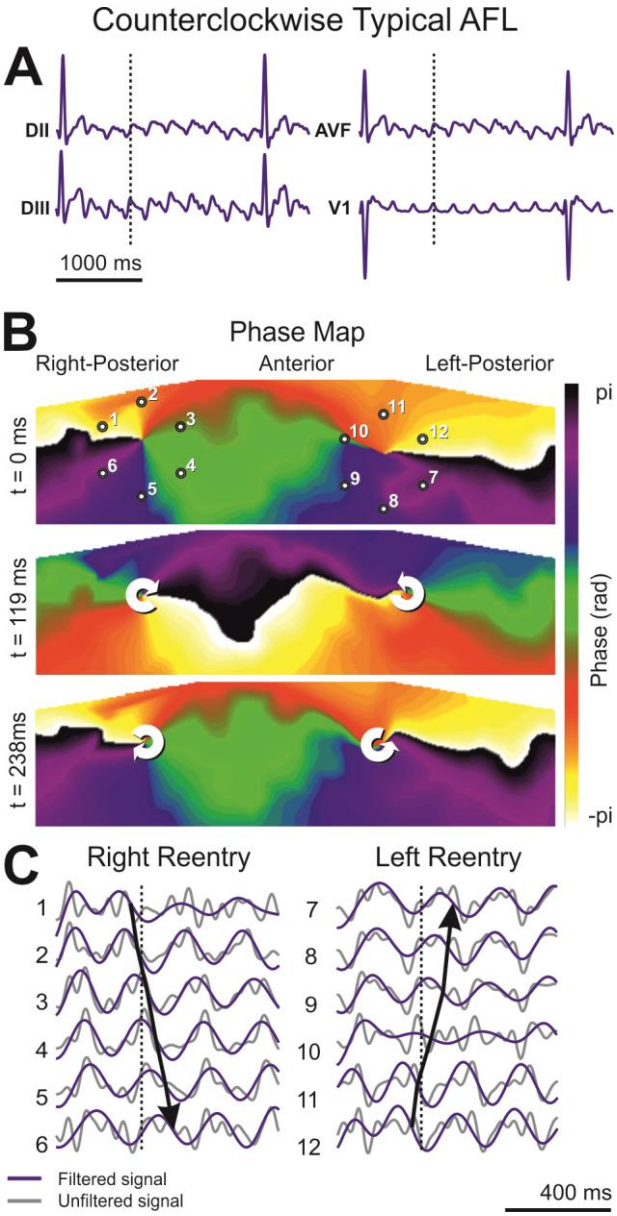

Figure 4.4 – Surface ECG tracings and phase maps in a counterclockwise typical AFL patient.

Panel A show inferior ECG leads and V1 for counterclockwise typical (CCW) AFL patient. Phase maps at three consecutive time instants are depicted for the same patient in panel B, evidencing stable rotational patterns. The maps represent the whole vest, the center of the maps corresponds with the chest while the left and right parts of the back are represented on the right and left respectively. Filtered and unfiltered ECG tracings around phase singularities (for locations represented

in panel B) are depicted in panel C. Doted vertical lines denote the time instant corresponding to the first phase map (t=0ms). Points of maximum descending slope of the band–pass filtered signals were connected to highlight the reentrant propagation in the torso. In CCW typical AFL a descending propagation in the anterior part of the torso followed by an ascending propagation in the back can be observed, with phase singularities placed in on both midaxillary lines.

ascending slope that ends with a positive deflection that connects with the following wave.

This rotational pattern can be deducted from the surface ECG signals (Panel C) but becomes more evident in the phase maps. It can be observed how band–pass filtering highlights the reentrant behavior, consistent with the results seen in the phase maps.

In a case of clockwise typical AFL, phase maps display a caudocranial propagation pattern on the anterior torso followed by propagation in the opposite direction in the back, consistent with a clockwise rotation around the tricuspid valve (see Figure 4.5). Again, two SPs appear on both midaxillary lines, as for the counterclockwise AFL patients. Panel C confirms again the propagation pattern observed in phase maps.

The leads shown in panel A are consistent with those observed in previous studies of typical AFL with a wide, negative and W shape V1 ***(Garcia-Cosio 2012)***. In the case of inferior leads complex tracings similar to those observed in counterclockwise typical AFL without silence periods because of the constant reentry can be observed.

An example of an atypical AFL patient is presented in Figure 4.6. In this case, the standard ECG does not allow identifying the circuit involved in the reentry (Panel C) as it does not present a recognizable pattern, positive deflections can be observed in the inferior leads and biphasic waves in V1, continuous waves with short silent periods can be observed in accordance with a constant reentry in the atria.

Phase maps show again two SPs, but in this case the locations differ from those observed in the case of typical AFL patients. In this case SPs are located in the anterior and right–posterior part of the torso, showing a counterclockwise propagation in the front.

Panel A of Figure 4.7 shows occurrence maps for SPs of both typical and atypical AFL patients. SPs of typical AFL patients are presented in the top panel, these SPs are clustered in the same region (midaxillary lines, displayed as shaded areas on the surface maps) regardless of the rotation direction. P1 (patient 1) corresponds with the CCW AFL patient presented in Figure 4.4 and P2 corresponds with the example of CW AFL patient presented in Figure 4.5.

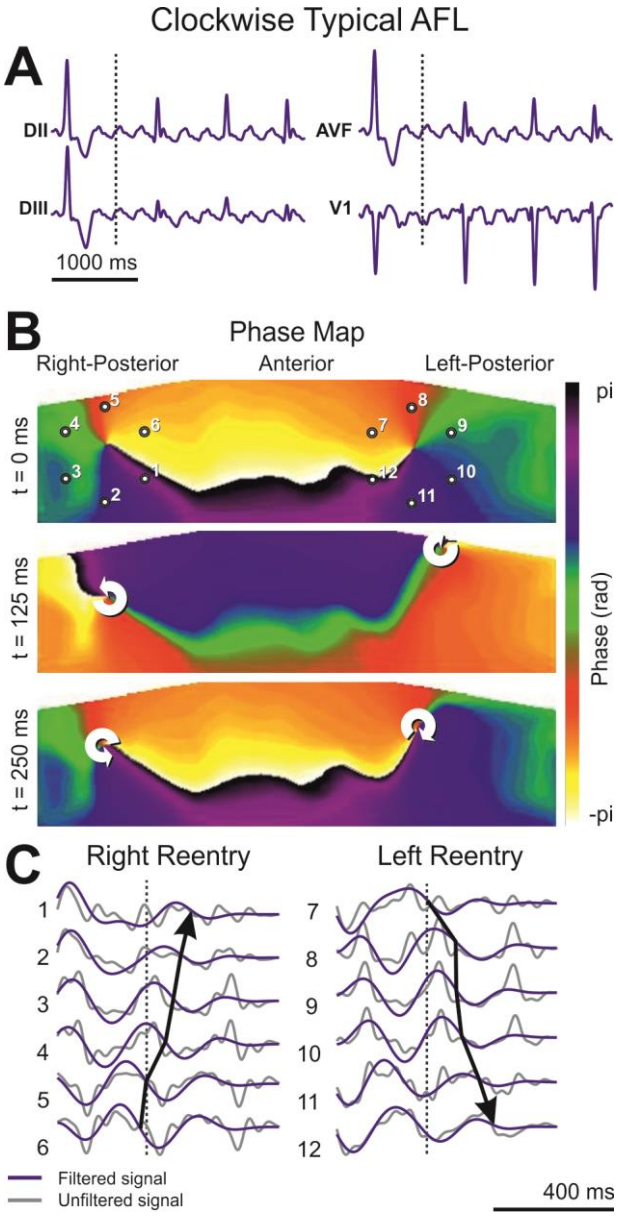

Figure 4.5 – Surface ECG tracings and phase maps in a clockwise typical AFL patient.

Panel A show inferior ECG leads and V1 for clockwise typical (CCW) AFL patient. Stable rotational patterns can be observed in phase maps. Filtered and unfiltered ECG tracings show a reentrant behavior in the torso. In CW typical AFL an ascending propagation in the anterior part of the torso followed by a descending propagation in the back can be observed, with phase singularities placed again in in both midaxillary lines.

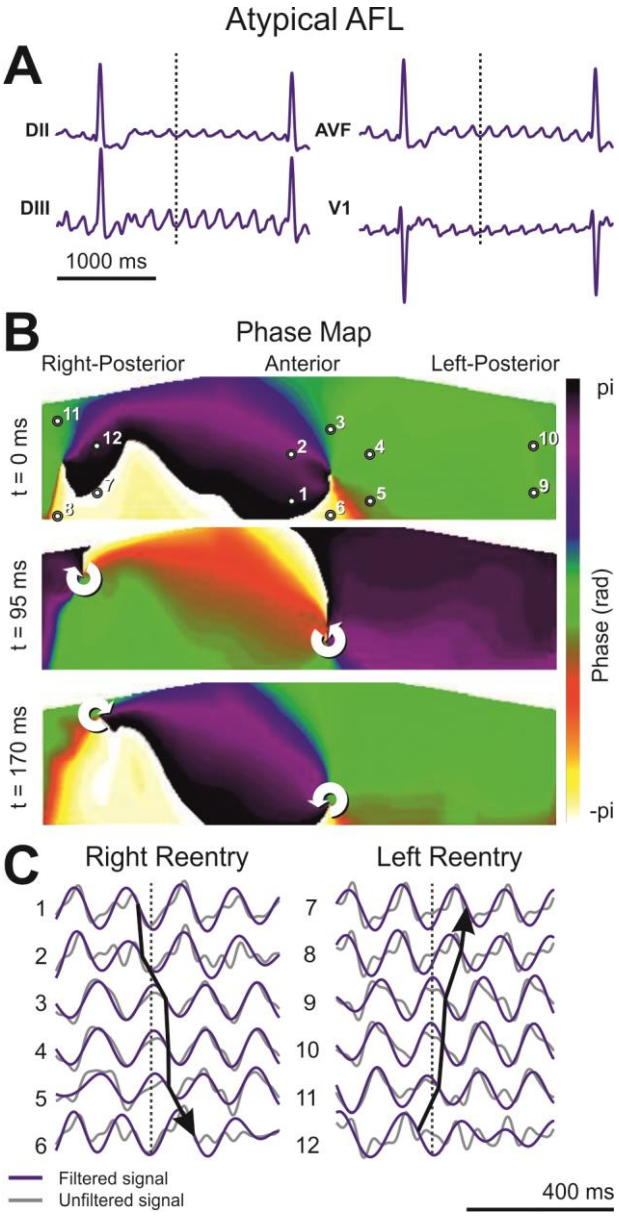

Figure 4.6 – Surface ECG tracings and phase maps in an example of atypical AFL patient.

Panel A show inferior ECG leads and V1 for a patient of atypical AFL. Stable rotational patterns can be observed in phase maps. Filtered and unfiltered ECG tracings show a reentrant behavior in the torso. This example of atypical AFL show a counterclockwise reentrant propagation centered in the in the anterior part of the torso associaded with a clockwise reentrant pattern in the back, with PS situated accordingly.

SPs of atypical AFL patients do not consistently match with the typical AFL SP locations. P9 in Figure 4.7 corresponds with the example shown in Figure 4.6. The presence of SPs is more predominant in the anterior and right–posterior part of the torso, as observed in Figure 4.6. P4 and P5 show a distribution of SPs similar to the observed in P9 anterior and right–posterior part of the torso but with different latitudes. Finally, P6, P7 and P8 presented a scattered distribution on the torso.

Note that in all cases the SPs are clustered in contralateral views of the torso, which is consistent with the figure–of–eight patterns shown in the phase maps. In the case of typical AFL patients and P6 the views correspond with the maxillary lines while in P4, P5 and P9 with the front and back of the torso.

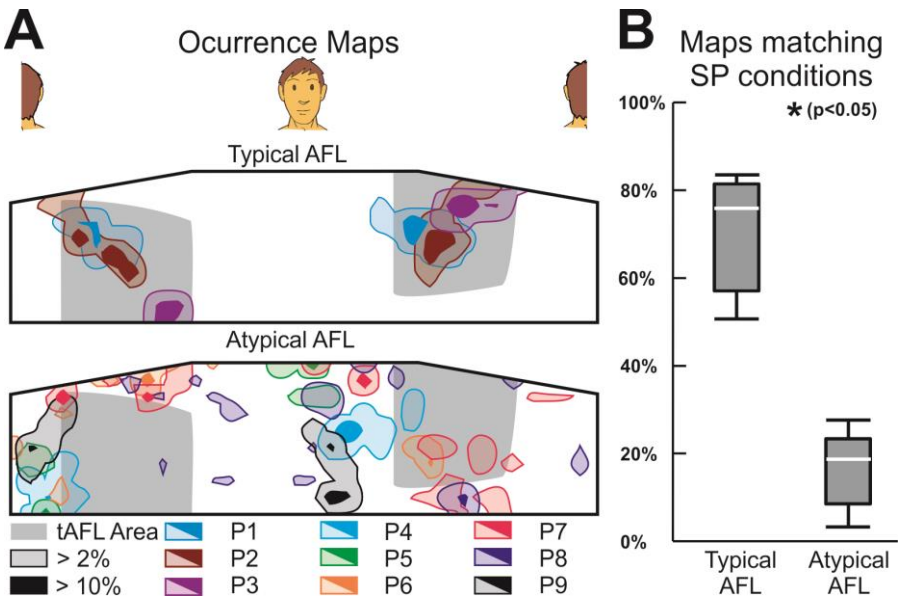

Figure 4.7 – Occurrence maps for singularity points (SP) typical and atypical atrial flutter (AFL) patients.

In panel A, the anatomical regions at which SPs were detected during more than the 10% (solid colors) and 2% (shaded colors) of the analyzed maps are depicted for each patient. Occurrence maps of typical AFL patients present clustered SPs whereas SPs in atypical AFL patients are more scattered and do not match with typical AFL locations. The gray shading represents the typical AFL area (tAFL), right and left areas were used to evaluate if the maps contained two simultaneous SPs in these regions. In Panel B, a box plot representing the percentage of maps that accomplished SP conditions for both typical and atypical AFL patients is shown. Significant differences can be observed between both groups.

By defining the shaded area in Panel A of Figure 4.7 as the typical AFL SP area (tAFL Area), we evaluated the number of maps for each patient that presented simultaneously an SP in each of the two defined tAFL areas. In the case of typical AFL patients 70.78±16.17% of their maps accomplished the conditions described. Opposedly, 5.15±10.99% ($p<0.05$) of maps matched these conditions for atypical AFL patients. It is depicted in the boxplot in Panel B.

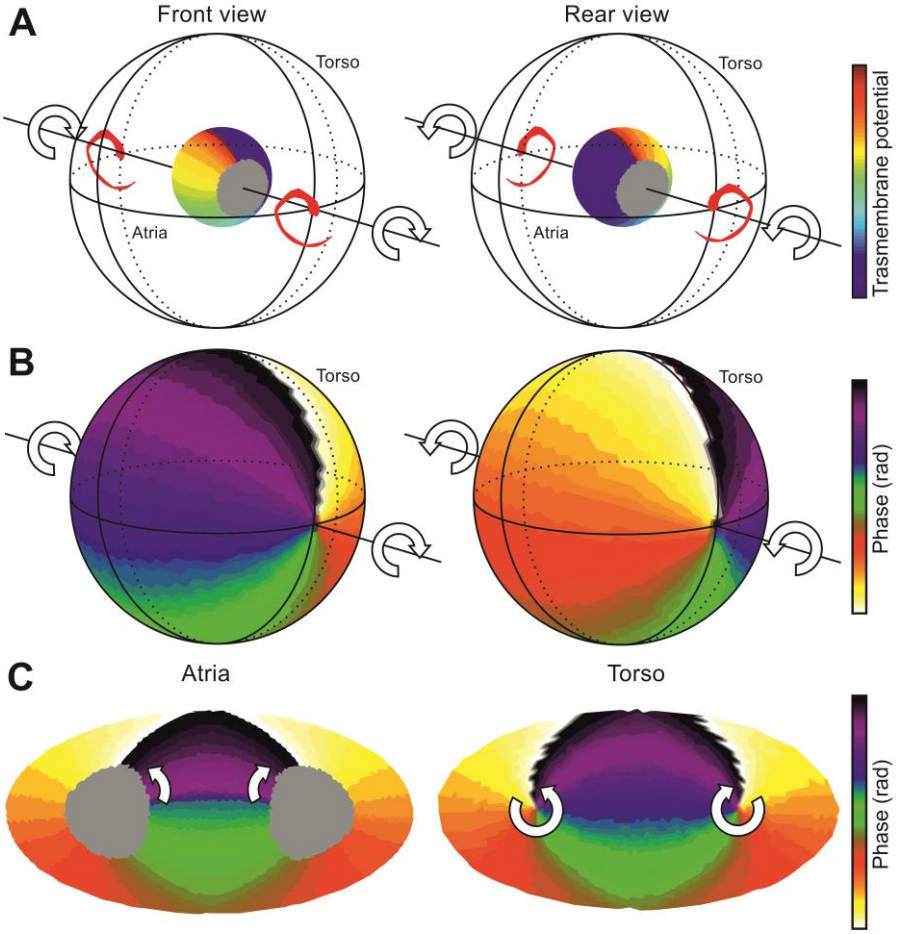

Figure 4.8 – Illustration of the torso representation of an anatomical reentry. *The figure shows two opposing viewpoints of a simulated activity in a model that includes atrial tissue, torso volume and torso surface. Atrial voltage maps are represented according to a color scale from blue to red (color bar scale). The atrial activity consists of a stable reentry around an anatomical obstacle (panel A). Propagation of electrical activity on the outer sphere results into a rotational pattern in the phase maps with singularity points at the rotation axis. Representation into an unfold sphere of the torso electrical activity appears as a figure–of–eight reentry that corresponds to a rotation in the atria (panel C).*

4.3.2 Understanding torso phase maps

Notice that the surface phase maps of AFL patients display a figure–of–eight pattern. Computer simulations of a rotational pattern in a spherical model show that this figure–of–eigth pattern appears as the projection of a single rotation on two contralateral views (see Figure 4.8) and does neither imply a dual–loop reentry nor the existence of functional rotors. SPs on the surface arise in the intersection of the axis of rotation of the propagation with the surface of the torso and thus appear at the same location for a given propagation circuit regardless of the rotation direction.

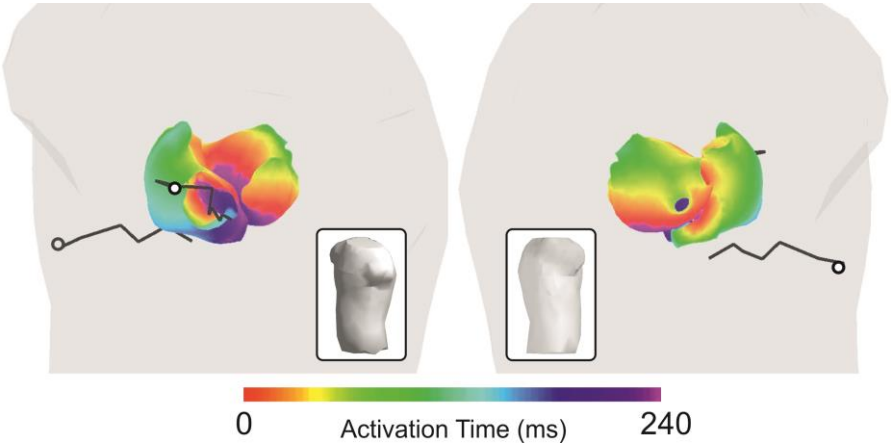

Figure 4.9 – Singularity points from atria to torso, in a simulation of typical AFL.
The figure shows both atria and torso, from two different angles; the left panel shows a view from the left–anterior part of the torso as depicts the sketch of the torso, and the right panel corresponds to a view from the left posterior part of the torso. Activation time of each part of the atria is presented in the model, a counterclockwise propagation around the tricuspid valve can be observed. SPs obtained in the nine layers covering the volume from the atria to the torso are connected with a black line, finally SPs in the torso are highlighted with a white dot.

The spherical model has the advantage that because of the geometrical simplicity the propagation in the torso is easily extrapolated from that observed in the atria. However, in the case of realistic atria the contribution of wave fronts propagating in different planes makes harder the estimation of torso propagation. With this aim we evaluated the location of SP from atria to torso by using the multilayer model shown in Figure 4.3.

Figure 4.9 shows the evolution of SPs from the atria to the torso, in the case of a typical AFL where a counterclockwise reentry around the tricuspid valve with an ascending propagation in the left atria can be observed. We define filament as the connection between SPs in the different layers. It can be observed how in the most internal layer SPs are closer to the center of the reentrant circuit, and how the filament is slightly deflected according to the weight of the electrical activity observed in the realistic model. It means that, as the descending propagation corresponds only to that observed in the right atria free wall and the ascending propagation both to the septum and left atria this imbalance of electric charge results in a deflection of the filament to the anterior part of the torso. This explains the placing of SPs depending on the reentrant circuit in the atria. The SPs in the outer layer occupy positions close to that previously observed in patients, as will be described in the following sections.

4.3.3 Surface representation of simulated typical and atypical atrial flutter episodes

In silico models were used to calculate torso phase maps in different episodes of macroreentrant tachycardias (i.e. typical and atypical flutters). With the atria and torso models depicted in Figure 4.2 and the methods described, it was possible to obtain occurrence maps of SPs to check the capabilities of phase maps as a technique to discriminate the circuits of AFL from the SPs detected in the torso. In parallel, the standard leads for each case were calculated and depicted in order to validate the results. Figure 4.2 shows the locations of the points used to calculate standard leads: Right Arm, Left Arm, Left Leg and V1.

Figure 4.10 shows, a simulation of counterclockwise typical AFL, in which a re–entry around the tricuspid valve can be observed. In the right atrial septum, the propagation has an upward direction, and then a downward propagation was observed in the right atrial free wall. Finally, the circuit crosses the tricuspid annulus and the inferior vena cava to restart the circuit. The whole reentry around this circuit has a period of 242 ms. On the other hand, in the left atrium, it is observed an upward propagation from the base to the pulmonary veins, that takes 175 ms. Both the highest (ms 130) and lowest (ms 195) part of both atria are reached at the same time.

Looking at phase maps (Panel B) we can observe three phase maps in three instants of the same period. A downward propagation in the front part of the torso followed by an ascending propagation in the back can be observed, as depicted in three sequential maps. Two SPs are fixed in the midaxillary lines, which is in accordance with the results observed in patients. Note that in silico phase maps show the whole torso from clavicles to the top of the pelvic region, while patient register only takes the rib cage.

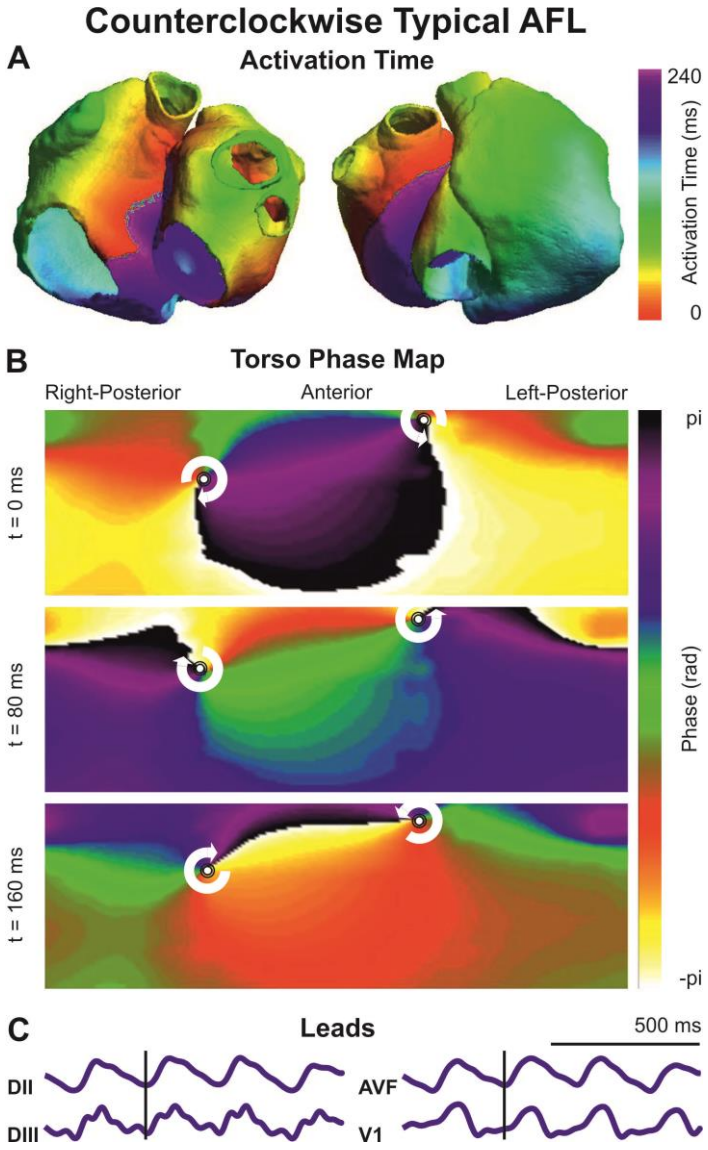

Figure 4.10 – Isochrone maps, phase maps and surface ECG tracings in a simulation of counterclockwise typical AFL.

Panel A shows the isochronal map in the atria illustrating a reentrant behavior around the tricuspid valve. Panel B shows the phase maps for three different instants in the same period, two SPs remain fixed in the midaxilliary lines and are surrounded by a craniocaudal propagation pattern on the anterior torso and the opposed direction on the back. Finally, panel C shows the standard derivations most representative of atrial flutter, the tracings representative of typical were observed in the inferior leads and positive deflections were obtained in V1.

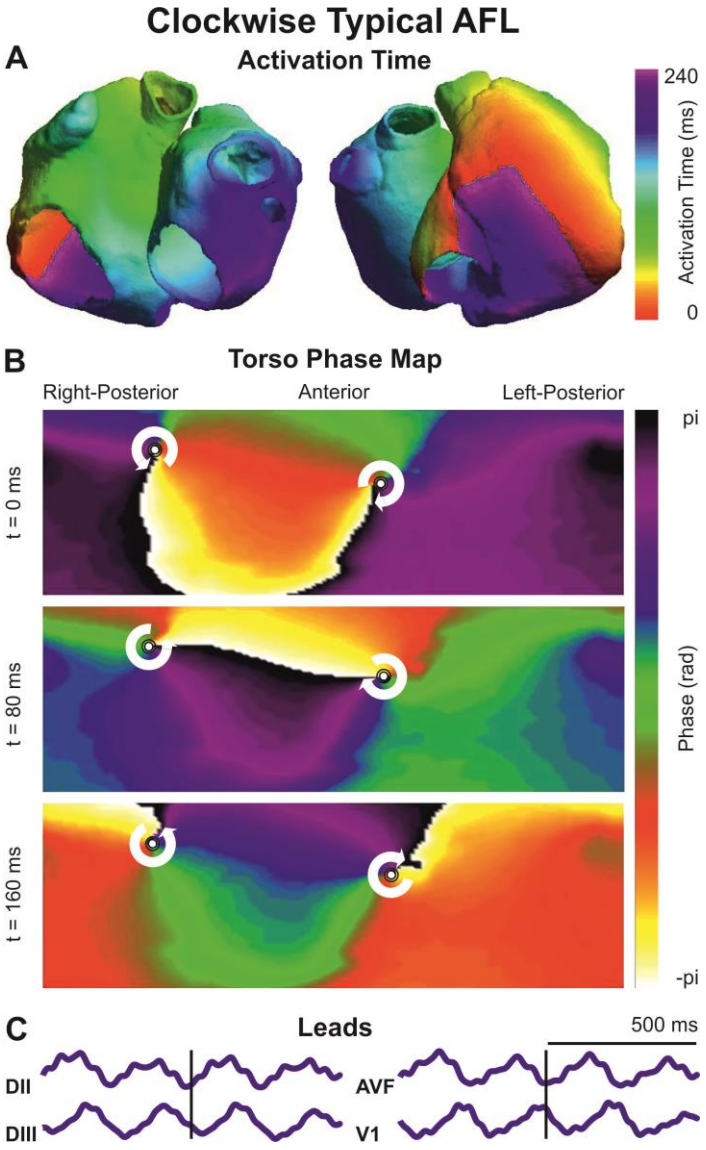

Figure 4.11 – Isochrone maps, phase maps and surface ECG tracings in a simulation of clockwise typical AFL.

Isochronal map in Panel A shows a clockwise reentry around the tricuspid valve. Phase maps present again two SPs in the midaxilliary lines, in this case a caudocranial propagation is observed in the front of the torso and a craniocaudal propagation in the back. It should be noted the W pattern presented by V1, which is representative of clockwise typical AFL. DII and AVF present fractionation due to the small distance between the right arm point and the SP, DIII shows the distinctive tracing of typical AFL.

With respect to standard leads, biphasic and positive deflections in V1, signal representative of counterclockwise typical AFL can be observed. Besides, the complex undulation in inferior leads is also obtained: a slow descending slope followed by a pronounced negative slope and finally an ascending slope that ends with a positive deflection that connects with the following period. In the case of DIII a fractionated signal can be observed due to the proximity between the recording point and a SP. The period of the signals corresponds to that observed in the reentry circuit, 242 ms.

According with previous works ***(Sasaki 2013)***, the ascending slope in AFL tracings corresponds with the depolarization of the upper part of the right atrial free wall, and the positive deflection with the lower part of the wall, the slow descending slope corresponds to the slow propagation across the cavotricuspid isthmus, finally the more pronounced descending slope corresponds to the propagation in the interatrial septum. The positive deflection in V1 corresponds to the wave propagation in the right atrial free wall.

Isocronal maps in Figure 4.11-A depict a clockwise reentrant activity around the tricuspid valve. An ascending propagation in the right atrial free wall was leaded by the crista terminalis, after 68ms the propagation reached the septum and started a descending propagation, that got the area of the tricuspid annulus in the milisecond 150. Then, the reentrant circuit crossed the area which includes the inferior vena cava and the tricuspid annulus to restart the following period after 242 ms.

With respect to the left atria the propagation got the structure through the Bachmann's bundle that is activated at ms 80, just after the superior vena cava had been fully activated. The whole left atrium was depolarized in millisecond 227, being the area between the mitral valve and the left pulmonary veins the last to be depolarized.

Regarding the phase maps, three different maps corresponding to three time instants in a single period can be observed in Figure 4.11-B. Two SPs remain in the midaxilliary lines surrounded by a caudocranial propagation pattern on the anterior part of the torso and the opposed direction on the back.

DII and AVF presented important fractionation, that is due to the proximity between an SP and the right arm ECG lead. In the case of DIII, the shape of the waveform is similar to that described for counterclockwise typical flutter according to that observed in patients. In parallel, V1 shows the negative waves with the W shape characteristic of counterclockwise AFL at the bottom of the signal. This W shape corresponds with the propagation through the right atrial free wall, which matches in time with the upward slope followed by a positive deflection observed in DIII.

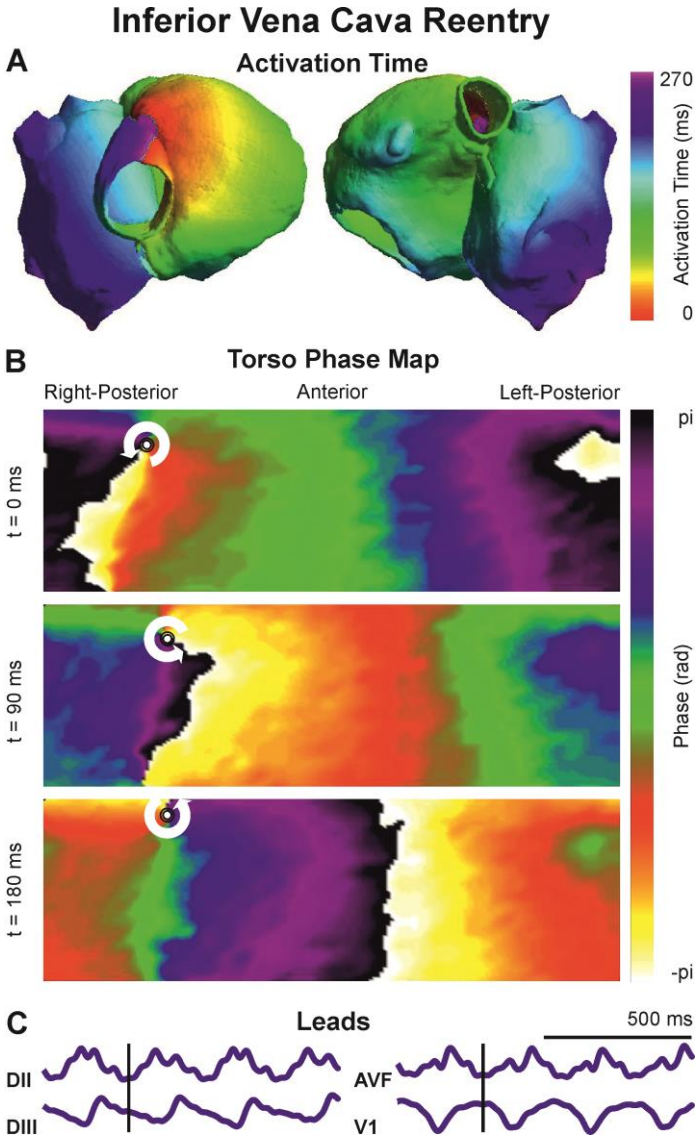

Figure 4.12 – Isochrone maps, phase maps and surface ECG tracings in a simulation of a clockwise reentry around the inferior vena cava.

With a period of 270ms, a clockwise reentry around inferior vena cava is presented in Panel A. A SP is located in the top of the right–posterior part of the torso, in the top of the left posterior part of the torso a point where phase propagation converge can be observed. Fractionated tracings can be observed in DII and AVF due to the proximity between the right arm lead and the SP, a positive wave with a pronounced upward slope followed by a smooth downward slope is present in DIII. V1 shows positive waves.

A simulation of a clockwise reentrant behavior around the inferior vena cava is described in Figure 4.12. We will start by describing the reentry from the area that connects the inferior vena cava and the crista terminalis: an spread towards the superior vena cava accompanied by the reentrant propagation through the inferior vena cava can be observed. After 120 ms, the propagation reaches the superior vena cava and the Bachmann's bundle In ms 199, the tricuspid valve was fully depolarized, whereas the whole atria was completely depolarized in ms 269, being the area between the left pulmonary veins and the mitral valve the last area to be depolarized. At this time a new cycle begins with the same propagation pattern.

Phase maps show a propagation from right to left on the front of the torso. A SP is also observed on the top of the right posterior part of the torso with a counterclockwise activity around it. It is also observed that there is a sink in the propagation of phase on the upper part of the posterior torso.

DII and AVF show fractionation due to the close distance between the right arm electrode and the SP. DIII shows a steep upward slope followed by a positive deflection and a gentle downward slope. V1 presents a negative deflection, both this deflection and the complex formed by the positive slope and the positive deflection in DIII, correspond to the depolarization of the right atrial wall. The period of the tracings is again 270 ms, which matches with the rotational period.

A macro–reentry around the 4 pulmonary veins with a functional block region is shown in Figure 4.13. Panel A shows a period of the re–entry. Starting with the left pulmonary veins we can observe a propagation that after 80 ms reaches the right pulmonary veins. Shortly after, the front invades the right atrium through the Bachmann's bundle. The counterclockwise cycle around the pulmonary veins ends in the left atrium after 240 ms. On its side, the right atrium completes its depolarization in coordination with the beginning of the new period with an irregular front around crista terminalis.

In panel B, phase maps show a counterclockwise reentrant activity in the upper portion of the posterior torso and a clockwise activity in the anterior torso, showing two SPs in these locations. Note that the upper part of the back is the closest to the pulmonary veins area.

With regard to standard leads, we can see that the inferior leads show no recognizable patterns but allow determining the reentrant rate, however minor alterations due to the low frequency activity promoted in the functional block area are also present. V1 has an important fractionation as it is near the area of the SP.

The simulation in Figure 4.14 corresponds with one similar to that shown in Figure 4.13, but because the decrease in conductivity in the functional block region was less prominent, the reentry managed to rotate around the left pulmonary veins, and the propagation crossed between left and right pulmonary veins. However, in this case, the irregular activity in the region of the pulmonary veins promoted a propagation pattern to the rest of the atria that differed from one period to the next in consecutive time periods.

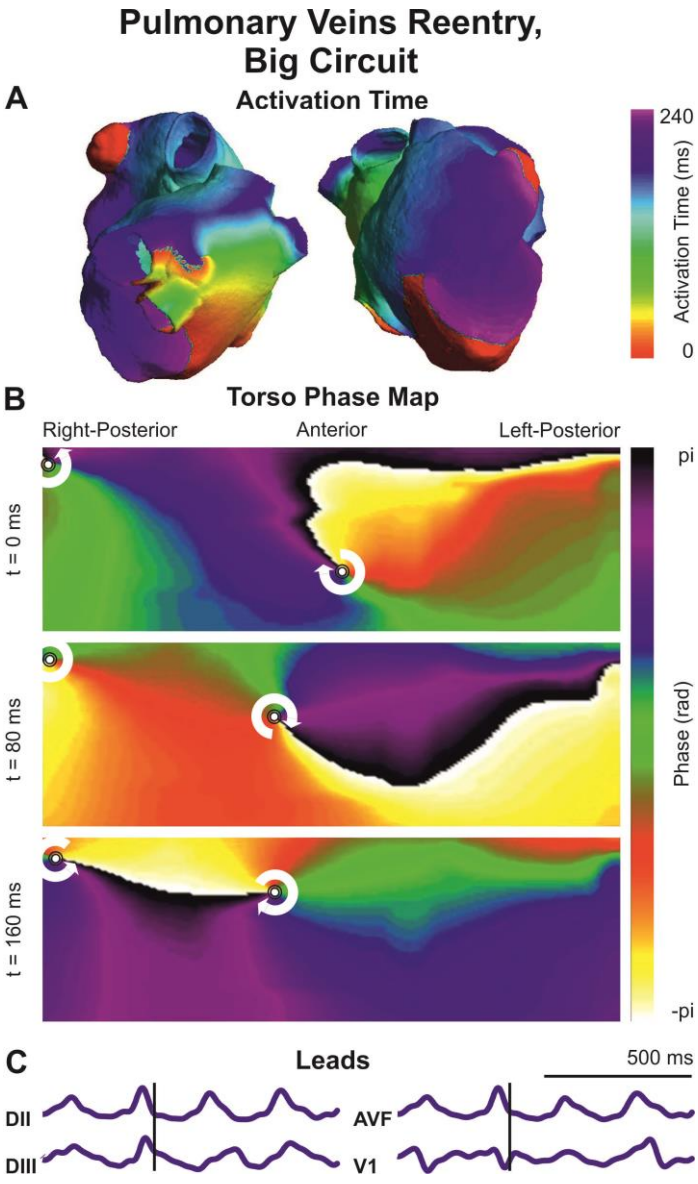

Figure 4.13 – Isochrone maps, phase maps and surface ECG tracings in a simulation of a counterclockwise reentry around the pulmonary veins.

Panel A shows isochrone maps in a case of a counterclockwise reentry around the pulmonary veins that acts as a functional block area.. Two SPs are located in the center of the front and back of the torso, with a clockwise propagation in the front and a counterclockwise propagation in the back. Tracings in the inferior leads show two to one patterns, V1 presents a fractionated signal according with the SP in the anterior part of the torso.

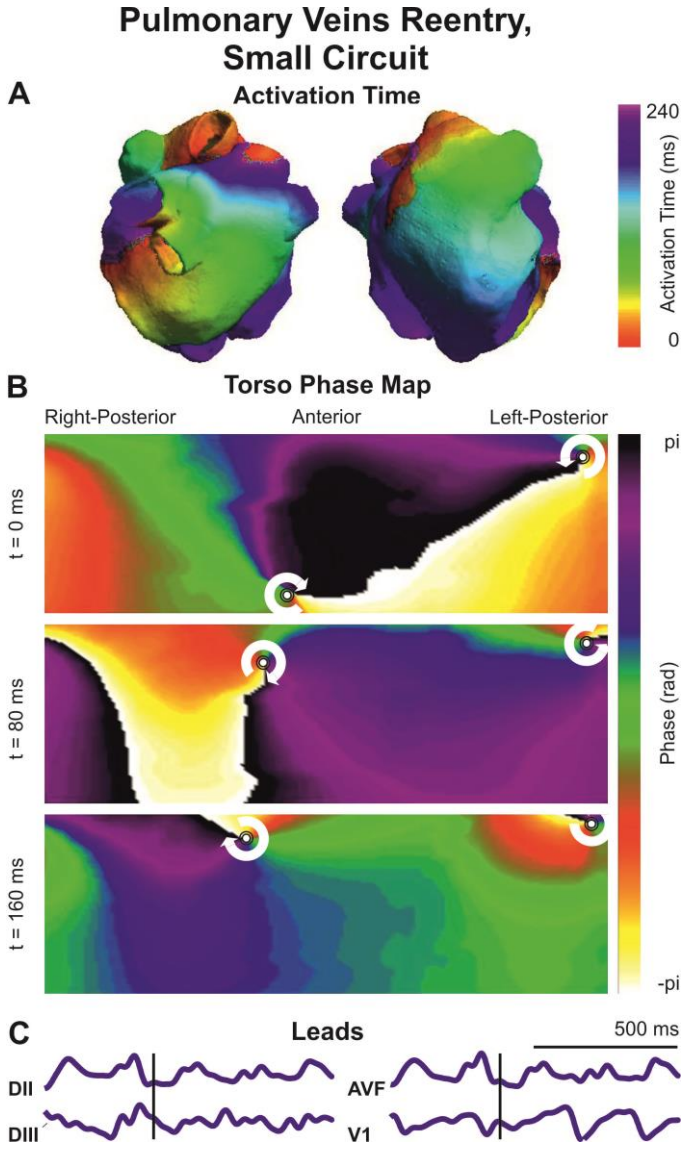

Figure 4.14 – Isochrone maps, phase maps and surface ECG tracings in a simulation of a counterclockwise reentry around the pulmonary veins.
Isochrone maps in Panel A corresponds to a simulation of a reentry around the left pulmonary veins. After band pass filtering around the frequency of the reentry, two SPs located in the center of the front and back of the torso, with a clockwise propagation in the front and a counterclockwise propagation in the back can be observed. In this case due to an irregular propagation in the whole atria irregular tracings are observed in the ECG leads.

The reported irregularity of the propagation pattern is reflected as irregular tracings in ECG leads and they resemble those reported in cases of atrial fibrillation. Phase maps after filtering show again a stable SP in the top of the back with a counterclockwise propagation according to that observed in the pulmonary veins and a counterclockwise propagation on the posterior part of the torso.

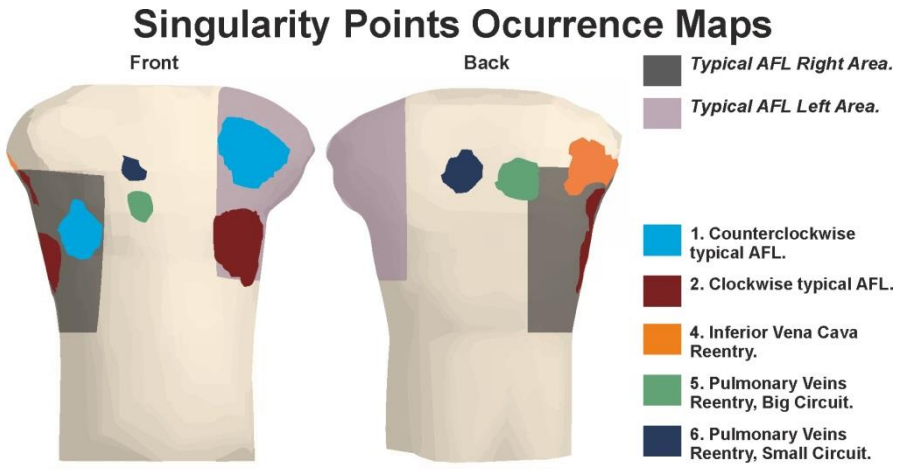

Figure 4.15 – Singularity Points occurrence maps in simulations.
The regions that show an occurrence of SPs higher than a 10% are depicted for each simulation. Gray shadings represent the typical AFL regions, right and left areas were used again to evaluate if the maps contained simultaneously a SP in each area.

Figure 4.15 shows the areas of the torso where a SP can be detected for more than 10% of the phase maps in each case. Typical AFL SP areas are depicted by the shaded areas in gray. As in the case of patients, the percentage of phase maps with points contained simultaneously in both areas has been evaluated. In the case of the counterclockwise and clockwise typical AFL, 100% and 69.87% of maps respectively satisfied the condition. However, in the case of atypical flutter simulations only 2.12% of maps satisfied this condition for the reentry around inferior vena cava and 0% and 6.98% in the big and small circuits around pulmonary veins. It reflects a significant difference using this criteria ($p<.01$).

It can be observed that the locations of SPs correspond to that described from Figure 4.10 to Figure 4.14 previous figures.

4.3.4 Detection of the reentrant frequency from the torso

Computer models were used to assess the ability to detect the rotation period of reentries in AFL from the torso surface. We used the Fast Fourier transform to detect both in the computed ECGs and EGMs the dominant frequency with resolution 0.5 Hz. In the case of typical AFL, the reentries around the inferior vena cava and the big circuit around pulmonary veins 91.20±8.63% ECG signals presented as dominant frequency the observed in the reentry. Moreover, in the EGMs, the frequency of reentry was detected in 90.19±10.63% nodes. The case of the small reentrant circuit in pulmonary veins showed the frequency of the reentry in the 56.87% of the EGs and in the 58.97% of the ECGs.

This shows the ability to estimate the dominant frequency of the reentry from the ECG leads in the case of AFL.

4.4. Discussion

4.4.1 Main findings

In this study, body surface phase maps are proposed as a non–invasive technique to distinguish between cavotriscupidius dependent and non–dependent atrial macroreentries. We show that phase maps of surface potentials from patients with AFL display characteristic figure–of–eight patterns that arise as a projection of a single rotation into two contralateral views. SPs location on surface phase maps is determined by the intersection of the rotation axis with the surface of the torso, and thus is distinct depending on the rotation circuit. This may allow a noninvasive determination of the rotation circuit in complex atypical AFL.

The technique has been evaluated both in patient recordings and by using computational modeling. For typical AFL patients we observed that SPs were located in limited regions around axillary lines. However, in the case of patients of atypical AFL the location of SPs were not included in these areas. The same applies in the case of computer modeling simulations where we verified that the location of the SPs depends on reentry circuit. It can be observed that in these cases the points may be associated with a projection of the obstacle on the surface of the torso, although some deviation is produced by the propagation through the rest of the atria, as depicted in Figure 4.9.

To stabilize the reentrant spread on the torso surface and help visualize the points, the signals at the torso were band–pass filtered with a bandwidth of 4 Hz around the frequency of re–entry. In the case of patient recordings, this frequency was estimated as the most repeated dominant frequency between all electrodes, it is consistent with the analysis of dominant frequencies in models presented. This is consistent with previous work by the group where it is used band–pass filtering to stabilize the points on the torso and to evaluate the projection of the filaments

(Rodrigo 2014b). Figure 4.14 shows how it is possible with this technique to identify the location of reentrant mechanisms both in the case of AFL and atrial fibrillation.

4.4.2 Noninvasive diagnosis of atrial flutter from the surface ECG

The surface ECG is routinely used for stablishing the diagnosis of AFL because of its characteristic ondulating pattern. The ECG can also be used for a first identification of the circuit involved in the reentry ***(Medi and Kalman 2008)***. A sawtooth pattern in the inferior ECG leads is suggestive of a CTI–dependent AFL. However, age–related fibrosis, pulmonary disease and prior surgery can alter the surface ECG signals ***(Krummen 2006, Saoudi 2001, Akar 2007)*** and 13% of patients with CTI–dependent circuits had neither sawtooth waves nor RR regularity ***(Krummen 2010)***. Our presented phase maps may be less sensitive to these alterations since subtle changes in propagation direction will not alter the overall rotational pattern.

Less commonly, the reentrant circuit involves anatomical locations different that the CTI. In these cases, classified as atypical atrial flutter, analysis of atrial waves on the standard ECG does not report feasible information about the reentrant circuit since there is high variability either in terms of shape, base line or frequency ***(Garcia-Cosio 2012, Jais 2000, Kall 2000, Yang 2001)***. In particular, differentiation between left and right AFL has motivated many previous works ***(Bochoeyer 2003)***. Left atrium AFL has been shown to present shorter cycle lengths than isthmus dependent AFL in post–radiofrequency MAZE patients ***(Akar 2007)*** and lower spatial coherence ***(Kahn 2007)***, which is consistent with our scattered SP histograms in some AFL patients.

As an alternative approach to the standard ECG, Sippensgroenewegen et al. ***(SippensGroenewegen 2000)*** proposed the use of integral maps obtained from body surface potential recordings to identify patients with typical AFL. However, it has not been shown that integral maps of atypical AFL patients allow discrimination from typical AFL patients. Here we have shown that phase maps of atypical AFL patients differ from those of typical AFL patients because of their different rotation axes and could be used for classification of patients into CTI–dependent or non–CTI–dependent groups.

4.4.3 Phase analysis of atrial arrhythmias

Phase maps and SPs are commonly used to identify re–entrant patterns in the atrial wall in animal models or in inverse–computed solutions ***(Yamazaki 2012, Zlochiver 2008, Haissaguerre 2013)*** since they allow summarizing the propagation pattern without the need for activation detections which are highly

sensitive to noise. More recently we have shown that they can also be used for characterizing spatial reentrant patterns in the torso surface of atrial fibrillation patients ***(Rodrigo 2014b)***. Here, we further explore the ability of phase maps to represent rotational patterns in the torso surface which may not be univocally linked to functional rotors but to rotations around anatomical obstacles as well. Although surface representation of both entities is similar, they can be easily differentiated because of the differences in the rotation frequency, below 5 Hz in AFL, and in their spatio–temporal stability, since centers of rotational activity in atrial fibrillation tend to drift.

4.4.4 Limitations and future work

In this work we have shown that the location of phase singularities in surface maps is different for typical and atypical AFL patients. However, because of the limited number of patients included in our study we could not quantify its diagnostic value. A prospective study in a larger database should be performed in order to determine the sensitivity and specificity of the proposed criterion for the diagnosis of CTI–dependent AFL circuits.

Since the identification of the reentrant circuit was not accomplished in the electrophysiological laboratory in non–CTI–dependent patients, we cannot relate the location of surface PSs and the anatomical location of the reentrant circuit in this group of patients. Further studies should be performed in order to explore the ability of surface phase maps to identify atypical AFL circuits.

Finally, the proposed phase map analysis requires at least two atrial waves free from ventricular content, to avoid detection of SPs corresponding to ventricular activity. In this work we have performed carotid sinus massage in order to reduce the heart rate, which should not be performed in patients with carotid sinus hypersensitivity.

With respect to computational modeling, we simulated a representative behavior for typical flutter or reentrant patterns around areas with low conductivity that promoted functional block areas or obstacles. However the variability of reentry circuits, conduction velocities etc. is very high in patients. Besides, the method of resolution of the forward problem considered the torso homogeneous medium, small deviations may be expected in SPs caused by refraction in different tissues, however main conclusions presented here should hold.

As presented in Figure 4.14 the technique can be extended for the detection of reentrant activity in atrial fibrillation episodes. For many authors ***(Atienza 2006, Rodrigo 2014b, Mansour 2001),*** high frequency rotors are nowadays the target for ablation in patients suffering of atrial fibrillation, so the noninvasive location of the regions containing rotors is an objective of our research group.

4.4.5 Conclusion

Using noninvasive phase mapping during atrial macroreentries, different propagation patterns can be identified that are dependent on the anatomical structure that sustain the reentrant circuit. This mapping procedure may help in patient treatment selection both to decide if an ablation procedure would be feasible and to plan the ablation procedure.

Chapter 5

Role of Main Ion Channel Currents on Atrial Fibrillation Electrophysiological Characteristics: An In Silico Inter–subject Variability Study

5.1. Introduction

Atrial fibrillation (AF) is the most common arrhythmia in the clinical practice ***(Haissaguerre 2000, Pedersen 2006)***. Treatment of the arrhythmia needs from a deeper understanding of the ionic mechanisms responsible of the maintenance of AF, as antiarrhythmic strategies used nowadays have a modest efficacy at the time of terminating the arrhythmia and sustaining sinus rhythm in patients with long–standing AF ***(Nattel 2008, Wettwer 2013)***. One of the main explanations for this lack of success on chronic AF patients is the modifications on AF substrate and perpetuation mechanisms due to prolonged episodes of the arrhythmia. Sustained AF promotes remodeling in the atrial substrate that modifies the characteristics of reentrant activity (e.g. dominant frequency, rotor tip meandering, wavefronts curvature, etc.) easing the susceptibility to maintain AF ***(Jalife 2011, Pandit and Jalife 2013)***. Understanding the ionic mechanisms that govern the maintenance of AF drivers under a remodeled substrate may allow the development of more effective antiarrhythmic drug treatments. However, the process of remodeling and its effects on the interaction between ion channel currents depends on the underlying clinical scenario and genetics of each patient ***(Walmsley 2013, Sanchez***

2014), which may result in different perpetuation mechanisms from patient to patient.

The goal of the present study is to identify the role of each ionic current in the characteristics of AF drivers in order to suggest personalized pharmacological strategies to terminate the arrhythmia. Specifically, a population of 173 mathematical models of human atrial tissue with realistic inter–subject variability was developed based on action potential biomarkers extracted from microelectrode recordings of patients diagnosed with AF. These mathematical models capturing variability in experimental measurements were used to evaluate the role of each ionic current in the dynamics of functional reentries and to test the hypothesis that the same antiarrhythmic treatment may have completely different effects on AF characteristics depending on the basal expression of different ion channels.

5.2. Methods

5.2.1 Experimental Dataset and Biomarkers

Right atrial appendages from 149 patients diagnosed with chronic AF and who underwent cardiac surgery for myocardial or mitral/aortic valve replacement revascularization were obtained. Experimental data was recorded from human samples conforming the declaration of Helsinki, additionally the study was approved by the Ethics Committee of the Dresden University of Technology (Nº EK790799). All patients gave written, informed consent. Antiarrhythmic medication was interrupted before the study ***(Sanchez 2014)***.

Standard intracellular microelectrodes were used to record action potentials (APs) in atrial trabeculae of the samples described (n=215 of 149 patients) ***(Wettwer 2004, Wettwer 2013)***. Properties of bath solution (in mM): NaCl 127, KCl 4.5, $MgCl_2$ 1.5, $CaCl_2$ 1.8, glucose 10, $NaHCO_3$ 22, NaH_2PO_4 0.42, equilibrated with O_2–CO_2 [95:5] at 36.5±0.58 °C, pH 7.4. The preparations were stimulated at 1 Hz no less than 1 h before data acquisition ***(Wettwer 2004, Wettwer 2013)***. A subset of this database (n=9 preparations) was also recorded at different pacing frequencies f = 1, 2, 3 and 4 Hz.

Variability in APs was quantified by the following biomarkers: APD (AP duration) at 20, 50, and 90% of repolarization (APD20, APD50, APD90 respectively), AP amplitude (APA), resting membrane potential (RMP) and AP plateau potential at 20% of APD90 (V20). Graphical representation of these parameters is given in Figure 5.1.B.

In addition to the 1Hz static biomarkers, a rate dependent biomarker (APDratio) was defined as the ratio between the APD at each certain rate (i.e. 2, 3 and 4Hz) divided by the APD at 1 Hz. This biomarker was measured for each pacing rate both for APD50 and APD90, as they were the most sensitive biomarkers to the pacing rate.

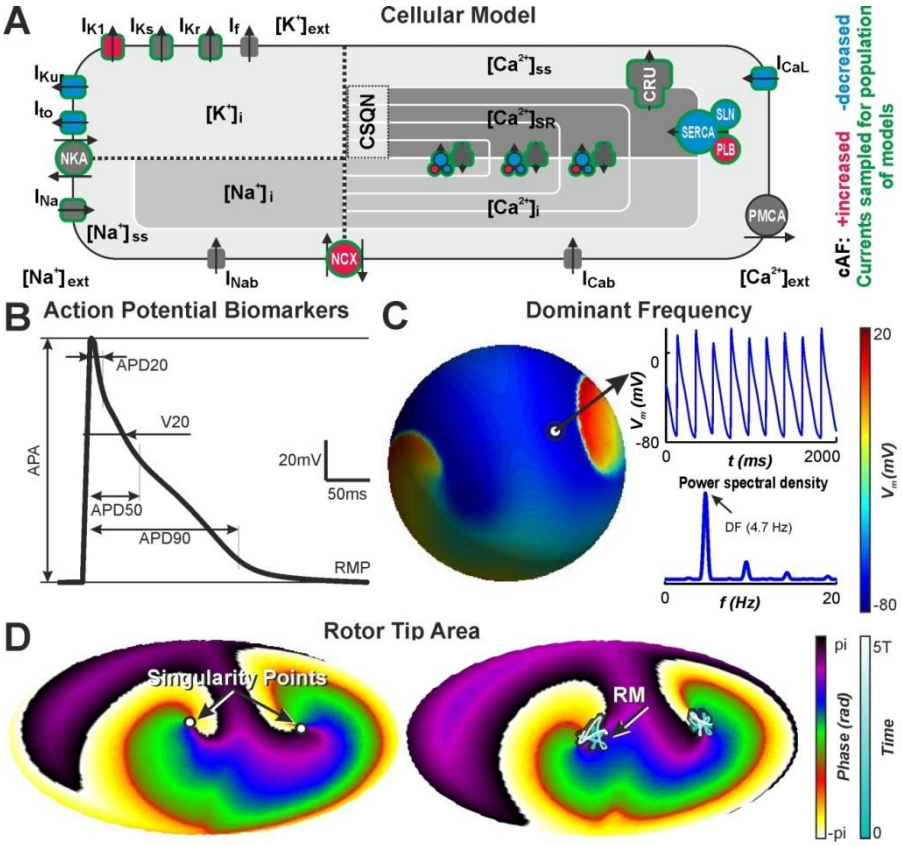

Figure 5.1 – Parameters and biomarkers evaluated in the study.

Panel A shows the Koivumaki original sinus rhythmn model. The modifications introduced to account for AF remodeling are depicted in red and blue and the currents that were sampled to obtain the population of models are highlighted in green. In Panel B biomarkers associated to the AP are represented: AP duration at 20, 50, and 90% of repolarization (APD20, APD50, APD90 respectively), AP amplitude (APA), resting membrane potential (RMP) and the potential at 20% of APD90 (V20). Panel C shows the membrane voltage in sphere simulations according to a color scale, transmembrane voltage and power spectral density are also depicted for a given node, illustrating the definition of dominant frequency (DF). Panel D shows phase maps in the sphere by using the Aitoff projection. The sphere on the left shows the detection of the rotor tip that corresponds with singularity points (SPs), the sphere on the right shows the meandering of the rotor tip according to a color scale.

5.2.2. Electrophysiological Cellular Model

As a basis of the study, the atrial myocyte model by Koivumaki et al ***(Koivumaki 2011)*** has been used. As depicted in panel A of Figure 5.1, some modifications have been applied to implement remodeling of chronic AF: I_{CaL} (–59%), I_{to} (–62%), I_{Kur} (–38%), I_{K1} (+ 62%), I_{NCX} (+ 50%), expression of SERCA (–16%) and PLB to SERCA (+ 18%) and SLN to SERCA (–40%). These variations are based on a literature study of different works facing atrial remodeling from different perspectives and with different databases, which are compiled in the work of Koivumaki et al. ***(Koivumaki 2014)***. We will refer to this model as 'baseline AF model'; the model with no modifications associated with the remodeling will be referred as 'Koivumaki original sinus rhythmn model'.

5.2.3. Population of Models

In order to model variability between subjects, a population of human atrial models was generated from the electrophysiological model described above (i.e. 'baseline AF model') by varying the set of parameters depicted in green in panel A of Figure 5.1 from –100% to +200% of the original value: g_{Na}, maximum I_{NaK}, g_{K1}, g_{CaL}, k_{NCX}, g_{to}, g_{Kur}, g_{Kr}, g_{Ks} as well as the expression of cpumps in SERCA and the availability of Ca^{2+} release channels from sarcoplasmic reticulum $J_{rel,RyR}$.

Latin Hypercube Sampling Method ***(Mckay 2000, Britton 2013)*** was used to generate 16.384 combinations of the currents listed above. The method allows the generation of a combination of the N=11 parameters by means of sampling the N–dimensional space with a high resolution, efficiently and without bias. It is implemented by stablishing the inferior and superior and bounds (–100 to +200%) and sampling the range in each parameter in M=16.384 intervals, which results in M^N locations in the N–dimensional space. Then, M of these locations are randomly chosen meeting that, for each dimension N, in no case each interval is chosen more than once.

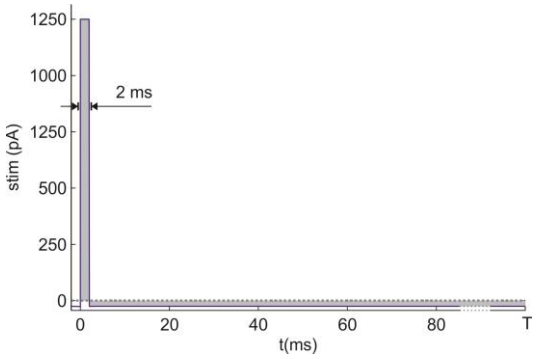

Figure 5.2 – Stimulus pattern used at different frequencies.

The resulting 16,384 unicellular models were simulated at different pacing frequencies: 1, 2, 3 and 4 Hz with square stimulus with duration 2 ms and amplitude 1250 pA (see Figure 5.2), followed by negative amplitude during the inactive time interval to maintain current conservation in the model, and simulate the effect of neighbouring cells in the tissue. Mathematical simulations were performed on the cardiac simulation GP–GPU platform described in Chapter 3. APs from period 91 to 100 were stored at sampling frequency of 1kHz and used to measure the AP biomarkers described above.

A subset of the initial population of 16,384 mathematical models was selected by identifying those that satisfy physiological ranges of the biomarkers identified by using the experimental recordings. The identification of that subset of models was carried out in two different steps.

First, only those models for which biomarkers APD90, APD50, APD20, APA, RMP and V20 at 1 Hz remain restricted to the maximum and minimum values measured experimentally in the 215 APs from right atrial appendages were selected. To ensure biological depolarization transient, two extra constraints in biomarkers were introduced, the time between the stimuli and AP peak must be lower than 20 ms and dV/dt_{max} higher than 20 V/s.

Next, with the aim to ensure that the resulting population reproduces rate dependent properties similar to those present in experimental data, only those models that reproduce physiological rate dependence were selected. Specifically, linear regressions of APDratios vs APD 1 Hz were computed for each frequency (i.e. 2, 3 and 4 Hz) and biomarker (i.e. APD50 and APD90) in the 9 samples recorded at different frequencies. The models that presented APDratios, for APD90 and APD50 at 2, 3 and 4Hz, with an error to the estimated line lower than the observed in experimental data were finally accepted (see panel B in Figure 5.3).

We will refer to the set of models which only satisfied the 1Hz biomarkers as the '1Hz population', whereas the set of models that satisfied both the 1Hz and rate dependent biomarkers will be referred as 'physiological population'.

5.2.4. Role of Ionic Currents on AF Reentrant Mechanisms

The models from the physiological population of models and the baseline AF model from Koivumaki were simulated on a spherical shell of active tissue as described in section 3.1. It consisted of a 3 cm radius sphere incorporating 163,842 nodes, with an average inter–nodal distance of 283.25 ± 18.42 μm ***(Rodrigo 2014b)***. Reentrant activity was induced in the spherical model by using a cross stimulation protocol.

Two seconds of transmembrane voltage maps were analyzed after five seconds of simulation. Fibrillation activity of models that could maintain a reentrant activity was characterized with two different AF characteristic

biomarkers: the dominant frequency (DF) and the area of rotor meandering (RM) (Figure 5.1). Specifically, DF was computed by using the Welch periodogram (1.25 second Hamming window with a 8192 point Fast Fourier Transform per window and 80% overlap). In order to measure RM, phase maps were computed and Singularity Points (SPs) were detected as described in section 3.4. Only SPs that accounted for at least 3 consecutive rotations were considered as sustained reentries. In sustained reentry models, RM was quantified for up to 5 consecutive rotations.

In order to identify main ion channel conductivities involved in the perpetuation of reentries, the 11 modified conductivities were compared between the group of physiological models with sustained reentries vs. models without sustained reentries. In addition, in order to identify the role of each ion current in the electrophysiological characteristics of the AF (i.e. DF and RM), the relation between modified conductivities, the 1Hz AP biomarkers and AF reentrant characteristics was analyzed.

5.2.5 Personalized Effects of Antiarrhythmic Treatments

Finally, in order to test the hypothesis that the same antiarrhythmic treatment may have different effects on the AF characteristics depending on the basal expression of different ion channels, the previous analysis was repeated after the reduction of a 50% of g_{CaL} in all the physiological model spheres that sustained reentries. Specifically, 3D models in which the reduction of I_{CaL} terminated the arrhythmia were compared with those that maintained the reentrant activity. In addition, the effect of I_{CaL} block in both DF and RM and its relation with conductivities and biomarkers was evaluated.

5.2.6. Statistical Analysis

Mann–Whitney U–test was used to evaluate statistical significance between variables, statistical significance was considered for $p<0.01$.

In order to evaluate the role of each parameter (i.e. g_{Na}, maximum I_{NaK}, g_{K1}, g_{CaL}, k_{NCX}, g_{to}, g_{Kur}, g_{Kr}, g_{Ks} and expression of cpumps in SERCA and Jrel in RyR) on each specific biomaker (i.e. V20, APA, RMP, APDs and APDratios), the partial correlation coefficient (PCr) was used. The PCr quantifies the correlation between the parameter (X) and the biomarker (Y) after accounting for the linear effects of one or more additional parameters (Z) ***(Marino 2008, Britton 2013)***, according to Equation 5.1:

$$PCr_{XY,Z} = \frac{r_{XZ} - r_{XZ}r_{YZ}}{\sqrt{1 - r_{XZ}^2} \cdot \sqrt{1 - r_{YZ}^2}} \tag{5.1}$$

where r_{XY} denotes the standard correlation coefficient between the parameter X and the biomarker Y.

5.3. Results

5.3.1. Experimental Dataset and Biomarkers

Minimum and maximum values of the biomarkers measured at a pacing frequency of 1Hz for the 215 analyzed cells are presented in Table 5.1. Notice that their range is too broad and a single mathematical model does not account for the observed variability.

	Minimum Value	**Maximum Value**
APD90 (ms)	140	330
APD50 (ms)	30	180
APD20 (ms)	1	75
APA (mV)	80	130
RMP (mV)	–85	–65
V20 (mV)	–30	20

Table 5.1 – Maximum and minimum values of biomarkers in 1Hz recordings on the 215 analyzed cells.

Regarding rate dependent biomarkers, minimum and maximum values measured in the subset of cells in which those experiments were performed (i.e. 9 cells) are presented in Table 5.2. Notice that not all biomarkers were affected by the increase in the pacing rate; whereas APD90 and APD50 presented a significant reduction at higher rates, the other biomarkers were not as dramatically affected.

5.3.2. Generation of the Physiological Population of Mathematical Models

From the total of 16,384 mathematical models with different combinations of ion channels expression that were analyzed, there were 945 (5.76%) mathematical models with biomarkers inside the measured ranges for 1Hz biomarkers reported in Table 5.1 and constituted our ‘1 Hz population’. Only 173 (1.06%) mathematical models also met the rate dependence constraints and constituted our ‘physiological population’. Therefore, although a large number of ion channel combinations reproduced 1Hz patch–clamp experiments for a pacing rate of 1 Hz, only few of them were physiologically realistic in terms of pacing rate dependence.

	1Hz		2Hz		3Hz		4Hz	
	Minimum Value	Maximum Value	Minimum Value	Maximum Value	Minimum Value	Maximum Value	Minimum Value	Maximum Value
APD90 (ms)	167	236	148	220	134	199	121	176
APD50 (ms)	59	121	65	118	62	108	56	96
APD20 (ms)	4	31	5	45	6	48	6	48
APA (mV)	93	116	93	115	83	113	82	113
RMP (mV)	-84	-69	-84	-71	-84	-74	-82	-70
V20 (mV)	-20	6	-18	8	-22	8	-17	6

Table 5.2 – Range of measured biomarkers for cells at different pacing rates.

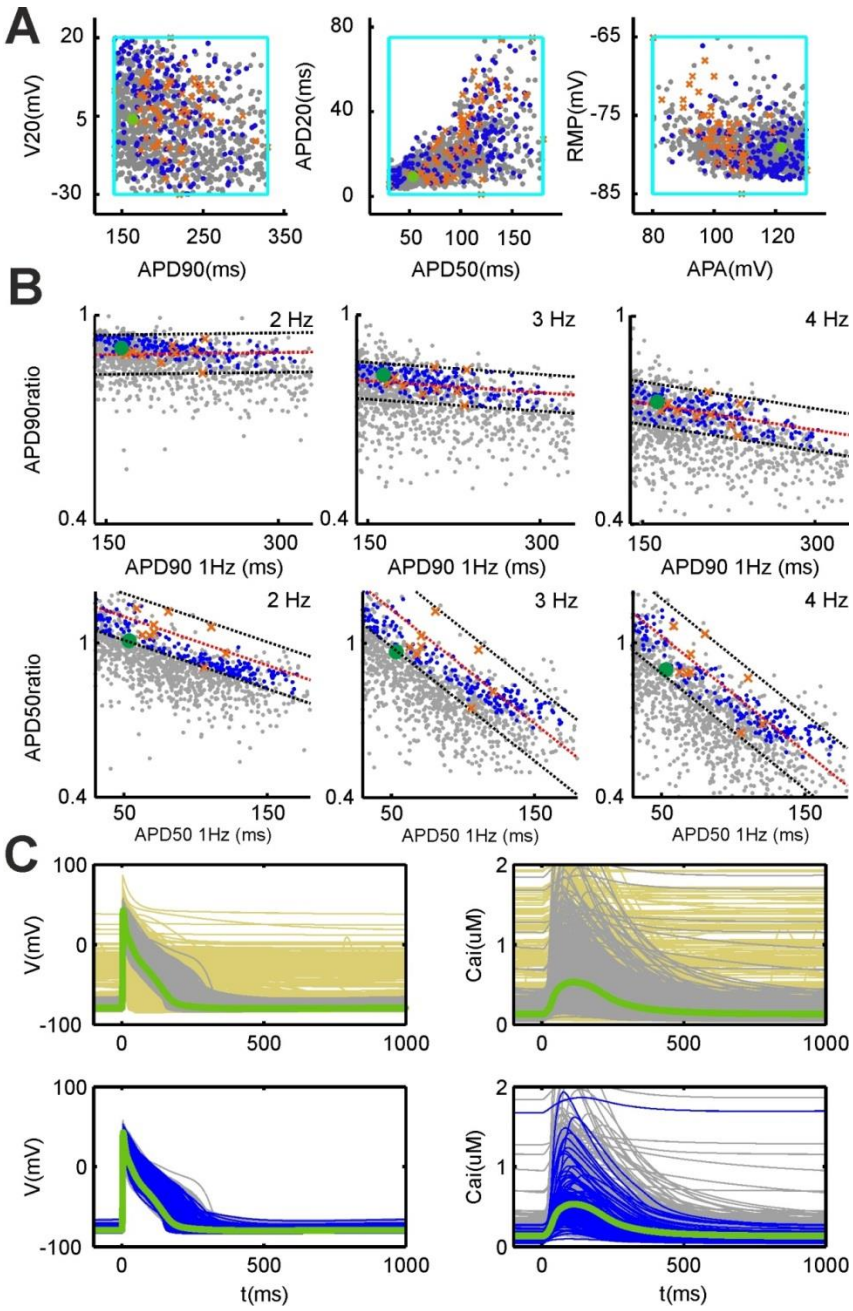

Figure 5.3 – Population of models calibration and biomarkers.

Panel A shows the values of the biomarkers –V20, APD20, APD50, APD90, RMP and APA–. The green dot represents the baseline AF model; blue and gray dots correspond to the 'physiological population' obtained with the calibration including rate dependence constraints (N=173) and those that fitted the conditions

of biomarkers at 1Hz but not those related with rate dependence (N=945). Orange marks correspond with a random sort of values measured in experimental preparations. Upper and lower bounds for 1 Hz biomarkers are marked in light blue. Panel B shows rate dependence of APDs and rate dependence bounds. Only the models with a deviation from regression lines –depicted in red– below the maximum deviation observed in experimental measurements were accepted. Note that models that fulfill one but not all criteria may appear as gray dots inside some upper and lower bonds for a given pair of biomarkers. Panel C depicts AP and intracellular calcium tracings, yellow tracings correspond to all the simulated models (N=16,384), the rest of color tracings correspond again with those described before.

In Figure 5.3, the variability of APs, calcium transients and biomarkers for the different groups is presented. In Panel A the simulated models, together with the experimental data are depicted (in gray: the 945 models that reproduced only in the 1Hz biomarkers, in blue: the 173 models that reproduced both 1Hz and rate dependent biomarkers; the green dot represent the baseline AF model) that fit into the limits of 1Hz biomarkers depicted in turquoise are depicted in comparison with the biomarkers obtained from experimental recordings (i.e. orange marks). Notice that the observed variability on experimental biomarker values is reasonably covered by the obtained populations of mathematical models.

Panel B shows the coverage of APD50 and APD90 ratios for the experimental data, and the models in our '1 Hz' and 'physiological' populations. It can be observed, both in experimental and simulated values, that the larger the APD at 1 Hz, the lower the APDratio. This reflects a pronounced shortening of the APD as a function of the pacing rate and baseline APD. Notice that many of the models in the '1 Hz population' do not reproduce the rate dependence measured in the experimental recordings, which highlights the importance of calibrating the population at multiple pacing frequencies.

The 'baseline AF model' (i.e. green point) met most constraints imposed, except for the APD50ratio at 3Hz. However, for some of the biomarkers the baseline AF model was close to the limits imposed, estimated frommicroelectrode recordings (i.e. APD90, APD50, APD20, APA, APD50ratio), which evidences that may not be representative of the actual range of recorded APs.

In panel C, APs and calcium transients of all populations of models are depicted. It is of note that imposition of only APD biomarkers at 1 Hz allows for the selection of a class of models with exacerbated calcium transients. However, imposition of rate-dependence biomarkers extracted from APD measurements allowed discarding those models with possibly non physiological calcium transient.

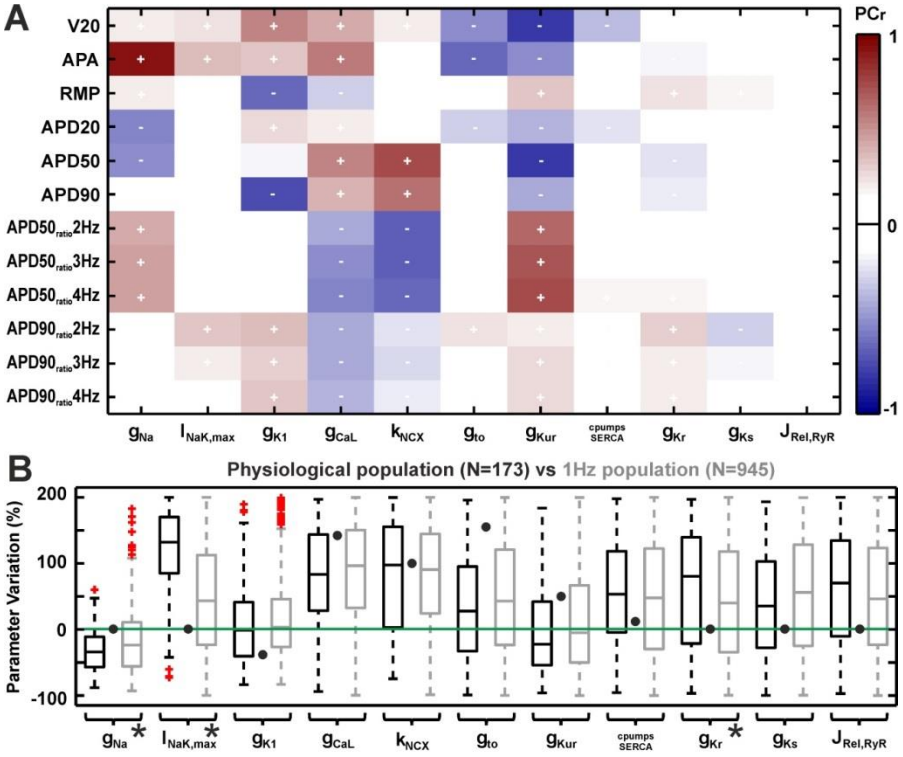

Figure 5.4 – Ionic current parameters and correlation with biomarkers.

*Panel A depicts correlation plots showing PCr values between pairs of parameters related with ionic currents and biomarkers. PCr values are represented with colors according to the color bar, darker colors represent stronger correlation. Partial correlation allows the evaluation of the effect between pairs of each parameter–biomarker mitigating the effect of other parameters. Box plot of the ionic current parameter variations in the population of models are depicted in Panel B. The boxplots in black correspond to the physiological population, fitting the constraints of biomarkers at 1Hz and rate dependence calibration. In gray the models corresponding to the 1Hz population (*p<0.01). The green line represents the baseline values while black dots represent the original Koivumaki original sinus rhythmn model. A high variability in conductances covering the whole range of values (from –100% to 200%) can be observed. It is also observed how the most constrained current is INa with limits in overexpression and blockade of +65% and –90% respectively in the resulting population.*

The specific effects of each parameter under study in each biomarker analyzed by partial correlation (PCr) on the physiological population are presented in Figure 5.4. In this graph direct correlations are marked in red whereas indirect correlations are plotted in blue, the intensity of the color depends on the magnitude of the correlation. This representation allows the identification of the main model parameters that strongly affect (direct or indirectly) several of the biomarkers (e.g. g_{Na}, g_{K1}, g_{CaL}, k_{NCX}, g_{Kur}) and those parameters which effect is restricted to few biomarkers (e.g. $I_{Nak,max}$, g_{to}), or even do not affect any of the studied biomarkers (e.g. g_{Kr}, g_{Ks} and those related with sarcoplasmic reticulum).

Thanks to this analysis it is possible to infer that an increase on sodium current conductivity (g_{Na}) is directly related to the amplitude of the AP (APA) and inversely related to APD50 and APD20, but not on APD90. ADP90, instead, was found to be inversely related to g_{K1} and g_{Kur} conductivities but directly related to the conductivities of g_{CaL} and k_{NCX}.

Regarding the modifications of action potential morphology due to the increase on the activation rate (i.e. APD ratios biomarkers), our results indicate that special attention needs to be played to g_{Na}, g_{CaL}, k_{NCX} and g_{Kur}. Notice that during atrial tachyarrhythmias such as AF, a fast activation rate is imposed and the rate dependent response may be crucial to either maintain or terminate the arrhythmia. Therefore, these currents appear as possible antiarrhythmic targets.

Panel B of Figure 5.4 shows the distribution of the variation in parameters for the 173 of models that reproduced both 1Hz and rate dependent biomarkers (i.e. physiological population) and those 945 models that reproduced only in the 1Hz biomarkers (i.e. 1Hz population).

As a result of accounting for physiological variability, it is of note that most currents inside the 1 Hz and physiological populations were not circumscribed to the midpoint of the simulated range (-100% to +200%) and showed median values that often diverged from the average baseline model. While the median values of g_{K1} and g_{Kur} matched with their baseline values, g_{Na} was clustered around lower values. On the other hand, g_{CaL} and k_{NCX} presented higher median values than the baseline model and closer to that of the control Koivumaki original sinus rhythmn model.

The parameters that differed from 1 Hz and physiological populations to a greater extent were g_{Na}, $I_{NaK,max}$ and g_{Kr} ($p<0.01$). In particular, g_{Na} tended to be lower while $I_{NaK,max}$ and g_{Kr} tended to be higher to fulfill the imposed rate-dependence criteria. This highlights the importance of I_{NaK} in AP rate adaptation, consistent with our PCr analysis results (Figure 5.4) and previous works ***(Bueno-Orovio 2013)***.

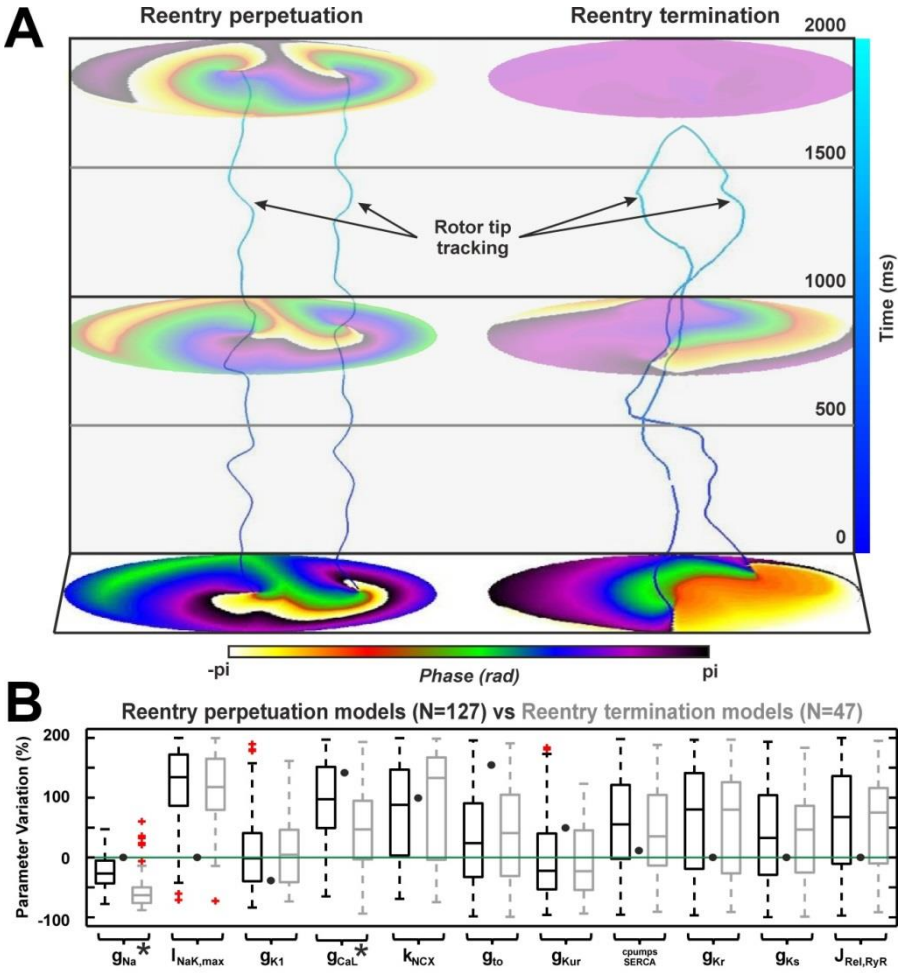

Figure 5.5 – End of functional reentry and ionic currents.

Phase maps and filaments representing rotor tip meandering in time are presented in Panel A. As it can be observed the example on the left presented more spatially stable rotors maintaining the reentrant activity during the whole simulation. On the contrary, the example on the right exhibited larger rotor meandering that resulted in the end of the reentrant activity by the collision of rotor tips. Panel B shows boxplots of the ionic current variations in models of the resulting population that maintained functional reentries in the sphere tissue –in black– vs those that did not maintain AF –in gray–. The green line and black dots represent both baseline AF model and Koivumaki original sinus rhythm models, respectively. Significant differences can be observed in g_{Na} and g_{CaL} (*), showing lower values when the reentry could not be maintained.

5.3.3. Role of Ionic Currents on Reentrant AF Mechanisms

The simulation of 174 different physiologic atrial tissue models –the physiological population plus the baseline AF model from Koivumaki– allowed us to (1) identify the differences between models that do and do not allow AF maintenance and (2) identify the role of each ion current conductivity on AF characteristics (i.e. dominant frequency, DF, and rotor meandering, RM).

Regarding the perpetuation of the arrhythmia, although the 174 models were based on biomarkers from cells from AF patients, in 47 (i.e. 27%) of them, reentries were self–terminated during the first seven seconds of the simulation. Temporal evolution of phase maps of one representative example of each subgroup can be observed in Figure 5.5. Notice that in the example on the left, reentries were stable during the entire simulation, and the arrhythmia was perpetuated. However, in the example on the right, although reentries start in a similar position, rotor tips were drifting up to an instant in which they collide and the arrhythmia terminated. This mechanism of termination (i.e. collision between rotors due to its larger RM) was present in all the 47 simulations in which the arrhythmia was not perpetuated. This result suggests that ion channel currents involved in RM may play a fundamental role in the perpetuation or termination of already stabilized AFs.

A comparison of the distribution of each ionic current parameter between the simulations in which the fibrillation terminated (i.e. 47) and those in which it was perpetuated (i.e. 127) is depicted in panel B of Figure 5.5. Notice that sodium and calcium conductivities (i.e. g_{Na} and g_{CaL}) were the only two parameters that presented significant differences between both groups highlighting their outstanding relevance as antiarrhythmic targets. Interestingly, no significant variations were observed on potassium repolarizing currents which have been also considered in the literature as potential antiarrhythmic targets for AF ***(Jalife 2011, Wettwer 2013, Ravens 2014)***.

The specific characteristics of AF on the models in which the arrhythmia was perpetuated is shown in Figure 5.6. Significant variability can be observed in the histogram distribution of DFs and RMs, which indicates that the new population of models developed in this study allows the simulation of several AF scenarios. Thanks to the inter–subject variability that this database introduces, the relation between ion channel parameters and AF biomarkers can be identified. For example, notice that a low direct correlation was observed between DF and RM (R^2= –0.44), which suggests that rotor drifting may not be significantly related with its reentry period. Nevertheless, the scatterpolot indicates that high DFs are most often related with low RMs whereas low DFs can be found with any RM value. This result takes additional relevance when related with the partial correlation analysis between AF biomarkers and ion channels conduction properties (in Panel B of Figure 5.6). The sodium conductivity (g_{Na}) plays a main role in both

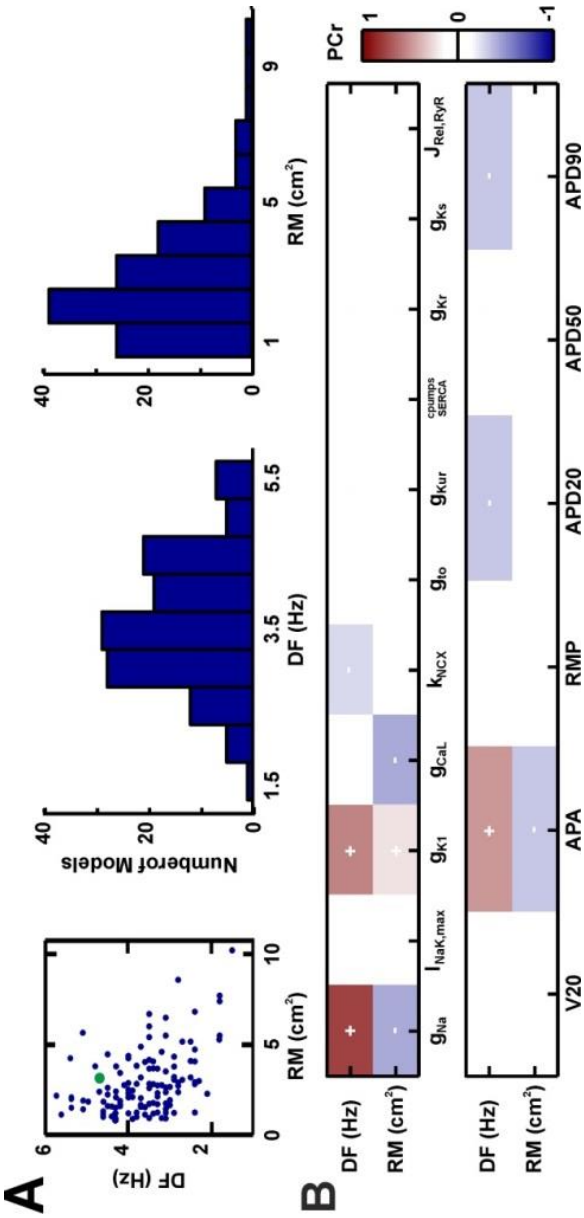

Figure 5.6 – Ionic currents and functional reentries.

Panel A histograms and scattergram of both DF and RM area showing the distribution of both variables for the 127 models that maintained the reentry. In Panel B, correlation plots showing PCr values between pairs of parameters related with ionic currents and reentry biomarkers (Top Panel) and biomarkers at 1Hz and reentry biomarkers (Bottom Panel) are presented. Note the positive correlation of g_{Na} and g_{K1} with DF and the negative correlation of g_{Na} and g_{CaL} with RM.

parameters: whereas an increase of g_{Na} would be correlated with an increase of DFs, it would also be related with a reduction of meandering. However, the lack of a strong direct correlation between DF and RM indicates that the effect of g_{Na} in both AF biomarkers is significantly affected by other conductivities. Specifically, our results suggest that, in addition to g_{Na}, DF is mainly governed by g_{K1} whereas RM is inversely related to g_{CaL}. None of the remaining studied parameters of the model presented a significant partial correlation with AF characteristics.

Regarding the relation between AF characteristics and action potential biomarkers, our results indicate that the amplitude of the action potential (i.e. APA) is the only biomarker that its related with both RM and DF. The large dependence of this amplitude with the sodium conductivity is in accordance with our results presented in Figure 5.4.A. In addition to APA, both APD20 and AP90 presented a slight correlation with DF, but we found no strong correlation between any biomarker and RM.

5.3.4. Personalized Effects of Antiarrhythmic Treatments

The efficacy of existent AF antiarrhythmic drugs is not homogeneous. One of the main applications of the developed database of different physiological AF tissues is the possibility to use it as a benchmark for drug testing and, even more interestingly, to unmask the differences between responder and non–responder subjects. In this section the presented database was used to illustrate the potential role of variability in ion channels expression as one of the possible causes for drug effects disparities. Indeed, the finding that RM plays a relevant role in the termination of AF due to collisions between rotors and that RM is mainly governed by g_{Na} and g_{CaL}, raises questions regarding which could be the different effects of a calcium channel blocker (i.e. verapamil) depending on the relative expression of other ion channel currents.

Specifically, effects on AF characteristics of a reduction of 50% of g_{CaL} were evaluated in the 127 models that maintained the fibrillation during basal conditions. In Figure 5.7 the opposite effect of this reduction on AF characteristics in two examples is depicted. Notice that in the example of panel A, the reduction of g_{CaL} produced a significant increase in the meandering of rotors and a decrease on the DF (4.4 vs. 3.8 Hz), whereas in the example on panel B, the reduction of g_{CaL} resulted in an increase of DF (4.6 vs. 5.1 Hz).

The reduction of g_{CaL} also had different degrees of success on AF termination depending on the specific characteristics of each model. After seven seconds of simulation under the effects of the g_{CaL} block, 38 of the 127 reentrant processes terminated (30%). The differences between ion channel properties in the cases in which the arrhythmia terminated after the I_{CaL} blockade and those in which the arrhythmia persisted are presented in Figure 5.8. As it can be observed in panel A, most significant differences were observed for I_{K1} and I_{Na} conductivities. Models in

which g_{CaL} block resulted in reentry termination presented lower expressions of both I_{K1} and I_{Na} in basal conditions. The trend observed for g_{Na} is suggestive of the potential implication of low sodium conductivities on a more prevalent antiarrhythmic effect of calcium channel blockers.

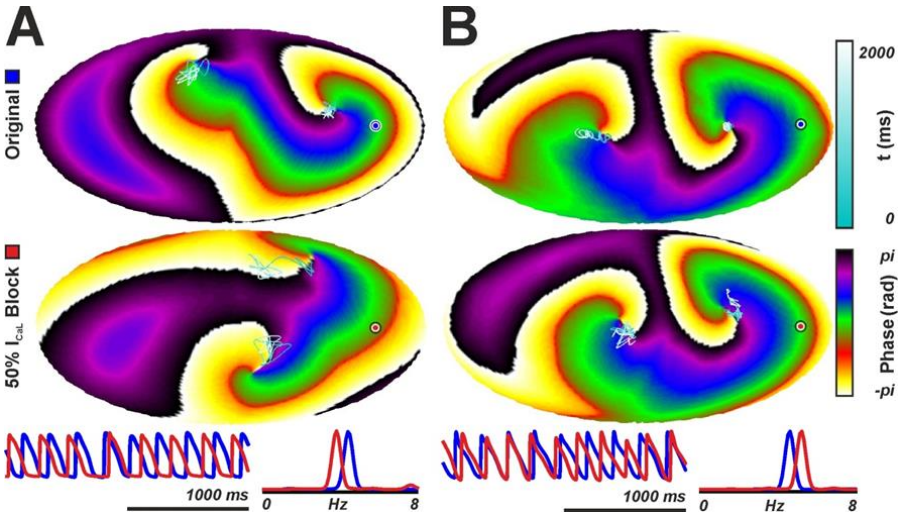

Figure 5.7 – Examples of the effect of a block of 20% in g_{CaL} in DF and RM. *Phase maps are depicted for one time instant according to a color scale together with the rotor tip meandering in light blue. Transmembrane voltages and power spectral density for selected nodes are presented on the bottom with different colors for baseline (blue) and 20% I_{CaL} reduction (red).*

The specific mechanisms by which the calcium block terminates AF are evaluated in panel B of Figure 5.8. As it can be observed the reduction in g_{CaL} resulted in an average increase in rotor meandering. However this effect was not uniform in the entire population and in some cases the g_{CaL} block resulted in a reduction of RM and therefore , an stabilization of the arrhythmia. Regarding the modifications on DF, no clear trends were observed. In addition, as during basal conditions, a weak inverse relationship between DFs and RMs was observed (R^2 = –0.48). The partial correlation between the variation of DFs and RMs and each of the parameters of the model can shed some light about the characteristics of calcium blockers responders and non–responders. As shown in panel C of Figure 5.8, sodium current conductivity (g_{Na}) was the main parameter correlated with both DF and RM changes. According to these results, the inverse correlation between g_{Na} and the change in RM indicates that calcium blockers produced an increase in the RM mainly in those cases in which the basal conductivity of the sodium

channel was low. This result suggests that the antiarrhythmic effect of calcium blockers could be subject to the degree of expression of the sodium current in each patient.

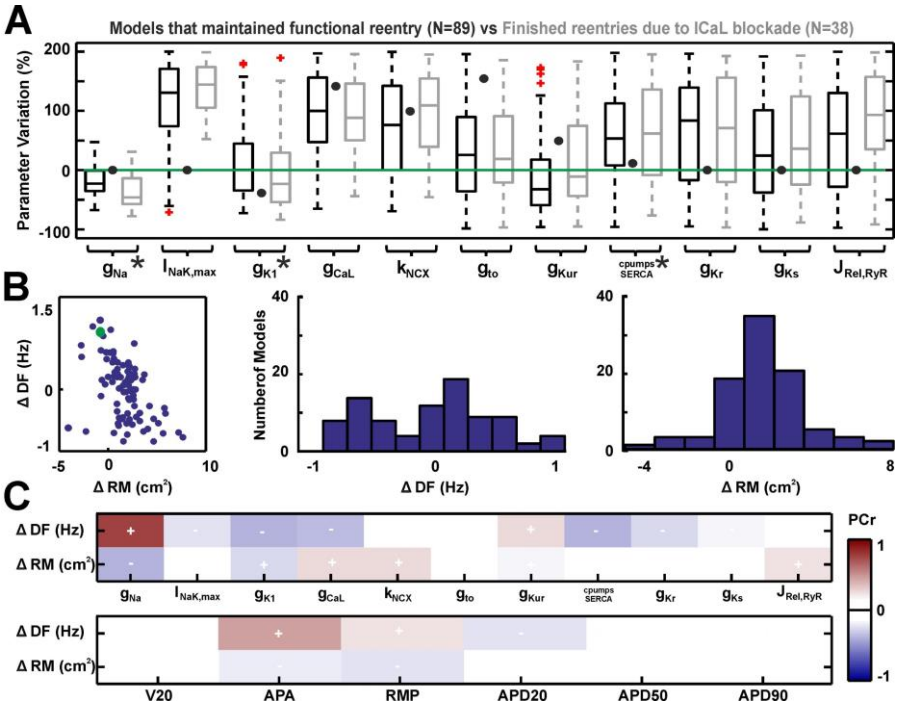

Figure 5.8 – I_{CaL} blockade in population of models.

Panel A shows boxplots of the ionic current parameter variations in models that maintained functional reentries(in black) vs those that finished the reentry due to I_{CaL} blockade (in gray). The green line and black dots represent both baseline AF model and Koivumaki original sinus rhythm model as described above. Significant differences can be observed in g_{K1} and g_{CaL}, showing lower values in the models that could not maintain the reentry. Panel B shows histograms and scattergram of the gradients observed in DF and RM in the models that perpetuated the reentry. It can be observed how models present both positive and negative gradients showing that the I_{CaL} block promotes different effects depending on the model. In Panel C correlation plots showing PCr values between pairs of parameters related with ionic currents and gradients of reentry biomarkers (Top Pannel) and biomarkers at 1Hz and gradients of reentry biomarkers (Bottom Pannel). Stronger colors represent stronger correlation. It is showed how models with a higher expression in g_{Na} tend to present increments in frequency and reduction in rotor tip area due to I_{CaL} block.

In the case of the DF, a more complex behavior is observed. The direct correlation between change in DF and g_{Na} is suggestive of an increase in DF due to calcium block in models with higher sodium channel conductivity. However, the inverse correlation between the change of DF and g_{K1} points to a reduction of DF in those models in which the g_{K1} conductivity was high. This multifactorial response to calcium block may explain the controversial correlation between calcium blockers and modifications on DFs reported in the literature.

5.4. Discussion

5.4.1. Major findings

In this work, a population of mathematical models of atrial tissues which mimics the inter–subject variability of AF patients including rate dependent response has been implemented. This in silico database consisting of 173 different AF computational models) has been used to evaluate the role of each ion channel current on AF reentry perpetuation mechanisms. The fundamental and interdependent role of I_{Na}, I_{CaL} and I_{K1} currents on AF dynamics has been shown. This physiological variability in ionic current densities may independently explain the observed disparity of antiarrhythmic drug effects, which can be related to the expression of other currents that may be unaltered by the drug. As shown here, this may be the case of calcium blockers, whose antiarrhythmic effect is dependent on sodium current densities, among others.

5.4.2. Inter–subject variability AF mathematical models population

Mathematical models have been used to evaluate hypotheses of AF perpetuation mechanisms and drug response from the beginning of computer technologies since the late fifties ***(Moe and Abildskov 1959)***. During the last decades, thanks to the increase in computing power together with a more extended research in cardiac ionic currents by patch–clamp experiments, more sophisticated electrophysiological models have been developed. This ionic current models have been used to evaluate the effect of antiarrhythmic treatments both on AP and rotors dynamics ***(Courtemanche 1999, Pandit 2005, Koivumaki 2014)***. However most of these in–silico studies have made of a single set of parameters fitted to an average of many experiments, often obtained from cells of different species. Although this approach has allowed the reproduction and a better understanding of AF mechanisms, hides the variability between patients observed in the clinical practice. Variability is present in the most of biological structures in nature; it

makes healthy individuals of the same species exhibit such differences in biomarkers which often hinder the definition of pathological behaviors, and its therapies. Scientific experiments are generally performed in highly controlled environments and models, plus the results obtained are usually averaged to reduce errors. AP is not an exception and presents important differences in morphology to the same species and area. As observed in our database and others ***(Muszkiewicz 2014, Sanchez 2014)***, AP of patients suffering of AF present significant differences in terms of temporal and rate dependent biomarkers. This variability may explain the contradictory responses to pharmacological treatments reported in the literature. New cardiac simulation platforms as the one presented in this thesis allow performing simulations of populations of models, accounting for the variability observed across subjects. However, to the best of our knowledge, this is the first study in which a population of models has been used to determine the ionic currents linked to arrhythmia perpetuation in a pseudo-3D model of atrial fibrillation.

In order to account for an extensive sampling of possible model parameters, an exhaustive sampling in the multidimensional sampling space is not feasible. Instead, latin hypercube sampling allows for a more efficient sampling, covering the range of biomarkers measured experimental preparations ***(Britton 2013)***.

After having established a wide population of models, AP markers allowed us for a selection of ionic current combinations that result in APs covering the observed experimental range. However, reproduction of AP biomarkers at a single pacing rate does not account for the observed rate dependence of ionic currents. As we have shown, cells with long basal APDs shorten their APDs under fast rates to a greater extent than models with short basal APDs. In order to account for this rate-dependence of cardiac electrophysiology we have included restrictions in our database of models that reproduce this observed trend. It is of note that the introduction of these rate-dependence bounds, obtained from AP measurements, resulted in the rejection of models with unrealistic calcium transients. According to our results, the single most relevant parameter to account for this rate dependence was I_{NaK}, which is in accordance with previous reports ***(Sanchez 2012, Bueno-Orovio 2013)***. However, this is the first time that APDratio, or the ratio between APD shortening and APD at different pacing cycles, has been used to select the most physiologically relevant models among a wider population.

By using our proposed approach we have been able to determine the range of parameters of the AF model reported by Koivumaki et al. ***(Koivumaki 2014)*** that better represent our database of cells recorded in experimental preparations. We have oberved that g_{K1}, g_{to} and g_{Kur} remodeling proposed by Koivumaki better fits to remodeled atrial cells than the control cell model. However, expressions on g_{CaL} and k_{NCX} present a better fit for the Koivumaki original sinus rhythm model than the baseline AF model. In addition, it is of note that a significant overexpression in $I_{NaK,max}$ is required, although it was not considered for the AF model.

5.4.3. Strategies for the development of new pharmacological therapies and reentrant biomarkers

Antiarrhythmic drugs are the main strategy for AF cardioversion and the maintenance of sinus rhythm, however they are associated with undesired secondary effects and proarrhythmia ***(Filgueiras-Rama 2012)***. For this reason, the development of new drugs based on mechanistic strategies has attracted the interest of pharmacological companies and research groups. The understanding of the mechanisms associated with rotors is important to develop new strategies to finish AF.

Current clinical and research studies on AF have evidenced the important role of rotors on AF maintenance ***(Narayan 2012, Haissaguerre 2014).*** Overexpression of repolarization currents, such as I_{K1} or I_{KACh} has demonstrated to accelerate atrial drivers as a consequence of APD shortening ***(Pandit 2010, Atienza 2009, VanWagoner 1997, Dobrev 2000, Voigt 2010)***, while I_{K1} block has shown to reduce the activation frequency ***(Warren 2003)***. In addition, to shortening of APD90, I_{K1} overexpression facilitates I_{Na} availability due to hyperpolarization associated I_{K1}, resulting in an acceleration of the rotor activity ***(Pandit 2010, Sekar 2009, Hou 2010)***. This is consistent with our finding of a significant correlation of I_{K1} with activation frequency during fibrillation, also related to APD shortening. However, pharmacological block of these currents has reported a modest effect on AF termination ***(Pandit 2011, Filgueiras-Rama 2012)***. We found that, indeed, there is no relation either between I_{K1}, I_{Kur}, I_{Kr} or I_{Ks} in terms of AF maintenance.

Our simulations suggest that AF maintenance may be more strongly related to the depolarizating currents I_{Na} and I_{CaL}. This may be related to the dynamics of rotation cores rather than APD elongation, since both currents affect rotor meandering with little or no effect on APD. A reduced availability of either I_{Na} or I_{CaL} results in a decreased excitability, which forces the rotor core to drift. This increased rotor meandering may facilitate annihilation of wavefronts due to collision, as found in the present study and others ***(Kneller 2005, Climent 2015a, Climent 2015b)***. It may independently explain the mechanism of action of I_{Na} block as an antiarrhythmic, especially effective paroxysmal AF patients ***(Kneller 2005, Conde 2013)***. However, I_{Na} block has also been associated with an increased vulnerability to ventricular fibrillation due to a reduction in conduction velocity ***(Filgueiras-Rama 2012)***.

Alternatively, AF termination might be approached by a pharmacological reduction of I_{CaL}. However, the role of I_{CaL} as an antiarrhythmic is yet controversial. While Chorro et al. reported that verapamil results in an acceleration of ventricular fibrillation ***(Chorro 2000)*** due to a reduction of the effective refractory period, others have reported a frequency reduction ***(Samie 2000, Climent 2015a)***. In the same direction, we did not find a significant correlation between I_{CaL} and DF. In fact, I_{CaL} block resulted in diverse effects on DF in our

population of models. This can be explained by its simultaneous effect of APD and rotor meandering, since it decreases APD (which would tend to increase DF) but at the same time increases rotor meandering (which, in turn, tends to decrease DF). The balance between these two opposed effects has been shown to be multifactorial, but strongly related to I_{Na} availability. Therefore, I_{CaL} may be effective for AF termination in the case of low availability of I_{Na}. This is consistent with previous works that linked Ca^{2+} currents to the propagation of APs under reduced I_{Na} availability ***(Samie 2000, Filgueiras-Rama 2012)***. According to our results, the antiarrhythmic effect of Ca^{2+} channel blockers may be more prominent in some patients than others, depending on their specific balance of ion channel currents, in particular I_{CaL} and I_{Na}. As an alternative approach, drugs that partially block both I_{CaL} and I_{Na} currents could be more effective for AF termination in a wider population of patients.

5.4.4. Limitations

Mathematical models are a partial representation of real objects and so the extrapolation of the results should be made with caution. Despite of that, the introduction of inter-subject variability approximates in-silico experiments to a more realistic clinical scenario.

Regarding more specific limitations of the study, due to technical and ethical limitations, the atrial tissue samples were taken from the right atrial appendage which may not representate all the complex behavior of left and right atrium of AF patients. Note that the tissue in the left atria is considered prominent in maintaining AF, at least in paroxysmal AF patients ***(Sarmast 2003, Atienza 2009, Voigt 2010, Doessel 2012, Rodrigo 2014b)*** and therefore right atrial tissue may harbor reentries with a larger rotation period and thus lower DFs. This may be one of the underlying mechanisms of our reported frequencies, which are lower than those typically found in AF patients. Another reason for the low DF frequencies in our models may be related to an inaccurate modelling of intercellular coupling that could not be fitted from our experimental preparations, which do not allow to record transmembrane voltages in coupled cardiomyocytes and measure conduction velocities.

Another limitation of the study is the lack of Ca^{2+} transient biomarkers to fit the models. However, it has been shown that these variables have modest impact on AP biomarkers. Recording of calcium transients with calcium-sentitive fluoroscopic dyes may allow including additional constraints to the model population. In either case, Ca^{2+} transients presented in Figure 5.3 show realistic shapes thanks to our imposed rate dependence constraints and, therefore, our results may not be conditioned by this limitation.

The selection of parameters to alter during the generation of the population of AF remodeled mathematical was based in previous works in which main ion

channel parameters that govern AF were suggested ***(Koivumaki 2014, Sanchez 2014, Britton 2013).*** Despite of that, AF has been demonstrated as a multifactorial phenomena, and the introduction of other variables such as ionic concentrations, time constants related to ionic currents or the diffusion coefficient in tissue simulations will allow the identification of its potential role during AF.

Regarding the morphology of simulated tissue does not reproduce the complex atrial anatomy in humans. In either case, introduction of anatomical heterogeneities would most likely increase the incidence of collisions and annihilation of wavefronts under an increased rotor meandering.

5.4.5. Conclusions

Populations of models adjusted to experimental biomarkers are presented as a useful tool when understanding the ionic mechanisms related with rotor dynamics and designing new antiarrhythmic pharmacological treatments for AF. As presented, the same pharmacological treatment (i.e. a blockade in I_{CaL}) can promote divergent effects in terms of DF and RM depending on the patient. Populations of models will improve viability studies of these treatments and will avoid unexpected side effects associated to inter-subject variability.

Chapter 6

Discussion and conclusion

In this chapter a global conclusion of the results given in this dissertation is presented. This chapter has been structured in three sections. First, the main findings of this thesis are discussed and compared with previous works; the limitations of the thesis are also introduced. Secondly, the main conclusions of this thesis are listed by assessing the resolution of the objectives. The chapter is closed with a guideline for future work, highlighting aspects of this work that can be improved and the range of future lines of research.

6.1. Discussion

6.1.1. Main findings

Pharmacological and radiofrequency ablation therapies are currently the preeminent strategies to deal with atrial reentrant tachyarrhythmia such as AFL and AF. Macro–reentrant mechanisms are accepted as the cause of AFL ***(Garcia-Cosio 2012)***, in the case of AF, although there is more discussion on the causes underlying the arrhythmia, functional ***(Pandit and Jalife 2013)*** or anatomical ***(Hansen 2015)*** micro–reentrant behaviors are gaining weight as main drivers of this arrhythmia.

Ablation procedures sometimes present difficulty to locate the driving circuit and thereby find the best way to terminate the arrhythmia. This difficulty is faced with invasive mapping of the atrium during the ablation procedure; however a non–invasive technology that allowed a planning of the intervention will improve the efficiency and efficacy resulting in significant economic and time savings.

In this thesis it has been proven that phase maps, obtained from body surface potential mapping electrocardiographic signals are able to locate in the torso surface singularity points that differ depending on the reentrant circuit responsible

of the maintenance of AFL. As it has been shown in patients and models, phase maps present figure–of–eight like patterns resulting of the projection of the rotation pattern on the torso surface. Singularity points determine the rotation axis non–invasively, and therefore differs depending on the rotation circuit and the contribution of different wavefronts arising in the atrium, which can facilitate the noninvasive determination of the different circuits responsible for atypical AFL. As it has been shown by our group, this technique can be extended to the diagnosis of patients with AF driven by rotors in the left or right atria ***(Rodrigo 2014b)***.

However, the number of patients suffering from atrial tachyarrhythmia is much higher than the number of ablation procedures that can be performed. In addition, a low success rate of actual ablation techniques in patients with high structural or electrical remodeling, produces that in most cases AF patients do not undergo ablation procedures. Instead, these patients are treated with pharmacological therapies. However, the efficacy of existent antiarrthmic drugs is limited and presents a high variability between patients. For this reason, it is necessary to understand the mechanisms responsible for maintaining reentrant activity in each individual patient and focus the antiarrhitmic treatment on them.

The strategies used to hinder the maintenance of the fibrillation process focus on increasing the area needed to maintain reentrant activity. Attending to the leading circle theory presented by Allessie et al. ***(Allessie 1977)***, pharmacological treatments have been traditionally addressed by increasing the refractory period of the cells and the equivalent wavelength. Another strategy recently discussed focuses on destabilizing the rotor core which results in displacement and extinction by collision with other wavefronts or anatomical obstacles ***(Climent 2015b)***.

This thesis has evaluated, by means of a population of models, the role of different ionic currents on action potential and reentry biomarkers. The results that reinforce previous analyses related with the strategy of increasing the resulting wavelength by lengthening the AP are described in Chapter 5.

Besides, thanks to the simulations of populations of models in tissue, this thesis shows the importance of I_{CaL} in reentry biomarkers. I_{CaL} is very important at the time of maintaining stable the rotor core, we hypothesize that it is due to its important role as depolarization current in areas of low availability of I_{Na} such as the core of the rotors where the cells do not reach the resting membrane potential prior to depolarization. Thus, the mechanism of class IV antiarrhythmic drugs, such as verapamil, for AF termination is elucidated by means of a population of models. The methodology also allowed explaining the divergence in previous studies, due to the high variability in the expressions of currents depending on the patient, a single drug therapy can have divergent effects depending on the patient. Thereby we see that the differences in previous studies ***(Chorro 2000, Samie 2000)*** can be justified by the double effect of I_{CaL} (refractoriness – excitability) more than because to the lack of specificity in the ionic currents of verapamil or other antiarrhythmic drugs. The results also show that the mechanism responsible of the

high efficacy of drugs that affect to different currents at the time of ending AF may be related with the simultaneous blockade of I_{Na} and I_{CaL}.

This thesis has shown the capabilities of populations of models adjusted to recorded AP biomarkers when assessing the effect of a specific drug therapy in a wide range of combinations in terms of ion channel expressions. Therefore, an increased knowledge of the ionic mechanisms responsible of reentrant mechanisms, together with anatomical and genetical studies, will accelerate the introduction of personalized drug treatments.

These results were obtained thanks to cardiac mathematical modeling, including from the subcellular structures to the in–silico ECG signal calculation, applied to the improvement of the diagnosis and treatment of reentrant atrial tachyarrhythmia. The work developed during this thesis has the simulation platform developed as an important outcome. The features of the GP–GPU platform, the geometrical model and the electrophysiological model implemented together with the tools designed with Matlab is comparable with that available internationally by the most important research groups in this field. It easies the design and test of the techniques developed in the group for invasive and non–invasive location of drivers sustaining AF.

6.1.2. Comparison with previous studies

The non–invasive diagnosis of atrial tachyarrhythmia is a research field which attracts the interest of many researchers and institutions. Our group develops state of the art techniques related with the analysis of body surface potential maps. Other research groups use BSP signals to reconstruct the electrical activity in the myocardium by means of the inverse problem of the electrocardiography or analyze ECG signals in time or frequency domains.

The inverse problem of electrocardiography reconstructs non–invasively the cardiac activity from the signals recorded on the torso surface and a reconstruction of the torso volume based on medical imaging. However due to the ill–posed nature and multiple solutions of the problem, the accuracy of inverse problem is very sensitive to the input signal to noise ratio, the geometrical input model errors, estimation of volume conductivities etc. Some authors have presented the location of macroreentries or drivers during AFL or other atrial tachycardia based on inverse problem solutions ***(Seger 2006, Roten 2012)***. The reconstruction of AF patterns for the location of drivers was performed by some authors ***(Cuculich 2010, Haissaguerre 2013)*** however they obtain smoothed results which result too simple compared to what is observed in in–vivo or ex–vivo recordings ***(Allessie 2010)***. As drivers of AF have been associated with high frequency sites ***(Mansour 2001, Atienza 2009, Narayan 2012)***, our group proposed the non–invasive

reconstruction of dominant frequency maps by means of the inverse problem of the electrocardiography ***(Pedron-Torrecilla 2014)***.

In the field of temporal and frequency ECG analysis, Jones et al. were able to distinguish with ECG analysis the patients with primary AF–sustaining sources in the left or the right atria, in both persistent or paroxysmal AF ***(Jones 2013)***. Differentiation between left and right AFL has motivated many previous works ***(Bochoeyer 2003)***. Left atrium AFL has been shown to present shorter cycle lengths than isthmus dependent AFL in post–radiofrequency MAZE patients ***(Akar 2007)*** and lower spatial coherence ***(Kahn 2007)***.

SippensGroenewegen et al. proposed the use of integral BSPM for the differentiation of typical and atypical AFL ***(SippensGroenewegen 2000)***, in our group Guillem et al. identified different AF patterns in BSP Maps ***(Guillem 2009b)*** and estimated non–invasively the location of AF highest dominant frequency sites ***(Guillem 2013)***. Phase analysis reduces the errors induced in voltage analysis when generating isochrones maps from BSPM recordings, it was introduced for the first time by Rodrigo et al. ***(Rodrigo 2014b)*** and was used to discriminate between left and right AF–sustaining rotors.

Regarding the reentry mechanism and its pharmacological therapies, both pharmacological and in–silico tissue studies have been presented. I_{Na} is presented as the most important current when in the propagation of wavefronts both in sinus rhythm and in during reentrant activity and a blockade of this current result in a deceleration of the reentrant activity ***(Kneller 2005, Pandit and Jalife 2013)***. In parallel, a blockade of I_{K1} or the acetylcholine–activated K^+ current, which present similar effects in action potential and reentrant activity, results in a reduction of the reentrant frequency due to the lengthening of the AP by means of a reduction in depolarizing currents and a reduction in the polarization during the resting state which is promoted by I_{K1} ***(Warren 2003, Pandit 2005, Atienza 2006)***. The role of I_{CaL} remains controversial and the in–silico population used in this thesis elucidated the two mechanisms that confront in this current, on the one hand the overexpression of this current results in longer effective refractory periods associated with AP lengthening ***(Koivumaki 2014)***, but at the same time, as a depolarization current, it has an important role in the propagation in conditions were I_{Na} is not available ***(Rohr and Kucera 1997, Shaw and Rudy 1997, Rohr 1998, Samie 2000, Climent 2015a)***, as it can be the center of rotors were the AP do not get the resting membrane potential prior to depolarization.

6.2. Limitations

Mathematical modelling is a useful tool at the time of explore or test new strategies for the diagnosis and treatment of cardiac arrhythmias. However, the results obtained with this methodology needs to be assessed with other experimental methods. Despite of that, the results obtained demonstrated that

mathematical modelling helps in the understanding of mechanisms associated with reentrant tachyarrhythmias.

Regarding the strategy used to simulate atrial flutter episodes, the atrial geometrical model used includes fiber orientation and variations in anisotropy depending on the area of the atria but we did not implement heterogeneity in the electrophysiology dependent of the area of the atria in our baseline model which have been researched in other works ***(Seemann 2006, Aslanidi 2011, Tobon 2013)***. We consider electrophysiological heterogeneity would not have major effect in the macro–reentrant circuits associated to AFL, and that these minor effects would not be perceptible in the singularity points observed on the torso surface due to the spatial (propagation atria–torso) and temporal filtering applied for the stabilization of singularity points. However, atrial heterogeneity may have an important role when simulating atrial fibrillation in realistic structures, as functional reentries tend to stabilize in areas with preponderance of some currents.

Another limitation with regard to the simulation strategy, affects the calculation of in–silico ECG signals which can be affected by the absence of heterogeneous conductivity structures such as lungs, rib cage etc in our torso volume. However, although these structures can have an important role when detecting small variations in the ECG signal, their impact was reduced in our methodology as we locate the main component of reentry. The extension of this simulation strategy for other applications requiring greater sensitivity to voltage levels will require prior checks.

Regarding the chronic AF population of models, the database of left atrial appendage cells can have an effect in the level of remodeling of the population as the most of the drivers of atrial fibrillation are found in the pulmonary veins ***(Narayan 2012)*** that are quite remote to this area. In addition, as populations of models are the result of variations of some parameters associated to a baseline model the results are somehow conditioned to this model.

The reduced number of samples is a recurrent limitation in clinical experimentation. In this thesis, the reduced number of recordings of AFL episodes and the lack of intracardiac recordings to confirm the reentrant circuit which promotes the singularity points observed in the atria, are a limitation of the work presented in chapter 4. This problem is in part solved with the use of mathematical models. However, the collaboration of the group with Hospital Gregorio Marañón in Madrid will make the database of patients wider, which will allow the verification of the results presented in a bigger population of patients. In the case of the generation of the population of models of AF, the use of samples of the tissue responsible of the maintenance of AF, would avoid the limitations associated with dominant frequency observed reinforcing the conclusions obtained in this thesis.

6.3. Conclusion

A brief answer to each of the objectives presented in section 1 is presented in this section:

Main objective

To propose and develop methods for the non–invasive location –which will ease ablation procedures– and pharmacological treatment of reentrant drivers of atrial tachyarrhythmia.

Answer: Phase analysis of BSPM recordings has allowed us to show that, in the case of AFL, different propagation patterns that are dependent on the anatomical structure sustaining the macro–reentrant circuit can be identified. Populations of models adjusted to experimental biomarkers have allowed us to show the relation between ionic currents and both AP and reentrant biomarkers, the blockade of the depolarizing L–type Ca^{2+} current I_{CaL} promotes the destabilization of rotors and helps in the extinction of micro–reentrant activity sustaining AF.

Secondary objectives:

- *To develop a GP–GPU based platform for the simulation of human atrial cell, tissue and geometrical models.*

  Answer: During the development of this thesis a platform for the simulation of cardiac models has been developed. We have shown its ability in the simulation of populations of single cell models, tissues –spherical models– and models with a realistic geometry. The platform enables the input of electrophysiological variations with different intensity in each cell; it also allows the configuration of different stimulation protocols. This, together with the use of the forward problem of electrocardiography, allows the group to perform simulations from the cell level to the ECG signals. Nowadays, the research group features an efficient simulation platform for cardiac research that has also been used in various research publications related to this thesis.

- *To obtain spatial parameters from Body Surface Potential Mapping (BSPM) recordings in patients able to improve the diagnosis of atrial flutter.*

  Answer: Phase maps obtained from AFL patients band pass filtered BSPM recordings, display characteristic figure–of–eight patterns with SPs in two contralateral views of the torso. The location of these SPs depends on the structure that describes the reentrant circuit maintaining the arrhythmia, allowing the discrimination between typical and atypical atrial flutter.

- *To simulate different patterns of macro–reentrant tachycardia in the atria and to evaluate the mechanisms reflected in the torso surface, and the diagnosis methods proposed.*

Answer: In chapter 4, different simulations of macro–reentrant arrhythmias sustained by a reentrant circuit around the tricuspid valve or not have been presented and described. According with the results observed in patients this activity is reflected in the torso as figure–of–eight patterns with SPs placed depending on the reentrant circuit. Multilayer forward problem has been used to observe the evolution of SPs in the torso and confirm that the SPs in the torso correspond with the reentrant axis in the atria.

- *To develop a population of cell models which reproduce the variability in action potential biomarkers observed in chronic atrial fibrillation patients.*
  Answer: In chapter 5, a population of models generated based on the AP biomarkers from a database of 215 samples from the right atrial appendage is described. The population of models includes rate dependence constraints and shows that despite the limited variability in the range of biomarkers it is possible to characterize realistic action potentials with a wide range of variations in ionic current parameters.

- *To evaluate in the population of models of chronic atrial fibrillation the effect of different currents in the action potential and reentrant biomarkers.*
  Answer: The population of models together with partial correlation analysis showed the relationship between ionic currents and AP and reentrant biomarkers. The technology used presented easies analysis of the relations between ionic currents and biomarkers obtaining results similar to that present in the bibliography. In addition, the results explained previous contradictory results regarding the blockade of I_{CaL} that could be due to the differences between experimental populations, and the mechanisms underlying the new drugs that focus in a multichannel blockade.

- *To propose and to evaluate pharmacological treatments with the objective of destabilize rotors by incrementing the area needed for the maintenance.*
  Answer: The population of models analysis highlighted that I_{Na} and I_{CaL} were the currents with a higher effect in the area used by the tip of the rotor. As a consequence, we proposed a blockade of 20% in I_{CaL} that resulted in the termination of the reentrant activity in the 22% of the models. Since we used a simple spherical model, termination never happened by collision with anatomical obstacles, which most likely takes place in real atria. Therefore, the effect of I_{CaL} blockade in a more realistic scenario would have a deeper impact of AF termination

6.4. Guidelines for future works

The research group is focused in the hypothesis that the areas occupied by the singularity points ***(Rodrigo 2014b)*** and highest dominant frequencies ***(Guillem 2013)*** detected on the torso surface can guide radiofrequency ablation procedures. However, our results need further evaluation to introduce our technology into the clinical practice. With this aim the research group collaborates with Hospital Gregorio Marañón in the simultaneous recording of BSPM and the global atrial activity by means of multiple channel electrogram recording. The simultaneous recording of intracardiac and BSPM electrical activity, will help in the validation of the results obtained by means of mathematical modelling or non-invasive BSPM recordings and it will accelerate the transfer of our technology developments to the industry.

At the same time, the population of models principle will be applied in the resolution of the forward problem with the aim of modifying the relationship between the atria and the torso in terms of orientation, size or position. It will be used to evaluate the role of these variables in the location of both singularity points or frequency areas, resulting in an improvement of the non–invasive prediction of the location of the mechanisms driving atrial tachyarrhythmia. At the same time the database of atrial tachyarrhythmia will be complemented by including post ablation AFL, or realistic episodes of AF. These populations of atrial tachyarrhythmia will be used both in BSPM analysis works and inverse problem research.

As introduced in the limitations section, the implementation of electrophysiological atrial heterogeneity in the atrial model will improve AF simulations. Another improvement to AF simulations will be the introduction of structural remodeling, with a special focus on introducing fibroblasts in the tissue,. It may improve the simulation of atrial fibrillation by shortening action potentials and making the wavefronts more irregular and reallistic ***(Aslanidi 2012)***.

Recent results presented optical mapping experiments showing anatomical micro–reentrant circuits as drivers of AF. These circuits were kept around pectinate muscles and other small bundles ***(Hansen 2015)***. This may result in limitations associated with modeling based in diffusion tensors associated with fiber orientation; or in a rethinking of anisotropy values associated to fibers. The high frequencies recorded –near 15 Hz– also may result in adjustments in the values of electrical remodeling.

In order to better understand the mechanisms underlying functional reentries, new populations of models can be constructed based in AP recordings classified in terms paroxysmal or chronic AF or dependent on the area of the atria the cells belong. This database of AP recording is available in Hospital Gregorio Marañón and will be another collaboration project.

These populations of models will be used to test different pharmacological strategies or to assess other structural or electrical variations in a wide range of models. The objective of this work will be the introduction of personalized pharmacological treatments based in the mechanisms underlying the arrhythmia and the best strategy to extinguish it in each patient. However the huge computational costs associated to this analysis may result in the need of the improvement of the features of our simulation platforms by means of the introduction of multi GP–GPU stations.

Populations of models and other in silico assessment strategies of drug safety have attracted the interest in the pharmaceutical industry. In–silico evaluation of pro–arrhythmic effects may avoid high costs in time and money associated with the development of drugs which at the end are unsafe in terms of cardiac rhythmogenesis. The introduction of populations of cardiac tissue models allows the analysis of propagation biomarkers in a wide range of models, this is why our group is working for the transference of this technology to pharmaceutical industry in collaboration with the University of Oxford.

Chapter 7

Contributions

7.1. Main contributions of this thesis

7.1.1. Journal papers

- **Liberos A**, Climent AM, Rodrigo M, Pedrón–Torrecilla J, Millet J, Atienza F, Berenfeld O, Quesada A, Guillem MS. Non–invasive Characterization of Atrial Macroreentries during Typical and Atypical Atrial Flutter. (In preparation)
- **Liberos A**, Bueno–Orovio A, Rodrigo M, Ravens U, Guillem MS, Rodriguez B*, Climent AM*. Balance between Sodium and Calcium Currents Underlying Chronic Atrial Fibrillation Termination: An In Silico Inter–subject Variability Study. (Submitted)

7.1.2. International conferences

- **Liberos A**, Climent AM, Rodrigo M, Pedrón–Torrecilla J, Millet J, Quesada A, Guillem MS. Non–Invasive Phase Analysis in Atrial Flutter Electrographic Maps. CARDIOSTIM 2014. S96:16.
- **Liberos A**, Pedrón–Torrecilla J, Rodrigo M, Millet J, Climent AM, Guillem MS. Body surface Potential Propagation Maps During Macroreentrant Atrial Arrhythmias: A Simulation Study. Computing in Cardiology 2013. 40:915–918.
- García–Mollá, VM, **Liberos A**, Climent AM, Vidal A, Millet J, Gonzalez A. An Adaptive Step Size GPU ODE Solver for Simulating the Electric Cardiac Activity. Computing in Cardiology 2011. 38:233–236.
- **Liberos A**, Bueno–Orovio A, Rodrigo M, Millet J, Ravens U, Hernandez I, Guillem MS, Rodriguez B, Climent AM. Inter–Subject variability in human atrial fibrillation. A computational population of models. ITACA–WIICT 2015.

7.1.3. National conferences

- **Liberos A**, Climent AM, Rodrigo M, Pedrón–Torrecilla J, Berenfeld O, Atienza F, Guillem MS, Fernandez–Avilés F. Análisis de fase en la cartografía eléctrica de superficie en episodios de flutter auricular. Estudio de simulación. Congreso de las Enfermedades Cardiovasculares 2015.
- **Liberos Mascarell A**, Pedrón Torrecilla J, Millet J, Quesada A, Climent AM, Guillem MS. Simulación de la actividad electrofisiológica auricular y mapas eléctricos de superficie en episodios de flutter auricular. XXX Congreso Anual de la Sociedad Española de Ingeniería Biomédica 2012.
- García–Mollá VM, **Liberos Mascarell A**, Climent AM, Vidal A, Millet J, Gonzalez A. Simulación de la actividad eléctrica cardiaca mediante algoritmos de resolución de paso adaptativo para GPU. XXIX Congreso Anual de la Sociedad Española de Ingeniería Biomédica 2011.

7.2. Contributions related to this thesis

7.2.1. Journal papers

- García–Mollá VM, **Liberos A**, Vidal A, Guillem MS, Millet J, Gonzalez A, Martínez–Zaldivar F, Climent AM. Adaptive step ODE algorithms for the 3D simulation of electric heart activity with graphics processing units. Comput Biol Med 2014. 44:15–26.
- Rodrigo M, Guillem MS, Climent AM, Pedrón–Torrecilla J, **Liberos A**, Millet J, Fernández–Avilés F, Atienza F, Berenfeld O. Body surface localization of left and right atrial high–frequency rotors in atrial fibrillation patients: a clinical–computational study. Heart Rhythm 2014. 11:1584–1591.
- García–Mollá, VM, Vidal A, **Liberos A**, Climent AM. Adaptación para múltiples GPU de un simulador de actividad eléctrica en el corazón. Multi–GPU adaptation of a simulator of heart electric activity. Revista Cubana de Ciencias Informáticas 2013. 7:100–111.
- Pedrón–Torrecilla J, Climent AM, **Liberos A**, Rodrigo M, Pérez–David E, Bermejo J, Arenal A, Millet J, Fernandez–Aviles F, Berenfeld O, Atienza F, Guillem MS. Noninvasive Estimation of Epicardial Dominant High–Frequency Regions during Atrial Fibrillation. Journal of Cardiovascular Electrophysiology 2015 (accepted).
- Rodrigo M, Climent AM, **Liberos A**, Calvo D, Fernandez–Aviles F, Berenfeld O, Atienza F, Guillem MS. Identification of Dominant Excitation Patterns and Sources of Atrial Fibrillation. Annals of Biomedical Engineering 2015(accepted).

7.2.2. Book chapter

- Rodrigo M, Pedrón–Torrecilla J, Hernández I, **Liberos A**, Climent AM, Guillem MS. Data Analysis in cardiac arrhythmias. Eds: Fernández–Llatas C, García–Gómez JM. Data Mining in Clinical Medicine. Methods in Molecular Biology 2014. 1246:217–236.

7.2.2. International conferences

- Atienza F, Rodrigo M, Climent AM, **Liberos A**, Fernández–Avilés F, Berenfeld O, Guillem MS. Electroanatomical identification of dominant propagation patterns during atrial fibrillation by causality analysis. Hearth Rhythm Scientific Sessions 2014. 11:S442.
- Atienza F, Pedrón–Torrecilla J, Climent AM, **Liberos A**, Pérez–David E, Millet J, Fernández–Avilés F, Berenfeld O, Guillem MS. Noninvasive Estimation of Dominant High–Frequency Regions during Atrial Fibrillation: Validation of the Inverse Problem Resolution. Hearth Rhythm Scientific Sessions 2014. 11:S440.
- Pedrón–Torrecilla J, Climent AM, **Liberos A**, Rodrigo M, Pérez–David E, Millet J, Fernández– Avilés F, Berenfeld O, Atienza F, Guillem MS. Accuracy of Inverse Solution Computation of Dominant Frequencies and Phases during Atrial Fibrillation. Computing in Cardiology 2014. 41:537–540.
- Rodrigo M, Climent AM, **Liberos A**, Pedrón–Torrecilla J, Millet J, Fernández–Avilés F, Atienza F, Berenfeld O, Guillem MS. Non–invasive detection of reentrant drivers during atrial fibrillation: a clinical–computational study. Computing in Cardiology 2014. 41:9–12.
- Rodrigo M, Guillem MS, Climent AM, **Liberos A**, Pedrón–Torrecilla J, Fernández–Avilés F, Atienza F, Berenfeld O. Body surface detection of reentrant activity during atrial fibrillation. CARDIOSTIM 2014. S96:17.
- Rodrigo M, Climent AM, **Liberos A**, Fernández–Avilés F, Berenfeld O, Atienza F, Guillem MS. Body surface detection of reentrant activity during atrial fibrillation. CARDIOSTIM 2014. S119:140.
- Pedrón–Torrecilla J, **Liberos A**, Rodrigo M, Millet Roig J, Felipe A, Berenfeld O, Climent AM, Guillem MS. Non–invasive imaging of the atrial arrhythmia sources: patient study during atrial tachyarrhythmia and atrial fibrillation. ITACA–WIICT 2014. 1:10–17.
- Rodrigo M, Climent AM, **Liberos A**, Pedrón–Torrecilla J, Millet J, Fernández–Avilés F, Atienza F, Berenfeld O, Guillem MS. Non–invasive location of re–entrant propagation patterns during atrial fibrillation. ITACA–WIICT 2014. 1:1–9.

- Pedrón–Torrecilla J, **Liberos A**, Millet J, Climent AM, Guillem MS. Accuracy of non–invasive frequency estimation using atrial fibrillation. Computing in Cardiology 2013. 40:1183–1186.
- Rodrigo M, **Liberos A**, Climent AM, Guillem MS. Identification of Ablation Sites in Atrial Flutter by Causal Method. Computing in Cardiology 2013. 40:707–710.
- Rodrigo M, Climent AM, **Liberos A**, Pedrón–Torrecilla J, Millet J, Fernández–Avilés F, Atienza F, Berenfeld O, Guillem MS. Non–invasive Location of Re–Entrant Propagation Patterns during Atrial Fibrillation. Computing in Cardiology 2013. 40:1235–1238.
- Berenfeld O, Rodrigo M, Climent AM, **Liberos A**, Pedrón–Torrecilla J, Millet J, Arenal A, Fernández–Avilés F, Atienza F, Guillem MS. Noninvasive identification of reentrant drivers of atrial fibrillation using multi–channel surface recordings. Hearth Rhythm Scientific Sessions 2013. 10:310.
- Pedrón–Torrecilla J, Climent AM, **Liberos A**, Pérez–David E, Millet J, Atienza F, Guillem MS. Noninvasive Estimation of the Activation Sequence in the Atria during Sinus Rhythm and Atrial Tachyarrhythmia. Computing in Cardiology 2012. 39:901–904.
- Rodrigo M, Guillem MS, **Liberos A**, Millet J, Berenfeld O, Climent AM. Identification of fibrillatory sources by measuring causal relationships. Computing in Cardiology 2012. 39:705–708.
- Rodrigo M, **Liberos A**, Guillem MS, Millet J, Climent AM. Causality relation map: a novel methodology for the identification of hierarchical fibrillatory processes. Computing in Cardiology 2011. 38:173–176.
- **Liberos A**, Guillem MS, Millet J, Climent AM. A LabVIEWTM Based Multichannel Recording Architecture for High Density Electrical Mapping. Computing in Cardiology 2010. 37:341–344.

7.2.3. National conferences

- Pedrón–Torrecilla J, MS Guillem, AM Climent, **Liberos Mascarell A**, Rodrigo Bort M, Berenfeld O, Atienza F, Fernández–Avilés F. Reconstrucción no invasiva de los mapas electroanatómicos de frecuencia dominante durante fibrilación auricular. Congreso de las Enfermedades Cardiovasculares 2014. 67:391.
- Rodrigo Bort M, Climent AM, **Liberos A**, Pedrón Torrecilla J, Fernández–Avilés F, Berenfeld O, Atienza F, Guillem MS. El análisis causal de la actividad eléctrica durante fibrilación auricular permite identificar los patrones de propagación dominante. Congreso de las Enfermedades Cardiovasculares 2013. 66:15–21.

- Rodrigo Bort M, Guillem MS, Climent AM, **Liberos Mascarell A**, Pedrón Torrecilla J, Millet Roig J, Berenfeld O, Atienza F. Identificación no invasiva de patrones fibrilatorios mediante registro electrocardiográfico de superficie. Congreso de las Enfermedades Cardiovasculares 2013. 66:15–21.
- Pedrón–Torrecilla J, Climent AM, **Liberos Mascarell A**, Pérez–David E, Millet J, Atienza F, Guillem MS. Estimación no invasiva de la secuencia de activación auricular durante el ritmo sinusal y taquiarritmia auricular. XXX Congreso Anual de la Sociedad Española de Ingeniería Biomédica 2012.
- Rodrigo Bort M, Guillem MS, **Liberos Mascarell A**, Millet J, Berenfeld O, Atienza F, Fernández–Avilés F, Climent AM. Identificación de fuentes fibrilatorias mediante la medida de relaciones causales. XXX Congreso Anual de la Sociedad Española de Ingeniería Biomédica 2012.
- Rodrigo Bort M, **Liberos Mascarell A**, Guillem MS, Millet J, Climent AM. Mapa de relación causal: una nueva metodología para la identificación de patrones fibrilatorios jerárquicos. XXIX Congreso Anual de la Sociedad Española de Ingeniería Biomédica 2011.
- **Liberos Mascarell A**, Martínez Climent A, Pedrón Torrecilla J, Millet Roig J, Guillem Sánchez MS. Arquitectura Reconfigurable para el Mapeo Eléctrico de Potenciales Cardiacos basada en LabVIEWTM XXVIII Congreso Anual de la Sociedad Española de Ingeniería Biomédica 2010. 2010:5–8.
- Pedrón–Torrecilla J, Climent AM, **Liberos A**, Millet J, Guillem MS. Estudio Comparativo de un Método Iterativo para la Resolución Indirecta del Problema Inverso de la Electrocardiografía. XXVIII Congreso Anual de la Sociedad Española de Ingeniería Biomédica 2010. 2010:1–4.
- **Liberos Mascarell A**, Guillem MS, Pedrón–Torrecilla J, Millet J, Climent AM. Arquitectura Reconfigurable para el Mapeo Eléctrico de Potenciales Cardiacos basada en LabVIEWTM. XXVIII Congreso Anual de la Sociedad Española de Ingeniería Biomédica 2010.

7.3. Research stay

During the development of this thesis A Liberos has completed a research stay at “University of Oxford”, Oxford, United Kingdom, in the “Computational Cardiovascular Science Team” in the “Department of Computer Science”, leaded by Pr. Blanca Rodríguez.

Dates: From 1st September until 30th November 2014.

During this stay a joint work presented in Chapter 5 was developed.

7.4. Research projects

This work has been developed within the framework of several research projects. The interest and relevance of the research activity carried out by our group has been acknowledged by public administrations by means of the following research projects in which the author has participated:

- Instituto de salud Carlos III

  ESTUDIO PRECLINICO DE LA IMPLANTACION DE PARCHES DE TEJIDO CARDIACO BIOARTIFICIAL ELECTROMECANICAMENTE ENTRENADOS EN UN MODELO DE INFARTO DE MIOCARDIO PORCINO. DESARROLLO DE BIOREACTORES CON ESTIMULACION ELECTROMECANICA.

  From Jan 1st, 2014 until Jan 1st, 2017.

  Main researcher: Guillem Sánchez, María de la Salud

- Generalitat Valenciana

  SIMULACIÓN DE TEJIDO CARDIACO EN SISTEMAS CON MÚLTIPLES TARJETAS GRÁFICAS DE USO GENERAL (MULTI–GPU) (SP20120483).

  From Jan 1st, 2012 until Jan 1st, 2014.

  Main researcher: Martínez Zaldívar, Francisco José

- Universitat Politècnica de València

  SIMULACIÓN DE TEJIDO CARDIACO EN SISTEMAS CON MÚLTIPLES TARJETAS GRÁFICAS DE USO GENERAL (MULTI–GPU) (SP20120483).

  From Dec 31st, 2012 until Dec 31st, 2013.

  Main researcher: García Mollá, Víctor Manuel

- Ministerio de Educación

  DESARROLLO DE TECNICAS AVANZADAS DE ANALISIS Y CARACTERIZACION DE MAPAS DE PROPAGACION PARA LA AYUDA AL DIAGNOSTICO ELECTROCARDIOGRAFICO (TEC2009–13939).

  From Apr 18th, 2010 until Oct 14th, 2010.

  Main researcher: Millet Roig, José

- Generalitat Valenciana

  PROMAPCOR: DESARROLLO DE TECNICAS AVANZADAS DE ANALISIS Y CARACTERIZACION DE MAPAS DE PROPAGACION PARA LA AYUDA AL DIAGNOSTICO ELECTROCARDIOGRAFICO (ACOMP/2010/176).

  From Apr 15th, 2010 until Oct 14th, 2010.

  Main researcher: Millet Roig, José

References

(Akar 2007) Akar JG, Al-Chekakie MO, Hai A, Brysiewicz N, et al. Surface electrocardiographic patterns and electrophysiologic characteristics of atrial flutter following modified radiofrequency MAZE procedures. *J Cardiovasc Electrophysiol* 2007. **18:** 349-355

(Allessie 1973) Allessie MA, Bonke FIM and Schopman FJ. Circus movement in rabbit atrial muscle as a mechanism of tachycardia. *Circ Res* 1973. **33:** 54-62

(Allessie 1976) Allessie MA, Bonke FIM and Schopman FJG. Circus movement in rabbit atrial muscle as a mechanism of tachycardia .2. role of nonuniform recovery of excitability in occurrence of unidirectional block, as studied with multiple microelectrodes. *Circ Res* 1976. **39:** 168-177

(Allessie 1977) Allessie MA, Bonke FIM and Schopman FJG. Circus movement in rabbit atrial muscle as a mechanism of tachycardia .3. leading circle concept - new model of circus movement in cardiac tissue without involvement of an anatomical obstacle. *Circ Res* 1977. **41:** 9-18

(Allessie 2010) Allessie MA, de Groot NMS, Houben RPM, Schotten U, et al. Electropathological substrate of long-standing persistent atrial fibrillation in patients with structural heart disease. *Circulation-Arrhythmia and Electrophysiology* 2010. **3:** 606-615

(Antz 1998) Antz M, Otomo K, Arruda M, Scherlag BJ, et al. Electrical conduction between the right atrium and the left atrium via the musculature of the coronary sinus. *Circulation* 1998. **98:** 1790-1795

(Aslanidi 2011) Aslanidi OV, Colman MA, Stott J, Dobrzynski H, et al. 3D virtual human atria: A computational platform for studying clinical atrial fibrillation. *Prog Biophys Mol Biol* 2011. **107:** 156-168

(Aslanidi 2012) Aslanidi OV, Al-Owais M, Benson AP, Colman M, et al. Virtual tissue engineering of the human atrium: Modelling pharmacological actions on atrial arrhythmogenesis. *Eur J Pharm Sci* 2012. **46:** 209-221

(Atienza 2006) Atienza F, Almendral J, Moreno J, Vaidyanathan R, et al. Activation of inward rectifier potassium channels accelerates atrial fibrillation in humans - evidence for a reentrant mechanism. *Circulation* 2006. **114:** 2434-2442

(Atienza 2009) Atienza F, Almendral J, Jalife J, Zlochiver S, et al. Real-time dominant frequency mapping and ablation of dominant frequency sites in atrial fibrillation with left-to-right frequency gradients predicts long-term maintenance of sinus rhythm. *Heart Rhythm* 2009. **6:** 33-40

(Bachmann 1916) Bachmann G. The inter-auricular time interval. *Am J Physiol* 1916. **41:** 309-320

(Beeler and Reuter 1977) Beeler GW and Reuter H. Reconstruction of action potential of ventricular myocardial fibers. *Journal of Physiology-London* 1977. **268:** 177-210

(Berenfeld 2000) Berenfeld O, Mandapati R, Dixit S, Skanes AC, et al. Spatially distributed dominant excitation frequencies reveal hidden organization in atrial fibrillation in the langendorff-perfused sheep heart. *J Cardiovasc Electrophysiol* 2000. **11:** 869-879

(Bers 1993) Bers D, Bassani R, Bassamo J, Baudet S, et al. Paradoxical twitch potentiation after rest in cardiac-muscle - increased fractional release of sr calcium. *J Mol Cell Cardiol* 1993. **25:** 1047-1057

(Blanc 2001) Blanc O, Virag N, Vesin JM and Kappenberger L. A computer model of human atria with reasonable computation load and realistic anatomical properties. *Ieee Transactions on Biomedical Engineering* 2001. **48:** 1229-1237

(Bochoeyer 2003) Bochoeyer A, Yang Y, Cheng J, Lee R, et al. Surface electrocardiographic characteristics of right and left atrial flutter. *Circulation* 2003. **108:** 60-66

(Bosch 1999) Bosch RF, Zeng XR, Grammer JB, Popovic K, et al. Ionic mechanisms of electrical remodeling in human atrial fibrillation. *Cardiovasc Res* 1999. **44:** 121-131

(Brandt 2000) Brandt MC, Priebe L, Bohle T, Sudkamp M, et al. The ultrarapid and the transient outward K+ current in human atrial fibrillation. their possible role in postoperative atrial fibrillation. *J Mol Cell Cardiol* 2000. **32:** 1885-1896

(Britton 2013) Britton OJ, Bueno-Orovio A, Van Ammel K, Lu HR, et al. Experimentally calibrated population of models predicts and explains intersubject variability in cardiac cellular electrophysiology. *Proc Natl Acad Sci U S A* 2013. **110:** E2098-E2105

(Brundel 2001) Brundel BJJM, Van Gelder IC, Henning RH, Tuinenburg AE, et al. Alterations in potassium channel gene expression in atria of patients with persistent and paroxysmal atrial fibrillation: Differential regulation of protein and mRNA levels for K+ channels. *J Am Coll Cardiol* 2001. **37:** 926-932

(Bruns 2002) Bruns HJ, Eckardt L, Vahlhaus C, Schulze-Bahr E, et al. Body surface potential mapping in patients with brugada syndrome: Right precordial ST segment variations and reverse changes in left precordial leads. *Cardiovasc Res* 2002. **54:** 58-66

(Bueno-Orovio 2013) Bueno-Orovio A, Sanchez C, Pueyo E and Rodriguez B. Na/K pump regulation of cardiac repolarization: Insights from a systems biology approach. *Pflugers Arch - Eur J Physiol* 2013. 1-11

(Burdumy 2012) Burdumy M, Luik A, Neher P, Hanna R, et al. Comparing measured and simulated wave directions in the left atrium - a workflow for model personalization and validation. *Biomedical Engineering-Biomedizinische Technik* 2012. **57:** 79-87

(Caballero 2010) Caballero R, Gonzalez de la Fuente M, Gomez R, Amoros I, et al. In humans, chronic atrial fibrillation decreases the transient outward current and ultrarapid component of the delayed rectifier current differentially on each atria and increases the slow component of the delayed rectifier current in both. *J Am Coll Cardiol* 2010. **55:** 2346-2354

(Calkins 2009) Calkins H, Reynolds MR, Spector P, Sondhi M, et al. Treatment of atrial fibrillation with antiarrhythmic drugs or radiofrequency ablation two systematic literature reviews and meta-analyses. *Circulation-Arrhythmia and Electrophysiology* 2009. **2:** 349-U49

(Calvo 2014) Calvo CJ, Deo M, Zlochiver S, Millet J, et al. Attraction of rotors to the pulmonary veins in paroxysmal atrial fibrillation: A modeling study. *Biophys J* 2014. **106:** 1811-1821

(Carley 2003) Carley SD. Beyond the 12 lead: Review of the use of additional leads for the early electrocardiographic diagnosis of acute myocardial infarction. *Emergency medicine (Fremantle, W.A.)* 2003. **15:** 143-54

(Chauvin 2000) Chauvin M, Shah DC, Haissaguerre M, Marcellin L, et al. The anatomic basis of connections between the coronary sinus musculature and the left atrium in humans. *Circulation* 2000. **101:** 647-652

(Chorro 2000) Chorro F, Canoves J, Guerrero J, Mainar L, et al. Alteration of ventricular fibrillation by flecainide, verapamil, and sotalol - an experimental study. *Circulation* 2000. **101:** 1606-1615

(Christ 2004) Christ T, Boknik P, Wohrl S, Wettwer E, et al. L-type Ca2+ current downregulation in chronic human atrial fibrillation is associated with increased activity of protein phosphatases. *Circulation* 2004. **110:** 2651-2657

(Clayton and Panfilov 2008) Clayton RH and Panfilov AV. A guide to modelling cardiac electrical activity in anatomically detailed ventricles. *Prog Biophys Mol Biol* 2008. **96:** 19-43

(Climent 2011) Climent AM, Guillem MS, Zhang Y, Millet J, et al. Functional mathematical model of dual pathway AV nodal conduction. *American Journal of Physiology-Heart and Circulatory Physiology* 2011. **300:** H1393-H1401

(Climent 2015a) Climent AM, Guillem MS, Fuentes L, Lee P, et al. The role of atrial tissue remodeling on rotor dynamics: An in-vitro study. *Am J Physiol Heart Circ Physiol* 2015a. ajpheart.00055.2015

(Climent 2015b) Climent AM, Guillem MS, Atienza F and Fernandez-Aviles F. Electrophysiological characteristics of permanent atrial fibrillation: Insights from research models of cardiac remodeling. *Expert review of cardiovascular therapy* 2015b. **13:** 1-3

(Conde 2013) Conde D, Costabel JP, Caro M, Ferro A, et al. Flecainide versus vernakalant for conversion of recent-onset atrial fibrillation. *Int J Cardiol* 2013. **168:** 2423-2425

(Corradi 2012) Corradi D, Callegari S, Maestri R, Ferrara D, et al. Differential structural remodeling of the left-atrial posterior wall in patients affected by mitral regurgitation with or without persistent atrial fibrillation: A morphological and molecular study. *J Cardiovasc Electrophysiol* 2012. **23:** 271-279

(Cosio 2003) Cosio F, Martin-Penato A, Pastor A, Nunez A, et al. Atypical flutter: A review. *PACE-Pacing Clin Electrophysiol* 2003. **26:** 2157-2169

(Courtemanche 1998) Courtemanche M, Ramirez RJ and Nattel S. Ionic mechanisms underlying human atrial action potential properties: Insights from a mathematical model. *Am J Physiol -Heart Circul Physiol* 1998. **275:** H301-H321

(Courtemanche 1999) Courtemanche M, Ramirez R and Nattel S. Ionic targets for drug therapy and atrial fibrillation-induced electrical remodeling: Insights from a mathematical model. *Cardiovasc Res* 1999. **42:** 477-489

(Cox 1991a) Cox JL, Canavan TE, Schuessler RB, Cain ME, et al. The surgical-treatment of atrial-fibrillation .2. intraoperative electrophysiologic mapping and description of the electrophysiologic basis of atrial-flutter and atrial-fibrillation. *J Thorac Cardiovasc Surg* 1991a. **101:** 406-426

(Cox 1991b) Cox JL, Schuessler RB, Dagostino HJ, Stone CM, et al. The surgical-treatment of atrial-fibrillation .3. development of a definitive surgical-procedure. *J Thorac Cardiovasc Surg* 1991b. **101:** 569-583

(Cox 1993) Cox JL, Boineau JP, Schuessler RB, Kater KM, et al. 5-year experience with the maze procedure for atrial-fibrillation. *Ann Thorac Surg* 1993. **56:** 814-824

(Cox 1995) Cox JL, Boineau JP, Schuessler RB, Jaquiss RDB, et al. Modification of the maze procedure for atrial-flutter and atrial-fibrillation .1. rationale and surgical results. *J Thorac Cardiovasc Surg* 1995. **110:** 473-484

(Cox 2000) Cox JL, Ad N, Palazzo T, Fitzpatrick S, et al. Current status of the maze procedure for the treatment of atrial fibrillation. *Semin Thorac Cardiovasc Surg* 2000. **12:** 15-9

(Cuculich 2010) Cuculich PS, Wang Y, Lindsay BD, Faddis MN, et al. Noninvasive characterization of epicardial activation in humans with diverse atrial fibrillation patterns. *Circulation* 2010. **122:** 1364-+

(Da Costa 2006) Da Costa A, Thevenin J, Roche F, Romeyer-Bouchard C, et al. Results from the loire-ardeche-drome-isere-puy-de-dome (LADIP) trial on atrial flutter, a multicentric prospective randomized study comparing amiodarone and radiofrequency ablation after the first episode of symptomatic atrial flutter. *Circulation* 2006. **114:** 1676-1681

(Dang 2005) Dang L, Virag N, Ihara Z, Jacquemet V, et al. Evaluation of ablation patterns using a biophysical model of atrial fibrillation. *Ann Biomed Eng* 2005. **33:** 465-474

(Difrancesco and Noble 1985) Difrancesco D and Noble D. A model of cardiac electrical-activity incorporating ionic pumps and concentration changes. *Philosophical Transactions of the Royal Society of London Series B-Biological Sciences* 1985. **307:** 353-398

(Dobrev 2000) Dobrev D, Kortner A, Himmel H, Hofmann M, et al. Chronic human atrial fibrillation downregulates inward rectifier potassium current I-K,I-ACh independent of G-protein beta 3-subunit C825T-polymorphism. *Circulation* 2000. **102:** 192-193

(Dobrev 2001) Dobrev D, Graf E, Wettwer E, Himmel HM, et al. Molecular basis of downregulation of G-protein-coupled inward rectifying K+ current (I-K,I-ACh) in chronic human atrial fibrillation - decrease in GIRK4 mRNA correlates with reduced I-K,I-ACh and muscarinic receptor-mediated shortening of action potentials. *Circulation* 2001. **104:** 2551-2557

(Doessel 2012) Doessel O, Krueger MW, Weber FM, Wilhelms M, et al. Computational modeling of the human atrial anatomy and electrophysiology. *Med Biol Eng Comput* 2012. **50:**

(Dokos 2007) Dokos S, Cloherty SL and Lovell NH. Computational model of atrial electrical activation and propagation. *2007 Annual International Conference of the Ieee Engineering in Medicine and Biology Society, Vols 1-16* 2007. 908-911

(Dubuc 1993) Dubuc M, Nadeau R, Tremblay G, Kus T, et al. Pace mapping using body-surface potential maps to guide catheter ablation of accessory pathways in patients with wolff-parkinson-white syndrome. *Circulation* 1993. **87:** 135-143

(Eckardt 2002) Eckardt L, Bruns HJ, Paul M, Kirchhof P, et al. Body surface area of ST elevation and the presence of late potentials correlate to the inducibility of ventricular tachyarrhythmias in brugada syndrome. *J Cardiovasc Electrophysiol* 2002. **13:** 742-749

(Einthoven 1906) Einthoven W. Le telecardiogramme. *Arch Internat Physiol* 1906. **4:** 132-164

(El Chemaly 2007) El Chemaly A, Magaud C, Patri S, Jayle C, et al. The heart rate-lowering agent ivabradine inhibits the pacemaker current I(f) in human atrial myocytes. *J Cardiovasc Electrophysiol* 2007. **18:** 1190-1196

(El-Armouche 2006) El-Armouche A, Boknik P, Eschenhagen T, Carrier L, et al. Molecular determinants of altered Ca2+ handling in human chronic atrial fibrillation. *Circulation* 2006. **114:** 670-680

(Ellis 2000) Ellis WS, SippensGroenewegen A, Auslander DM and Lesh MD. The role of the crista terminalis in atrial flutter and fibrillation: A computer modeling study. *Ann Biomed Eng* 2000. **28:** 742-754

(Farber 2011) Farber R. CUDA application design and development. 2011.

(Filgueiras-Rama 2012) Filgueiras-Rama D, Castrejon S, Calvo C, Estrada A, et al. [Basic mechanisms of the new antiarrhythmic drugs in atrial fibrillation]. *Archivos de cardiologia de Mexico* 2012. **82:** 139-52

(Finlay 2005) Finlay DD, Nugent CD, McCullagh PJ and Black ND. Mining for diagnostic information in body surface potential maps: A comparison of feature selection techniques. *Biomedical engineering online* 2005. **4:** 51-51

(Frank 1954) Frank E. An equivalent circuit for the human heart-body electrical system. *Am Heart J* 1954. **48:** 738-745

(Fuster 2006) Fuster V, Ryden LE, Cannom DS, Crijns HJ, et al. ACC/AHA/ESC 2006 guidelines for the management of patients with atrial fibrillation - executive summary. *J Am Coll Cardiol* 2006. **48:** 854-906

(Gaborit 2005) Gaborit N, Steenman M, Lamirault G, Le Meur N, et al. Human atrial ion channel and transporter subunit gene-expression remodeling associated with valvular heart disease and atrial fibrillation. *Circulation* 2005. **112:** 471-481

(Garcia-Cosio 2012) Garcia-Cosio F, Pastor Fuentes A and Nunez Angulo A. Clinical approach to atrial tachycardia and atrial flutter from an understanding of the mechanisms. electrophysiology based on anatomy. *Rev Esp Cardiol* 2012. **65:** 363-375

(Garcia-Molla 2014) Garcia-Molla VM, Liberos A, Vidal A, Guillem MS, et al. Adaptive step ODE algorithms for the 3D simulation of electric heart activity with graphics processing units. *Comput Biol Med* 2014. **44:** 15-26

(Garrey 1924) Garrey WE. Auricular fibrillation. *Physiol Rev* 1924. **4:** 215-250

(Grammer 2000) Grammer JB, Bosch RF, Kuhlkamp V and Seipel L. Molecular remodeling of Kv4.3 potassium channels in human atrial fibrillation. *J Cardiovasc Electrophysiol* 2000. **11:** 626-633

(Grandi 2011) Grandi E, Pandit SV, Voigt N, Workman AJ, et al. Human atrial action potential and Ca2+ model sinus rhythm and chronic atrial fibrillation. *Circ Res* 2011. **109:** 1055-1066

(Gray and Jalife 1998) Gray RA and Jalife J. Ventricular fibrillation and atrial fibrillation are two different beasts. *Chaos* 1998. **8:** 65-78

(Guillem 2009a) Guillem MS, Quesada A, Donis V, Climent AM, et al. Surface wavefront propagation maps: Non-invasive characterization of atrial flutter circuit. *International Journal of Bioelectromagnetism* 2009a. **11:** 22-26

(Guillem 2009b) Guillem MS, Climent AM, Castells F, Husser D, et al. Noninvasive mapping of human atrial fibrillation. *J Cardiovasc Electrophysiol* 2009b. **20:** 507-513

(Guillem 2010) Guillem MS, Climent AM, Millet J, Berne P, et al. Conduction abnormalities in the right ventricular outflow tract in brugada syndrome detected body surface potential mapping. *Conference proceedings : Annual International Conference of*

the IEEE Engineering in Medicine and Biology Society.IEEE Engineering in Medicine and Biology Society.Conference 2010. **2010:** 2537-40

(Guillem 2013) Guillem MS, Climent AM, Millet J, Arenal A, et al. Noninvasive localization of maximal frequency sites of atrial fibrillation by body surface potential mapping. *Circulation.Arrhythmia and electrophysiology* 2013. **6:** 294-301

(Haissaguerre 1998) Haissaguerre M, Jais P, Shah DC, Takahashi A, et al. Spontaneous initiation of atrial fibrillation by ectopic beats originating in the pulmonary veins. *N Engl J Med* 1998. **339:** 659-666

(Haissaguerre 2000) Haissaguerre M, Jais P, Shah DC, Arentz T, et al. Catheter ablation of chronic atrial fibrillation targeting the reinitiating triggers. *J Cardiovasc Electrophysiol* 2000. **11:** 2-10

(Haissaguerre 2013) Haissaguerre M, Hocini M, Shah AJ, Derval N, et al. Noninvasive panoramic mapping of human atrial fibrillation mechanisms: A feasibility report. *J Cardiovasc Electrophysiol* 2013. **24:** 711-717

(Hansen 2015) Hansen BJ, Zhao J, Csepe TA, Moore BT, et al. Atrial fibrillation driven by micro-anatomic intramural re-entry revealed by simultaneous sub-epicardial and sub-endocardial optical mapping in explanted human hearts. *Eur Heart J* 2015. **36:** 2390-2401

(Harrild and Henriquez 2000) Harrild DM and Henriquez CS. A computer model of normal conduction in the human atria. *Circ Res* 2000. **87:** E25-E36

(Hocini 2015) Hocini M, Shah AJ, Neumann T, Kuniss M, et al. Focal arrhythmia ablation determined by high-resolution noninvasive maps: Multicenter feasibility study. *J Cardiovasc Electrophysiol* 2015. **26:** 754-760

(Hodgkin and Huxley 1952) Hodgkin AL and Huxley AF. A quantitative description of membrane current and its application to conduction and excitation in nerve. *Journal of Physiology-London* 1952. **117:** 500-544

(Hoekema 1999) Hoekema R, Uijen GJH and van Oosterom A. On selecting a body surface mapping procedure. *J Electrocardiol* 1999. **32:** 93-101

(Hoppe and Beuckelmann 1998) Hoppe UC and Beuckelmann DJ. Characterization of the hyperpolarization-activated inward current in isolated human atrial myocytes. *Cardiovasc Res* 1998. **38:** 788-801

(Horacek and Clements 1997) Horacek BM and Clements JC. The inverse problem of electrocardiography: A solution in terms of single- and double-layer sources on the epicardial surface. *Math Biosci* 1997. **144:** 119-154

(Hou 2010) Hou L, Deo M, Furspan P, Pandit SV, et al. A major role for hERG in determining frequency of reentry in neonatal rat ventricular myocyte monolayer. *Circ Res* 2010. **107:** 1503-+

(Iyer 2004) Iyer V, Mazhari R and Winslow RL. A computational model of the human left-ventricular epicardial myocyte. *Biophys J* 2004. **87:** 1507-1525

(Jacquemet 2006) Jacquemet V, van Oosterom A, Vesin J and Kappenberger L. Analysis of electrocardiograms during atrial fibrillation - A biophysical model approach. *Ieee Engineering in Medicine and Biology Magazine* 2006. **25:** 79-88

(Jais 1997) Jais P, Haissaguerre M, Shah DC, Chouairi S, et al. A focal source of atrial fibrillation treated by discrete radiofrequency ablation. *Circulation* 1997. **95:** 572-576

(Jais 2000) Jais P, Shah D, Haissaguerre M, Hocini M, et al. Mapping and ablation of left atrial flutters. *Circulation* 2000. **101:** 2928-2934

(Jalife 2002) Jalife J, Berenfeld O and Mansour M. Mother rotors and fibrillatory conduction: A mechanism of atrial fibrillation. *Cardiovasc Res* 2002. **54:** 204-216

(Jalife 2009) Jalife J, Delmar M, Anumonwo J, Berenfeld O, et al. Basic cardiac electrophysiology for the clinician, second edition. 2009.

(Jalife 2011) Jalife J. Deja vu in the theories of atrial fibrillation dynamics. *Cardiovasc Res* 2011. **89:** 766-775

(Jones 2013) Jones AR, Krummen DE and Narayan SM. Non-invasive identification of stable rotors and focal sources for human atrial fibrillation: Mechanistic classification of atrial fibrillation from the electrocardiogram. *Europace* 2013. **15:** 1249-1258

(Kahn 2007) Kahn AM, Krummen DE, Feld GK and Narayan SM. Localizing circuits of atrial macroreentry using electrocardiographic planes of coherent atrial activation. *Heart Rhythm* 2007a. **4:** 445-451

(Kall 2000) Kall J, Rubenstein D, Kopp D, Burke M, et al. Atypical atrial flutter originating in the right atrial free wall. *Circulation* 2000. **101:** 270-279

(Kalman 1997) Kalman J, Olgin J, Saxon L, Lee R, et al. Electrocardiographic and electrophysiologic characterization of atypical atrial flutter in man: Use of activation and entrainment mapping and implications for catheter ablation. *J Cardiovasc Electrophysiol* 1997. **8:** 121-144

(Kleber and Rudy 2004) Kleber A and Rudy Y. Basic mechanisms of cardiac impulse propagation and associated arrhythmias. *Physiol Rev* 2004. **84:** 431-488

(Kneller 2005) Kneller J, Kalifa J, Zou R, Zaitsev A, et al. Mechanisms of atrial fibrillation termination by pure sodium channel blockade in an ionically-realistic mathematical model. *Circ Res* 2005. **96:** E35-E47

(Koivumaki 2011) Koivumaki JT, Korhonen T and Tavi P. Impact of sarcoplasmic reticulum calcium release on calcium dynamics and action potential morphology in human atrial myocytes: A computational study. *PLoS Comput Biol* 2011. **7:** e1001067

(Koivumaki 2014) Koivumaki JT, Seemann G, Maleckar MM and Tavi P. In silico screening of the key cellular remodeling targets in chronic atrial fibrillation. *PLoS Comput Biol* 2014. **10:** e1003620

(Krueger 2013) Krueger MW, Seemann G, Rhode K, Keller DUJ, et al. Personalization of atrial anatomy and electrophysiology as a basis for clinical modeling of radio-frequency ablation of atrial fibrillation. *Medical Imaging, IEEE Transactions on* 2013. **32:** 73-84

(Krueger 2011) Krueger MW, Schmidt V, Tobon C, Weber FM, et al. Modeling atrial fiber orientation in patient-specific geometries: A semi-automatic rule-based approach. *Functional Imaging and Modeling of the Heart* 2011. **6666:** 223-232

(Krummen 2006) Krummen DE, Feld GK and Narayan SM. Diagnostic accuracy of irregularly irregular RR intervals in separating atrial fibrillation from atrial flutter. *Am J Cardiol* 2006. **98:** 209-214

(Krummen 2010) Krummen DE, Patel M, Nguyen H, Ho G, et al. Accurate ECG diagnosis of atrial tachyarrhythmias using quantitative analysis: A prospective diagnostic and cost-effectiveness study. *J Cardiovasc Electrophysiol* 2010. **21:** 1251-1259

(Kucera 1998) Kucera JP, Kleber AG and Rohr S. Slow conduction in cardiac tissue, II - effects of branching tissue geometry. *Circ Res* 1998. **83:** 795-805

(Lemery 2003) Lemery R, Guiraudon G and Veinot JP. Anatomic description of bachmann's bundle and its relation to the atrial septum. *Am J Cardiol* 2003. **91:** 1482-1485

(Lemery 2007) Lemery R, Birnie D, Tang ASL, Green M, et al. Normal atrial activation and voltage during sinus rhythm in the human heart: An endocardial and epicardial mapping study in patients with a history of atrial fibrillation. *J Cardiovasc Electrophysiol* 2007. **18:** 402-408

(Li 2011) Li M, Li T, Lei M, Tan X, et al. [Increased small conductance calcium-activated potassium channel (SK2 channel) current in atrial myocytes of patients with persistent atrial fibrillation]. *Zhonghua Xin Xue Guan Bing Za Zhi* 2011. **39:** 147-51

(Lionetti 2010) Lionetti FV, McCulloch AD and Baden SB. Source-to-source optimization of CUDA C for GPU accelerated cardiac cell modeling. *Euro-Par 2010 Parallel Processing, Pt i* 2010. **6271:** 38-49

(Luo and Rudy 1991) Luo CH and Rudy Y. A model of the ventricular cardiac action-potential - depolarization, repolarization, and their interaction. *Circ Res* 1991. **68:** 1501-1526

(Luo and Rudy 1994) Luo CH and Rudy Y. A dynamic-model of the cardiac ventricular action-potential .1. simulations of ionic currents and concentration changes. *Circ Res* 1994. **74:** 1071-1096

(Maclachlan 2007) Maclachlan MC, Sundnes J and Spiteri RJ. A comparison of non-standard solvers for ODEs describing cellular reactions in the heart. *Comput Methods Biomech Biomed Engin* 2007. **10:** 317-26

(Macleod 1991) Macleod R, Johnson C and Ershler P. Construction of an inhomogeneous model of the human torso for use in computational electrocardiography. 1991. 688-689

(Maesen 2013) Maesen B, Zeemering S, Afonso C, Eckstein J, et al. Rearrangement of atrial bundle architecture and consequent changes in anisotropy of conduction constitute the 3-dimensional substrate for atrial fibrillation. *Circulation-Arrhythmia and Electrophysiology* 2013. **6:** 967-975

(Maleckar 2008) Maleckar MM, Greenstein JL, Trayanova NA and Giles WR. Mathematical simulations of ligand-gated and cell-type specific effects on the action potential of human atrium. *Progress in Biophysics & Molecular Biology* 2008. **98:** 161-170

(Malmivuo and Plonsey 1995) Malmivuo J and Plonsey R. Bioelectromagnetism. 1995a. 482

(Mansour 2001) Mansour M, Mandapati R, Berenfeld O, Chen J, et al. Left-to-right gradient of atrial frequencies during acute atrial fibrillation in the isolated sheep heart. *Circulation* 2001. **103:** 2631-2636

(Marino 2008) Marino S, Hogue IB, Ray CJ and Kirschner DE. A methodology for performing global uncertainty and sensitivity analysis in systems biology. *J Theor Biol* 2008. **254:** 178-196

(Marsh 2012) Marsh ME, Ziaratgahi ST and Spiteri RJ. The secrets to the success of the rush-larsen method and its generalizations. *Ieee Transactions on Biomedical Engineering* 2012. **59:** 2506-2515

(Mayer 1916) Mayer AG. Nerve conduction, and other reactions in cassiopea. *Am J Physiol* 1916. **39:** 375-393

(McAllister 1975) McAllister RE, Noble D and Tsien RW. Reconstruction of electrical-activity of cardiac purkinje-fibers. *Journal of Physiology-London* 1975. **251:** 1-59

(Mckay 2000) Mckay M, Beckman R and Conover W. A comparison of three methods for selecting values of input variables in the analysis of output from a computer code. *Technometrics* 2000. **42:** 55-61

(Medi and Kalman 2008) Medi C and Kalman JM. Prediction of the atrial flutter circuit location from the surface electrocardiogram. *Europace* 2008. **10:** 786-796

(Mines 1913) Mines GR. On dynamic equilibrium in the heart. *Journal of Physiology-London* 1913. **46:** 349-383

(Moe 1956) Moe GK. Experimental methods for the evaluation of drugs in various disease states .3. cardiac arrhythmias - introductory remarks. *Ann N Y Acad Sci* 1956. **64:** 540-542

(Moe and Abildskov 1959) Moe GK and Abildskov JA. Atrial fibrillation as a self-sustaining arrhythmia independent of focal discharge. *Am Heart J* 1959. **58:** 59-70

(Moe 1962) Moe GK. On multiple wavelet hypothesis of atrial fibrillation. *Arch Int Pharmacodyn Ther* 1962. **140:** 183-&

(Morady 1999) Morady F. Drug therapy - radio-frequency ablation as treatment for cardiac arrhythmias. *N Engl J Med* 1999. **340:** 534-544

(Muszkiewicz 2014) Muszkiewicz A, Bueno-Orovio A, Liu X, Casadei,B, et al. Constructing human atrial electrophysiological models mimicking a patient-specific cell group. *Computing in Cardiology (Cinc)* 2014. **41:** 761-764

(Nademanee 2004) Nademanee K, McKenzie J, Kosar E, Schwab M, et al. A new approach for catheter ablation of atrial fibrillation: Mapping of the electrophysiologic substrate. *J Am Coll Cardiol* 2004. **43:** 2044-2053

(Narayan 2012) Narayan SM, Krummen DE, Shivkumar K, Clopton P, et al. Treatment of atrial fibrillation by the ablation of localized sources CONFIRM (conventional ablation for atrial fibrillation with or without focal impulse and rotor modulation) trial. *J Am Coll Cardiol* 2012. **60:** 628-636

(Nattel 1998) Nattel S. Experimental evidence for proarrhythmic mechanisms of antiarrhythmic drugs. *Cardiovasc Res* 1998. **37:** 567-577

(Nattel and Singh 1999) Nattel S and Singh BN. Evolution, mechanisms, and classification of antiarrhythmic drugs: Focus on class III actions. *Am J Cardiol* 1999. **84:** 11R-19R

(Nattel 2002) Nattel S. New ideas about atrial fibrillation 50 years on. *Nature* 2002. **415:** 219-226

(Nattel 2008) Nattel S, Burstein B and Dobrev D. Atrial remodeling and atrial fibrillation mechanisms and implications. *Circulation-Arrhythmia and Electrophysiology* 2008. **1:** 62-73

(Nimmagadda 2012) Nimmagadda VK, Akoglu A, Hariri S and Moukabary T. Cardiac simulation on multi-GPU platform. *J Supercomput* 2012. **59:** 1360-1378

(Noble 1962) Noble D. A modification of the Hodgkin–Huxley equations applicable to purkinje fibre action and pacemaker potentials. *JPhysiol* 1962. **160:** 317-352

(Noble 2012) Noble D, Garny A and Noble PJ. How the hodgkin-huxley equations inspired the cardiac physiome project. *J Physiol -London* 2012. **590:** 2613-2628

(Nygren 1998) Nygren A, Fiset C, Firek L, Clark JW, et al. Mathematical model of an adult human atrial cell - the role of K+ currents in repolarization. *Circ Res* 1998. **82:** 63-81

(Olgin 1995) Olgin JE, Kalman JM, Fitzpatrick AP and Lesh MD. Role of right atrial endocardial structures as barriers to conduction during human type-i atrial-flutter - activation and entrainment mapping guided by intracardiac echocardiography. *Circulation* 1995. **92:** 1839-1848

(Olsson 2001) Olsson S. Atrial fibrillation - where do we stand today? *J Intern Med* 2001. **250:** 19-28

(Oral 2002) Oral H, Knight BP, Tada H, Ozaydin M, et al. Pulmonary vein isolation for paroxysmal and persistent atrial fibrillation. *Circulation* 2002. **105:** 1077-1081

(Oral 2007) Oral H, Chugh A, Good E, Wimmer A, et al. Radiofrequency catheter ablation of chronic atrial fibrillation guided by complex electrograms. *Circulation* 2007. **115:** 2606-2612

(Pandit 2011) Pandit SV, Zlochiver S, Filgueiras-Rama D, Mironov S, et al. Targeting atrioventricular differences in ion channel properties for terminating acute atrial fibrillation in pigs. *Cardiovasc Res* 2011. **89:** 843-851

(Pandit 2010) Pandit SV, Warren M, Mironov S, Tolkacheva EG, et al. Mechanisms underlying the antifibrillatory action of hyperkalemia in guinea pig hearts. *Biophys J* 2010. **98:** 2091-2101

(Pandit and Jalife 2013) Pandit SV and Jalife J. Rotors and the dynamics of cardiac fibrillation. *Circ Res* 2013. **112:** 849-862

(Pandit 2005) Pandit S, Berenfeld O, Anumonwo J, Zaritski R, et al. Ionic determinants of functional reentry in a 2-D model of human atrial cells during simulated chronic atrial fibrillation. *Biophys J* 2005. **88:** 3806-3821

(Pedersen 2006) Pedersen OD, Sondergaard P, Nielsen T, Nielsen SJ, et al. Atrial fibrillation, ischaemic heart disease, and the risk of death in patients with heart failure. *Eur Heart J* 2006. **27:** 2866-2870

(Pedron-Torrecilla 2012) Pedron-Torrecilla J, Climent AM, Liberos A, Perez-David E, et al. Non-invasive estimation of the activation sequence in the atria during sinus rhythm and atrial tachyarrhythmia. *2012 Computing in Cardiology (Cinc)* 2012. **39:** 901-904

(Pedrón-Torrecilla 2013) Pedrón-Torrecilla J, Liberos A, Millet J, Climent AM, et al. Accuracy of non-invasive frequency estimation using atrial fibrillation. *Computing in Cardiology (Cinc)* 2013. **40**

(Pedron-Torrecilla 2014) Pedron-Torrecilla J, Climent AM, Liberos A, Rodrigo M, et al. Accuracy of inverse solution computation of dominant frequencies and phases during atrial fibrillation. *Comput Cardiol 2014* 2014. **41:** 537-540

(Perego and Veneziani 2009) Perego M and Veneziani A. An efficient generalization of the rush-larsen method for solving electro-physiology membrane equations. *Electronic Transactions on Numerical Analysis* 2009. **35:** 234-256

(Porciatti 1997) Porciatti F, Pelzmann B, Cerbai E, Schaffer P, et al. The pacemaker current I(f) in single human atrial myocytes and the effect of beta-adrenoceptor and A1-adenosine receptor stimulation. *Br J Pharmacol* 1997. **122:** 963-969

(Qi 2015) Qi D, Yang Z, Robinson VM, Li J, et al. Heterogeneous distribution of INa-L determines interregional differences in rate adaptation of repolarization. *Heart Rhythm* 2015. **12:** 1295-1303

(Ravens 2014) Ravens U. New developments in the antiarrhythmic therapy of atrial fibrillation. *Herzschrittmacherther Elektrophysiol* 2014. **25:** 41-46

(Reumann 2008) Reumann M, Bohnert J, Seemann G, Osswald B, et al. Preventive ablation strategies in a biophysical model of atrial fibrillation based on realistic anatomical data. *Ieee Transactions on Biomedical Engineering* 2008. **55:** 399-406

(Robbins and Dorn 2000) Robbins J and Dorn GW. Listening for hoof beats in heart beats. *Nat Med* 2000. **6:** 968-970

(Rodrigo 2014a) Rodrigo M, Pedrón–Torrecilla J, Hernández I, Liberos A, Climent AM, Guillem MS. Data Analysis in cardiac arrhythmias. Eds: Fernández–Llatas C, García–Gómez JM. *Data Mining in Clinical Medicine. Methods in Molecular Biology* 2014. **1246:**217–236.

(Rodrigo 2014b) Rodrigo M, Guillem MS, Climent AM, Pedron-Torrecilla J, et al. Body surface localization of left and right atrial high-frequency rotors in atrial fibrillation patients: A clinical-computational study. *Heart Rhythm* 2014. **11:** 1584-1591

(Rohr and Kucera 1997) Rohr S and Kucera J. Involvement of the calcium inward current in cardiac impulse propagation: Induction of unidirectional conduction block by nifedipine and reversal by bay K 8644. *Biophys J* 1997. **72:** 754-766

(Rohr 1998) Rohr S, Kucera JP and Kleber AG. Slow conduction in cardiac tissue, I - effects of a reduction of excitability versus a reduction of electrical coupling on microconduction. *Circ Res* 1998. **83:** 781-794

(Rohr 1999) Rohr S, Kleber AG and Kucera JP. Optical recording of impulse propagation in designer cultures - cardiac tissue architectures inducing ultra-slow conduction. *Trends Cardiovasc Med* 1999. **9:** 173-179

(Roten 2012) Roten L, Pedersen M, Pascale P, Shah A, et al. Noninvasive electrocardiographic mapping for prediction of tachycardia mechanism and origin of atrial tachycardia following bilateral pulmonary transplantation. *J Cardiovasc Electrophysiol* 2012. **23:** 553-555

(Rush and Larsen 1978) Rush S and Larsen H. Practical algorithm for solving dynamic membrane equations. *Ieee Transactions on Biomedical Engineering* 1978. **25:** 389-392

(Samie 2000) Samie F, Mandapati R, Gray R, Watanabe Y, et al. A mechanism of transition from ventricular fibrillation to tachycardia - effect of calcium channel blockade on the dynamics of rotating waves. *Circ Res* 2000. **86:** 684-691

(Sanchez 2012) Sanchez C, Corrias A, Bueno-Orovio A, Davies M, et al. The Na+/K+ pump is an important modulator of refractoriness and rotor dynamics in human atrial tissue. *American Journal of Physiology-Heart and Circulatory Physiology* 2012. **302:** H1146-H1159

(Sanchez 2014) Sanchez C, Bueno-Orovio A, Wettwer E, Loose S, et al. Inter-subject variability in human atrial action potential in sinus rhythm versus chronic atrial fibrillation. *PLoS One* 2014. **9:** e105897

(Sanchez-Quintana 2002) Sanchez-Quintana D, Anderson RH, Cabrera JA, Climent V, et al. The terminal crest: Morphological features relevant to electrophysiology. *Heart* 2002. **88:** 406-411

(Sanders 2005) Sanders P, Berenfeld O, Hocini MZ, Jais P, et al. Spectral analysis identifies sites of high-frequency activity maintaining atrial fibrillation in humans. *Circulation* 2005. **112:** 789-797

(Saoudi 2001) Saoudi N, Cosio F, Waldo A, Chen S, et al. A classification of atrial flutter and regular atrial tachycardia according to electrophysiological mechanisms and anatomical bases - A statement from a joint expert group from the working group of arrhythmias of the european society of cardiology and the north american society of pacing and electrophysiology. *Eur Heart J* 2001. **22:** 1162-1182

(Sarmast 2003) Sarmast F, Kolli A, Zaitsev A, Parisian K, et al. Cholinergic atrial fibrillation: I-K,I-ACh gradients determine unequal left/right atrial frequencies and rotor dynamics. *Cardiovasc Res* 2003. **59:** 863-873

(Sasaki 2013) Sasaki K, Sasaki S, Kimura M, Owada S, et al. Revisit of typical counterclockwise atrial flutter wave in the ECG: Electroanatomic studies on the determinants of the morphology. *Pace-Pacing and Clinical Electrophysiology* 2013. **36:** 978-987

(Sato 2009) Sato D, Xie Y, Weiss JN, Qu Z, et al. Acceleration of cardiac tissue simulation with graphic processing units. *Med Biol Eng Comput* 2009. **47:** 1011-1015

(Schotten 2001) Schotten U, Ausma J, Stellbrink C, Sabatschus I, et al. Cellular mechanisms of depressed atrial contractility in patients with chronic atrial fibrillation. *Circulation* 2001. **103:** 691-698

(Schotten 2002) Schotten U, Greiser M, Benke D, Buerkel K, et al. Atrial fibrillation-induced atrial contractile dysfunction: A tachycardiomyopathy of a different sort. *Cardiovasc Res* 2002. **53:** 192-201

(Seemann 2006) Seemann G, Hoper C, Sachse F, Dossel O, et al. Heterogeneous three-dimensional anatomical and electrophysiological model of human atria. *Philos Trans R Soc A-Math Phys Eng Sci* 2006. **364:** 1465-1481

(Seemann 2010) Seemann G, Bustamante PC, Ponto S, Wilhelms M, et al. Atrial fibrillation-based electrical remodeling in a computer model of the human atrium. *Computing in Cardiology, 2010* 2010. 417-420

(Seger 2006) Seger M, Modre R, Pfeifer B, Hintermüller C, et al. Non-invasive imaging of atrial flutter. *Computing in Cardiology 2006* 2006. **33:** 601-604

(Sekar 2009) Sekar RB, Kizana E, Cho HC, Molitoris JM, et al. I-K1 heterogeneity affects genesis and stability of spiral waves in cardiac myocyte monolayers. *Circ Res* 2009. **104:** 355-U158

(Shanmugam 2011) Shanmugam M, Molina CE, Gao S, Severac-Bastide R, et al. Decreased sarcolipin protein expression and enhanced sarco(endo)plasmic reticulum Ca2+ uptake in human atrial fibrillation. *Biochem Biophys Res Commun* 2011. **410:** 97-101

(Shaw and Rudy 1997) Shaw R and Rudy Y. Ionic mechanisms of propagation in cardiac tissue - roles of the sodium and L-type calcium currents during reduced excitability and decreased gap junction coupling. *Circ Res* 1997. **81:** 727-741

(SippensGroenewegen 1998) SippensGroenewegen A, Peeters HAP, Jessurun ER, Linnenbank AC, et al. Body surface mapping during pacing at multiple sites in the human atrium - P-wave morphology of ectopic right atrial activation. *Circulation* 1998. **97:** 369-380

(SippensGroenewegen 2000) SippensGroenewegen A, Lesh MD, Roithinger FX, Ellis WS, et al. Body surface mapping of counterclockwise and clockwise typical atrial flutter: A comparative analysis with endocardial activation sequence mapping. *J Am Coll Cardiol* 2000. **35:** 1276-1287

(Skasa 2001) Skasa M, Jungling E, Picht E, Schondube F, et al. L-type calcium currents in atrial myocytes from patients with persistent and non-persistent atrial fibrillation. *Basic Res Cardiol* 2001. **96:** 151-159

(Spach 1985) Spach MS, Dolber PC and Sommer JR. Discontinuous propagation - an hypothesis based on known cardiac structural complexities. *Int J Cardiol* 1985. **7:** 167-174

(Sundnes 2009) Sundnes J, Artebrant R, Skavhaug O and Tveito A. A second-order algorithm for solving dynamic cell membrane equations. *IEEE Trans Biomed Eng* 2009. **56:** 2546-2548

(Taccardi 1963) Taccardi B. Distribution of heart potentials on thoracic surface of normal human subjects. *Circ Res* 1963. **12:** 341-&

(Taccardi 1998) Taccardi B, Punske BB, Lux RL, MacLeod RS, et al. Useful lessons from body surface mapping. *J Cardiovasc Electrophysiol* 1998. **9:** 773-786

(ten Tusscher 2004) ten Tusscher KHWJ, Noble D, Noble PJ and Panfilov AV. A model for human ventricular tissue. *American Journal of Physiology-Heart and Circulatory Physiology* 2004. **286:** H1573-H1589

(Tobon 2008) Tobon C, Ruiz C, Saiz J, Heidenreich E, et al. Reentrant mechanisms triggered by ectopic activity in a three-dimensional realistic model of human atrium. a computer simulation study. *Computers in Cardiology, 2008* 2008. 629-632

(Tobon 2010) Tobon C, Ruiz C, Rodriguez JF, Hornero F, et al. A biophysical model of atrial fibrillation to simulate the maze III ablation pattern. *Computing in Cardiology 2010, Vol 37* 2010. **37:** 621-624

(Tobon 2013) Tobon C, Ruiz-Villa CA, Heidenreich E, Romero L, et al. A three-dimensional human atrial model with fiber orientation. electrograms and arrhythmic activation patterns relationship. *Plos One* 2013. **8:** e50883

(Trayanova 2006) Trayanova N. Defibrillation of the heart: Insights into mechanisms from modelling studies. *Exp Physiol* 2006. **91:** 323-337

(van Dam and van Oosterom 2003) van Dam PM and van Oosterom A. Atrial excitation assuming uniform propagation. *J Cardiovasc Electrophysiol* 2003. **14:** S166-S171

(Van Wagoner 1999) Van Wagoner DR, Pond AL, Lamorgese M, Rossie SS, et al. Atrial L-type Ca2+ currents and human atrial fibrillation. *Circ Res* 1999. **85:** 428-436

(VanWagoner 1997) VanWagoner D, Pond A, McCarthy P, Trimmer J, et al. Outward K+ current densities and Kv1.5 expression are reduced in chronic human atrial fibrillation. *Circ Res* 1997. **80:** 772-781

(Vaughan Williams 1984) Vaughan Williams EM. A classification of antiarrhythmic actions reassessed after a decade of new drugs. *J Clin Pharmacol* 1984. **24:** 129-47

(Vigmond 2001) Vigmond EJ, Ruckdeschel R and Trayanova N. Reentry in a morphologically realistic atrial model. *J Cardiovasc Electrophysiol* 2001. **12:** 1046-1054

(Vigmond 2009) Vigmond EJ, Boyle PM, Leon L and Plank G. Near-real-time simulations of biolelectric activity in small mammalian hearts using graphical processing units. *Conference proceedings : ...Annual International Conference of the IEEE Engineering in Medicine and Biology Society.IEEE Engineering in Medicine and Biology Society.Conference* 2009. **2009:** 3290-3

(Virag 2002) Virag N, Jacquemet V, Henriquez CS, Zozor S, et al. Study of atrial arrhythmias in a computer model based on magnetic resonance images of human atria. *Chaos* 2002. **12:** 754-763

(Voigt 2009) Voigt N, Trafford AW, Ravens U and Dobrev D. Cellular and molecular determinants of altered atrial Ca2+ signaling in patients with chronic atrial fibrillation. *Circulation* 2009. **120:** S667-S668

(Voigt 2010) Voigt N, Trausch A, Knaut M, Matschke K, et al. Left-to-right atrial inward rectifier potassium current gradients in patients with paroxysmal versus chronic atrial fibrillation. *Circ -Arrhythmia Electrophysiol* 2010. **3:** 472-U78

(Walmsley 2013) Walmsley J, Rodriguez JF, Mirams GR, Burrage K, et al. mRNA expression levels in failing human hearts predict cellular electrophysiological remodeling: A population-based simulation study. *Plos One* 2013. **8:** e56359

(Wang 1995) Wang K, Ho SY, Gibson DG and Anderson RH. Architecture of atrial musculature in humans. *Br Heart J* 1995. **73:** 559-565

(Warren 2003) Warren M, Guha P, Berenfeld O, Zaitsev A, et al. Blockade of the inward rectifying potassium current terminates ventricular fibrillation in the guinea pig heart. *J Cardiovasc Electrophysiol* 2003. **14:** 621-631

(Wettwer 2004) Wettwer E, Hala O, Christ T, Heubach J, et al. Role of I-kur in controlling action potential shape and contractility in the human atrium - influence of chronic atrial fibrillation. *Circulation* 2004. **110:** 2299-2306

(Wettwer 2013) Wettwer E, Christ T, Endig S, Rozmaritsa N, et al. The new antiarrhythmic drug vernakalant: Ex vivo study of human atrial tissue from sinus rhythm and chronic atrial fibrillation. *Cardiovasc Res* 2013. **98:** 145-154

(Workman 2001) Workman AJ, Kane AK and Rankin AC. The contribution of ionic currents to changes in refractoriness of human atrial myocytes associated with chronic atrial fibrillation. *Cardiovasc Res* 2001. **52:** 226-235

(Wu 1998) Wu TJ, Yashima M, Xie FG, Athill CA, et al. Role of pectinate muscle bundles in the generation and maintenance of intra-atrial reentry - potential implications for the mechanism of conversion between atrial fibrillation and atrial flutter. *Circ Res* 1998. **83:** 448-462

(Yamazaki 2012) Yamazaki M, Mironov S, Taravant C, Brec J, et al. Heterogeneous atrial wall thickness and stretch promote scroll waves anchoring during atrial fibrillation. *Cardiovasc Res* 2012. **94:** 48-57

(Yang 2001) Yang YF, Cheng J, Bochoeyer A, Hamdan MH, et al. Atypical right atrial flutter patterns. *Circulation* 2001. **103:** 3092-3098

(Yokokawa 2013) Yokokawa M, Latchamsetty R, Ghanbari H, Belardi D, et al. Characteristics of atrial tachycardia due to small vs large reentrant circuits after ablation of persistent atrial fibrillation. *Heart Rhythm* 2013. **4:** 469-76

(Yu 2012) Yu T, Deng C, Wu R, Guo H, et al. Decreased expression of small-conductance Ca2+-activated K+ channels SK1 and SK2 in human chronic atrial fibrillation. *Life Sci* 2012. **90:** 219-227

(Zhang 2009) Zhang H, Garratt CJ, Kharche S and Holden AV. Remodelling of cellular excitation (reaction) and intercellular coupling (diffusion) by chronic atrial fibrillation represented by a reaction-diffusion system. *Physica D-Nonlinear Phenomena* 2009. **238:** 976-983

(Zhao 2009) Zhao J, Trew ML, Legrice IJ, Smaill BH, et al. A tissue-specific model of reentry in the right atrial appendage. *J Cardiovasc Electrophysiol* 2009. **20:** 675-684

(Zlochiver 2008) Zlochiver S, Yamazaki M, Kalifa J and Berenfeld O. Rotor meandering contributes to irregularity in electrograms during atrial fibrillation. *Heart Rhythm* 2008. **5:** 846-854

(Zorn-Pauly 2004) Zorn-Pauly K, Schaffer P, Pelzmann B, Lang P, et al. If in left human atrium: A potential contributor to atrial ectopy. *Cardiovasc Res* 2004. **64:** 250-259